A METABOLOMIC INVESTIGATION OF KEY CELLULAR PROCESSES RELATING TO CANCER DEVELOPMENT AND PROGRESSION

A Thesis Submitted to the College of
Graduate Studies and Research
in Partial Fulfillment of the Requirements
for the Degree of Doctor of Philosophy
in the Department of Biochemistry
University of Saskatchewan
Saskatoon

By

Erin Jennifer Bingham

PERMISSION OF USE

In presenting this thesis in partial fulfilment of the requirements for a Postgraduate degree from the University of Saskatchewan, I agree that the Libraries of this University may make it freely available for inspection. I further agree that permission for copying of this thesis in any manner, in whole or in part, for scholarly purposes may be granted by the professor or professors who supervised my thesis work or, in their absence, by the Head of the Department or the Dean of the College in which my thesis work was done. It is understood that any copying or publication or use of this thesis or parts thereof for financial gain shall not be allowed without my written permission. It is also understood that due recognition shall be given to me and to the University of Saskatchewan in any scholarly use which may be made of any material in my thesis.

Requests for permission to copy or to make other use of material in this thesis in whole or part should be addressed to:

Head of the Department of Biochemistry
University of Saskatchewan
Saskatoon, Saskatchewan

ABSTRACT

Recent advancements in mass spectrometry have facilitated new analytical approaches capable of comprehensively characterizing metabolites in biological samples. Fourier transform ion cyclotron resonance mass spectrometry (FTICR-MS) combines excellent mass accuracy (ppm<1) and ultra-high resolution, which enables the separation and identification of individual components within complex mixtures, and the determination of elemental composition for each detected mass. FTICR-MS is an ideal method for non-targeted metabolomics as the majority of small molecular compounds (100-1000 Da) in a biological sample can be detected. The objective of this research was to investigate metabolomic alterations associated with key cellular processes deemed fundamental to cancer development and progression.

Differentiating U937 cells, fibroblasts synchronously progressing through the cell cycle and a transformed cell line containing a temperature sensitive oncogene were collected and subject to FTICR-MS analysis for non-targeted comprehensive metabolomics. Putative metabolite identifications were confirmed with targeted metabolite analysis using multiple reaction monitoring triple quadrupole mass spectrometry. Analysis of the resulting metabolic profiles revealed robust metabolic alterations associated with fundamental cellular processes. Changes in glycerolipid content were observed in all cellular processes studied. During cell cycle progression, elevated levels of triacylglycerols and vinyl acylglycerols were detected as cells approached mitosis; increased levels of plasmalogens were detected during the induced differentiation of human leukemic cells and activation of the oncogene $p130^{gag\text{-}fps}$ in fibroblasts resulted in increased levels of phospholipids, including plasmalogens. When *de novo* fatty acid synthesis was inhibited in the differentiation cell model, the cells were not able to complete the differentiation process. Removal of the inhibitor resulted in increased lipid content, particularly plasmalogens, and the continuation of differentiation, suggesting a requirement for the *de novo* synthesis of lipids during this cellular process.

This work demonstrates the advantages of non-targeted metabolic profiling for identifying non-intuitive metabolic associations with specific cellular processes. Collectively,

the results of this thesis have implicated glycerolipids, in particular phospholipids, in the processes of cell cycle progression, differentiation and tumourigenic transformation. A broadened understanding of the role of global lipid metabolism during fundamental cellular processes may one day lead to new approaches for their modulation, and potentially new therapeutic strategies.

ACKNOWLEDGEMENTS

The research presented in this thesis could not have been completed without the significant contributions made by my supervisors, Dr. Shawn Ritchie and Dr. Rob Warrington. Their unwavering guidance and support have made my graduate studies a wonderful experience. A very special thank you is extended to Dr. Dayan Goodenowe and John Hyshka, of Phenomenome Discoveries, for allowing me to work on this very exciting project. Recognition is also given to the members of my Advisory Committee: Dr. Bill Roesler, Dr. Mary Pato, Dr. Darrell Mousseau, Dr. Ramji Khandelwal and Dr. Stan Moore for their assistance and encouragement. I would also like to thank my external examiner, Dr. Grant Hatch, from the University of Manitoba for his participation in my defence and for his enthusiasm towards my work.

Appreciation is also extended to all employees at Phenomenome Discoveries, for their guidance and assistance with all aspects of my project. I would like to acknowledge, and thank, Dr. Gerald Davies for his help with the Western blot analyses. I would also like to show my gratitude to the Department of Biochemistry at the University of Saskatchewan for allowing me to complete my graduate work with them. Special thank you to Alison Meinert for all of her help formatting this thesis.

Lastly, I would like to thank my family and close friends for their love, support and encouragement. I am very thankful for everything they have done for me and the opportunities they have provided me throughout my life. I especially thank my parents for teaching me at a very early age that I can achieve anything I put my mind to, and for this I am forever grateful.

This research was supported fully by scholarships from the Natural Sciences and Engineering Research Council of Canada and Phenomenome Discoveries Inc, as well as devolved scholarships from the Department of Biochemistry.

TABLE OF CONTENTS

LIST OF TABLES

LIST OF FIGURES

LIST OF ABBREVIATIONS

AGPAT	Acyl-Glycerol-3-Phosphate Acyltransferase
amu	atomic mass unit
APCI	Atmospheric Pressure Chemical Ionization
ATP	Adenosine Triphosphate
BTA	1,2,3-Benzenetricarboxylic acid
Cdc2	Cell Division Control Protein 2 Homolog
CDK1	Cyclin Dependent Kinase 1
cDNA	Complementary DNA
CoA	Coenzyme A
DAG	Diacylglycerol
DHAPAT	Dihydroxyacetone-Phosphate Acyltransferase
DMSO	Dimethyl Sulfoxide
DNA	Deoxyribonucleic Acid
ER	Endoplasmic Reticulum
ESI	Electrospray Ionization
FASN	Fatty Acid Synthase
FSV	Fujinami Sarcoma Virus
FT	Fourier Transform
FTICR-MS	Fourier Transform Ion Cyclotron Resonance Mass Spectrometry
GC-MS	Gas Chromatography-Mass Spectrometry
GLUT	Glucose Transporter
GPAT	Glycerol-3-Phosphate Acyltransferase
HCA	Hierarchical Cluster Analyses
HIF1α	Hypoxia Inducible Factor 1 alpha
ICR	Ion Cyclotron Resonance
ITGAV	αV-Integrin
KEGG	Kyoto Encyclopedia of Genes and Genomes
LC-MS	Liquid Chromatography-Mass Spectrometry
LC-MS/MS	Liquid Chromatography-Tandem Mass Spectrometer
LPA	Lysophosphatidic Acid
M Phase	Mitotic Phase
m/z	Mass to Charge

MIF	Macrophage Migration Inhibitory Factor
mRNA	messenger Ribonucleic Acid
MS	Mass Spectrometry
MS-MS	Tandem Mass Spectrometry
NMR	Nuclear Magnetic Resonance
OAA	Oxaloacetic Acid
PAF	Platelet Activating Factor
PAFs	Polyunsaturated Fatty Acids
PBS	Phosphate Buffered Saline
PC	Principal Component
PCA	Principal Component Analysis
PCR	Polymerase Chain Reaction
PDK1	Pyruvate Dehydrogenase Kinase 1
PKC	Protein Kinase C
PLC	Phospholipase C
PMA	Phorbol 12-Myristate 13-Acetate
ppm	parts per million
PtdCho	Phosphatidylcholine
PtdEtn	Phosphatidylethanolamine
PtdSer	Phosphatidylserine
QAQC	Quality Assurance and Quality Control
RF	Radio Frequency
RNA	Ribonucleic Acid
ROS	Reactive Oxygen Species
RT-PCR	Real Time Polymerase Chain Reaction
S Phase	Synthesis Phase
SAGE	Serial Analysis of Gene Expression
TAG	Triacylglycerol
TC	Tricarboxylate Carrier
TCA Cycle	Tricarboxylic Acid Cycle or Citric Acid Cycle
TKTL1	Transketolase Like Gene
TOF	Time-of-Flight
TQ-MRM	Multiple Reaction Monitoring Triple Quadrupole
VAG	2-Acyl-1-(1-alkenyl)-sn-glycerol, or Vinyl Acylglycerol

1 OVERVIEW

The use of functional genomics and systems biology approaches in combination with mathematical modeling and advancements in bioinformatics has continued to increase our understanding of cancer development and progression. The systematic analysis of cancer is well on its way due to the availability of high-throughput genomic and proteomic technologies. However, changes that occur in the genome, transcriptome or proteome do not necessarily correspond to phenotypic alterations. Metabolomics is a logical progression from the analyses of genes, RNA and protein at the systems level. It provides the correlation between genes and the functional phenotype of an organism, which is the ultimate purpose of a functional genomics approach. Surprisingly, few studies have been carried out to investigate the comprehensive metabolic composition of cancer cells, and metabolism associated with cancer development and progression.

The objective of this research was to investigate phenotypic changes associated with key cellular processes deemed fundamental to cancer development. Using a non-targeted global metabolomics strategy, I have investigated the metabolic changes associated with cell cycle progression, cellular differentiation and tumourigenic transformation. Non-targeted metabolomics is a non-conventional biochemical analysis. The results obtained can be used to generate a data-driven hypothesis rather than to prove a theoretical hypothesis.

There are many stages required in a metabolomics analysis. Initially it must be decided if a targeted or non-targeted approach should be applied. This decision will be based on whether a specific aspect of the metabolome is to be studied, in which case a targeted analysis can be used to accurately quantify the metabolites of interest. On the other hand, if little is known about the expected metabolome changes and therefore no hypothesis can be formed, a global non-targeted metabolic analysis should be utilized. An analytical technology must then be selected to detect, quantify or structurally elucidate the metabolites. Such technologies include mass spectrometry (MS) or nuclear magnetic resonance (NMR), depending on the type of analysis required.

If a non-targeted metabolomics approach is selected, a bioinformatics platform is often required to organize and visualize the immense amounts of data produced from the analysis. Non-targeted metabolomics datasets are often large and likely not easy to comprehend in their raw form. Unsupervised statistical approaches can be used to reduce the complexity of metabolomics data and to visualize patterns of metabolite expression across samples. Metabolite identifications can then be made based on databases of known metabolites, formula assignments based on accurate masses or further analyses such as a targeted strategy or structural elucidation using NMR.

Our metabolomic investigation of cancer development and progression has identified a potential role of lipids in key cellular processes that are fundamental to the malignant phenotype. Lipids are a very diverse group of metabolites with a wide variety of biological functions in the cell, including structural components in cellular membranes, storage of fatty acids and cell signalling. To our knowledge, this is the first comprehensive metabolomic investigation of key cellular processes associated with cancer development and progression.

2 LITERATURE REVIEW

2.1 Understanding Biological Processes Using Systems Approaches

2.1.1 Functional Genomics

There have been many scientific discoveries and technological advances over the past fifty years that have allowed the study of biological systems at levels of complexity once never thought possible. In 1953, James D. Watson and Francis H. Crick introduced the structure of the deoxyribonucleic acid (DNA) helix (Watson and Crick, 1953). With this discovery, comprehension of the basic mechanisms of DNA replication, gene expression and protein synthesis followed closely behind. In the 1970s a group of researchers from Johns Hopkins University discovered type II restriction endonucleases and DNA ligases, enzymes capable of cutting and re-joining DNA at specific sequences sites (Smith and Wilcox, 1970; Danna and Nathans, 1971). It was quickly realized that these enzymes could be used to create recombinant DNA molecules, a fundamental technique upon which the science of biotechnology relies. Over the next decade further advancements in technology were made, including polymerase chain reaction (PCR) (Mullis, 1990) and automated DNA sequencing (Sanger *et al.*, 1977). Each of these very important milestones in molecular science has led to the completion of numerous large-scale genome sequencing projects, including that of the human genome.

The completion of the Human Genome Project (Lander *et al.*, 2001) has had a major impact on life science research, in particular human health and molecular medicine. The manner in which biological research is viewed, and approached, has changed dramatically throughout the post-genomic era. The genome project permitted the development of numerous high-throughput technologies and created the requirement for computer science, mathematics and statistics in molecular science (Hood, 2003). The sequencing of all human genes also brought hope for improved diagnosis, preventative medicine, earlier detection of genetic predispositions to disease, gene therapy and personalized drug design. Although the completion

of the human genome project was a significant milestone, it has not led to the advancements in molecular medicine which were predicted. This is because genomics represents only one piece of a very complicated puzzle. To fully understand the responses of a biological system, one must consider all of its components (Butcher *et al.*, 2004). Omics, systems biology and functional genomics are all terms for a similar goal: that is, to describe and understand the operation of a complex biological system through the analyses of its molecular building blocks (genes, RNAs, proteins and metabolites). Functional genomics allows the system-wide analysis from genotype to phenotype (Edwards and Batley, 2004). This global approach enables the identification of interactions between macromolecules, the determination of functional linkages between phenotypic expressions, and the construction of models which quantitatively describe the dynamics of the biological system (Bino *et al.*, 2004). Combining the analyses of genes, gene expression, proteins and metabolites could provide the insights required to understand the processes within a cell, and allow the progression from prediction to experimental validation of gene expression (Bino *et al.*, 2004; Heijne *et al.*, 2005).

2.1.2 OMICS

OMICS is a term that informally encompasses all of the molecular fields of study that end in *omics*, including genomics, transcriptomics, epigenomics, proteomics, and metabolomics. The omics technologies provide the molecular tools to analyze large sets of biological molecules such as DNA, RNA, protein and metabolites. The technical advancements in the omics assays have allowed analyses of entire signalling pathways, complete genomes, and all cellular components. For many years scientists were only able to analyze a single gene at a time. However, the discovery of high-throughput technologies brought the ability to study the genome of a system as a whole. Genomics involves studying the genome through the analysis of the nucleotide sequence, genome structure and its composition. Determining the composition of the genome can lead to the elucidation of molecular mechanisms which control a system. One of the main limitations of genomics is that the analysis often leads to the identification of a gene; however, the function of this gene at the biochemical level is typically not identified or is simply inferred from homology of previously investigated sequences (Fridman and Pichersky, 2005). Transcriptomics is the global analysis of all transcripts in a given organism. This molecular approach determines changes in gene

expression through the measurement of messenger ribonucleic acid (mRNA) and non-coding RNA levels in a system under a specific condition. The most common types of analysis used for transcriptomics are Northern Blots (Alwine *et al.*, 1977), Real-time PCR (RT-PCR) (Higuchi *et al.*, 1993), Serial Analysis of Gene Expression (SAGE) (Velculescu *et al.*, 1995) and DNA microarrays (Schena *et al.*, 1995). The study of gene expression can provide significant insight towards the cellular mechanisms that are affected at the gene expression level by the disease or drug treatment. Depending on the systems being compared, there can be either relatively few or thousands of differences. Understanding how all of these changes fit together can be very challenging. Proteomics is the analysis of the proteins synthesized under a given set of conditions. Proteomics has significant prospects for advancing our understanding of the life sciences, due to its direct relationship with gene and transcript data. However; the measurement of proteins can be complex due to their different properties, such as mass, isoelectric point, solubility, stability and post-translational modifications (Heijne *et al.*, 2005). There is also still a need for a high-throughput analysis for protein expression patterns. Metabolomics might be considered by some to be the key to integrated systems biology because it represents a direct measurement of the phenotype, measuring quantitative and qualitative traits (Fiehn, 2002). "Metabolomics is a burgeoning science that brings together analytical technology, genomics and computation, and lies at the core of the systems biology agenda" (Kell, 2004).

2.1.3 Metabolomics

Although genomics has dominated the scientific community for the past few decades, the analysis of metabolism and the correlations of specific metabolites to human health have taken place for centuries. Metabolomics is a scientific discipline that aims to identify and quantify the metabolome, which is the total quantitative collection of small molecular compounds present in an organism or biological sample. Metabolomics was first discussed in 1998 by Stephen Oliver, who not only coined the term but saw the enormous potential of the application of metabolomics for functional genomics (Oliver *et al.*, 1998). Metabolites are the reactants and products of a metabolic network; therefore, the quantification of the metabolome provides a direct method for the analysis of internal metabolism kinetics (Buchholz *et al.*, 2002). Metabolomics is a logical progression from the analyses of genes, RNA and protein at

the systems level. It provides the correlation between genes and the functional phenotype of an organism, which is the ultimate purpose of a functional genomics approach. In contrast to transcriptomics and proteomics, metabolomics can provide direct evidence rather than indications of changes in biochemical pathways (Heijne *et al.*, 2005). Metabolomics is considered to be a downstream analysis, in that the changes occurring in the metabolome reflect amplifications of the changes that occurred in the transcriptome and the proteome (Kell, 2005). Another benefit of metabolomics is that, unlike a transcript or protein, a given metabolite is the same in every organism that contains it.

Although the development of metabolomic methods and technologies is progressing rapidly, there are still issues and drawbacks that must be considered. DNA, RNA and proteins all have some structural properties in common, allowing the development of analytical methods that apply to basically all members of the class. On the other hand, metabolites within a cell have no shared chemical features on which a single general isolation, separation or identification method can be developed (Fridman and Pichersky, 2005). The number of metabolites and derivatives of known metabolites expected in mammals, plants and bacteria is still largely unknown. The metabolome is made up of very diverse compounds, ranging from ionic inorganic species to hydrophobic lipids, in a dynamic range of concentrations (Villas-Boas *et al.*, 2005b). Many major advances in the design and applications of analytical instrumentation for metabolomics have been made over the past few decades, allowing a broader and more comprehensive study of small molecules. However, in order for the true potential of metabolomics to be realized, efforts must be focused on improving sensitivity as a truly comprehensive analysis of the metabolome is not yet technically possible.

2.2 Metabolomics profiling technologies

There are numerous technologies available for studying the metabolome, each with advantages and limitations. There are two fundamental approaches that can be used when analyzing metabolites: targeted and non-targeted. A targeted analysis is restricted to the analysis of a single class of compounds or a specific pathway. A non-targeted approach, however, is aimed at identifying a large number of different metabolites in a sample with no prior knowledge about the sample itself. The power of a non-targeted approach allows for the generation of a data-driven hypothesis, whereas a targeted approach is intended to answer a

hypothesis and not generate one. To date there is not a single analytical method capable of detecting and quantifying all metabolites in a system. This is largely due to the chemical complexity of compounds that comprise the metabolome. However, there have been many advances made in metabolomics analyses and the combination of these technologies may make the detection of all metabolites attainable in the near future. Mass spectrometry (MS) and nuclear magnetic resonance (NMR) are the most commonly applied analytical technologies in metabolomics studies. NMR is a powerful technique and is particularly useful in the structure elucidation of unknown organic compounds. The main limitations of this approach are the complex computational requirements to resolve complex mixtures, the low sensitivity and that the cost of the NMR equipment can be significantly more expensive than MS-based technologies (Villas-Boas *et al.*, 2005a). Mass spectrometry is a widely applied technology in the study of metabolites as it provides a system which is both sensitive and capable of identifying and quantifying a wide range of metabolites (Dunn *et al.*, 2005). Mass spectrometry was the profiling technique utilized in this thesis and will be further explained in the following sections.

2.2.1 Types of Mass Spectrometry

The technology of mass spectrometry is based on the principle that molecules can be ionized into charged particles and detected, allowing both the determination of the mass and the structure of the ion. The mass spectrometer uses a beam of high-energy electrons to ionize organic molecules in a sample, which are then separated on the basis of their mass-to-charge (*m/z*) ratios and measured for relative abundance in the sample. The spectrum that is produced from a mass spectrometry approach is simply a display of the masses of the ionized molecules in a sample versus the relative intensity of each of the molecules. Mass spectrometers consist of an ionization source, ion filters or traps, an ion detector, vacuum pumps, and a data collection system (Figure 2.1). The sample is injected into the mass spectrometer at the inlet where it undergoes vaporization and ionization in the ionization source. There are numerous methods available for generating ionized molecules, including electrospray ionization (ESI) and atmospheric pressure chemical ionization (APCI), both of which are commonly used sources of ionization (Werner *et al.*, 2008). ESI generates ionized molecules through the use of a fine needle, to which a voltage is applied, which in turn causes the spray to be charged as it is

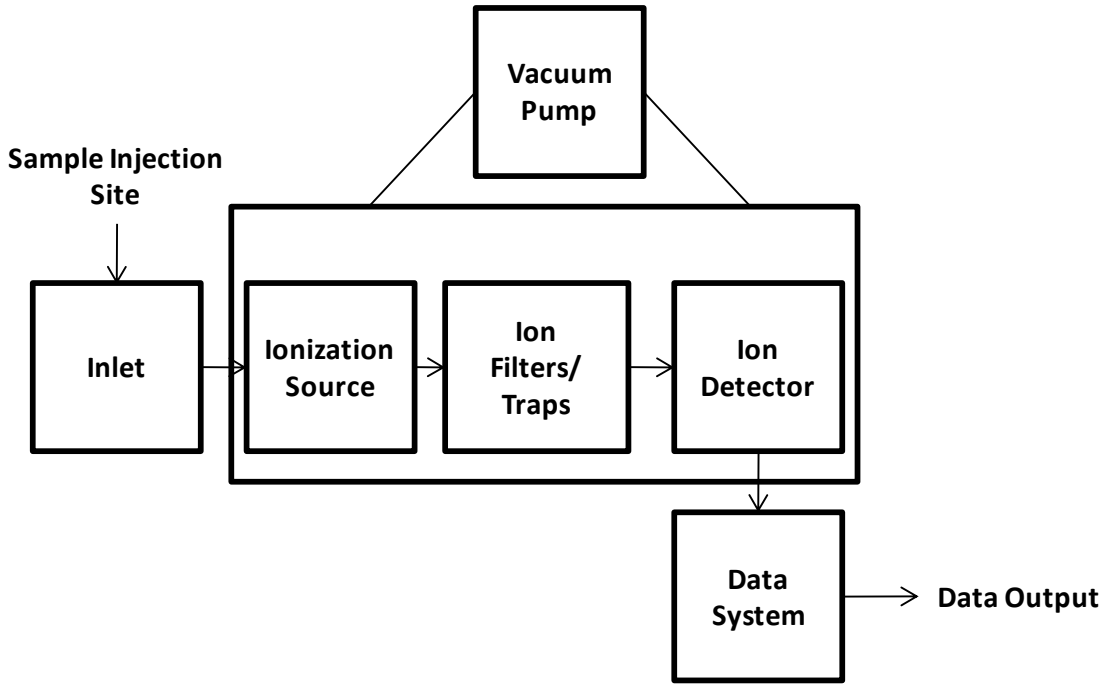

Figure 2.1 A generalized schematic of the main components of a mass spectrometer.
The sample is injected into the mass spectrometer at the inlet. The molecules of the sample are then ionized into charged particles at the ionization source. These charged particles are then separated by mass or charge depending on the type of mass analyzer being used. The ions then travel to the ion detector under vacuum pressure to the detector. When the ion hits the detector either the charge that is induced or the current that is produced is recorded.

nebulised. The sample is forced through the needle and uniformly charged droplets are produced. The droplets continue to break down, due to the evaporation of the solvent, resulting in individually charged ions. In comparison, APCI utilizes a co-axial flow of nitrogen, heat and a corona discharge needle to create ions from the injected liquid sample. The APCI source is more suitable for the study of less polar compounds as compared to the ESI source (Villas-Boas *et al.*, 2005a).

The ions are then filtered or trapped by the mass analyzer, such as time-of-flight (TOF), quadropole or cyclotron resonance (Werner *et al.*, 2008). With time-of-flight, ions travel through a vacuum tube to a detection plate, and the speed at which the ion travels through the tube is proportional to its mass (Lewandrowski *et al.*, 2005). The quadropole mass analyzer detects ions by scanning a radiofrequency for each mass across four parallel rods, and also measures the number of ions that passes through at each frequency (Bajad *et al.*, 2006). Ion cyclotron resonance detects ions through the measurement of an image current that is produced when ions, in the presence of a magnetic field, move in a cyclotron motion, which is the motion of a charged particle in a constant magnetic field, (Reemtsma, 2009). Ion cyclotron resonance is discussed further in the following section.

If the analyte components are separated prior to ionization, the capability of the mass spectrometer can be greatly increased. Gas or liquid chromatography are commonly used as separation methods and have been found to improve sensitivity and resolution of mass spectrometers (Werner *et al.*, 2008). Traditionally, gas chromatography-mass spectrometry (GC-MS) and liquid chromatography-mass spectrometry (LC-MS) have been used to study metabolites in a biological system. GC-MS can be used for the simultaneous separation, identification and quantification of volatile and non-volatile metabolites. The advantages of using GC-MS for the analysis of biological metabolites are the high chromatographic resolution and the ability to simultaneously analyze different classes of metabolites (Villas-Boas *et al.*, 2005a). The major drawbacks of this technology are that non-volatile compounds must be derivatized before they can be analyzed, large thermally-liable compounds cannot be detected due to their limited volatility, and that electron impact causes fragmentation (Dunn *et al.*, 2005; Villas-Boas *et al.*, 2005a). LC-MS is also capable of separating, identifying and quantifying a broad range of metabolites, especially metabolites with similar molecular masses. The advantages of this approach are that derivatization is not needed and thermo-labile metabolites

can be analyzed; however, the potential for identification can be a limitation unless a MS-MS fragmentation approach is used (Dunn *et al.*, 2005).

Fourier Transform Ion Cyclotron Resonance-Mass Spectrometry (FTICR-MS) is a mass spectrometry platform which is highly attractive for non-targeted metabolic profiling as it offers the highest mass accuracy and resolution of any other mass spectrometry technology.

2.2.2 FTICR-MS

FTICR-MS is derived from ion cyclotron resonance (ICR) spectrometry and is based on the principle of a charged particle orbiting in the presence of a strong magnetic field (Marshall, 2002). FTICR-MS have excellent mass accuracy and ultra-high resolution. Mass accuracy (measured in parts per million (ppm)) is a measurement of how well the observed mass-to-charge (*m/z*) correlates with the actual true mass of a specific elemental composition (Barrow *et al.*, 2005). FTICR mass spectrometers typically have mass accuracies less than 1 ppm, which allow for the elemental composition of each mass detected during the analysis to be determined. Metabolites with different molecular formulas have a different accurate mass. Therefore, if the mass of a metabolite can be accurately determined it will be possible to determine the corresponding molecular formula. However, before one can calculate the accurate mass of a metabolite, one must first be able to resolve the mass from the other masses in the sample. The FTICR-MS is currently the highest resolution mass spectrometer available, with a resolving power sufficient enough that individual components of a complex mixture can be identified and quantified without any prior separation (Werner *et al.*, 2008). Resolution is extremely important in mass spectrometry, as high resolution imparts the ability to separate closely spaced signals that occur in complex mixtures. Masses differing by only hundredths of a Dalton (Da) can be resolved, which is why there is no need for chromatography when using FTICR-MS (Stenson *et al.*, 2003). The FTICR-MS is therefore ideal for non-targeted, metabolomic analyses, and when properly deployed, can rapidly identify the similarities and dissimilarities between numerous types of biological samples (Bhalla *et al.*, 2005).

As reviewed by Barrow *et al*, there are five main components to a FTICR-MS; an ionization source, a vacuum system, a superconducting magnet, an analyzer cell, and a data converting and collecting system (Figure 2.2). Samples are directly injected into an ionization

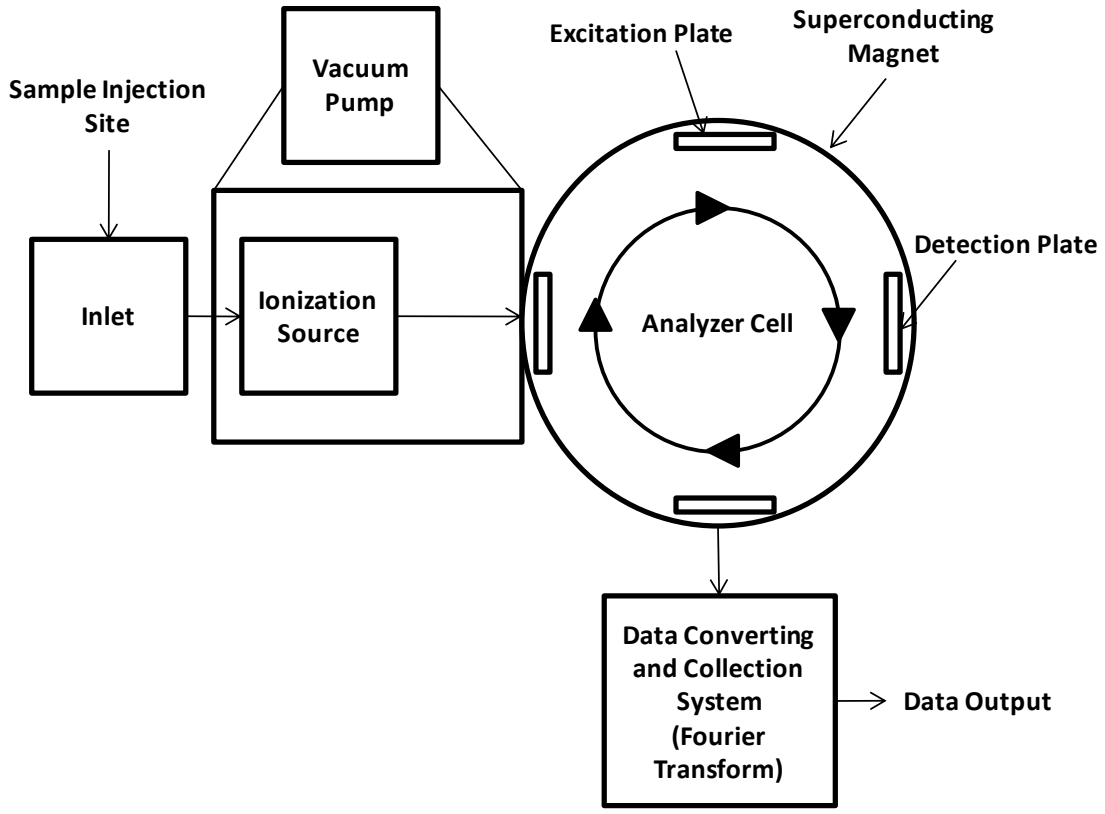

Figure 2.2 A generalized schematic of the main components of a Fourier transform ion cyclotron resonance mass spectrometer (FTICR-MS).
The sample is injected into the mass spectrometer at the inlet. The molecules of the sample are then ionized into charged particles at the ionization source. The ions then travel under vacuum pressure to the mass analyzer cell located inside a superconducting magnet. The ions each move in a cyclotron motion as a result of the opposing Lorentz force and radial forces. Through the use of a radio frequency (RF) potential, which is applied to the two excitation plates located in the analyzer cell, the orbiting radius of the cycling ions becomes larger and detectable. The frequency at which the ions cycle in the cell is then converted to a mass spectrum (m/z) using the mathematical procedure known as a Fourier transform.

source, most commonly with electrospray ionization (ESI) or an atmospheric pressure chemical ionization (APCI) source, which vaporizes and ionizes the injected sample. The vaporized sample then travels under vacuum pressure towards the analyzer cell which is located within the strong magnetic field of a superconducting magnet (Barrow *et al.*, 2005). The ions each move in a cyclotron motion as a result of the opposing Lorentz force, the force exerted on a charged particle in an electromagnetic field, and centrifugal (or radial) forces (Heeren *et al.*, 2004). The cyclotron orbits are too small to be detected when they initially enter the analyzer cell; however, through the use of a radio frequency (RF) potential, which is applied to the two excitation plates located in the analyzer cell, the orbiting radius of the cycling ions becomes larger and detectable (Barrow *et al.*, 2005). The frequency at which the ions cycle in the cell is then converted to a mass spectrum (*m/z*) using the mathematical procedure known as a Fourier Transform (FT) (Barrow *et al.*, 2005).

I have exploited the analytical power of the FTICR-MS to generate a non-targeted metabolomics platform. The combination of metabolite extraction, FTICR-MS analysis, and bioinformatics software enables the detection and identification of nearly all metabolites in a biological sample. A detailed description of the metabolite extraction and analysis is provided in the materials and methods section of this thesis.

Although this analytical technique is very powerful, and extremely useful in metabolomic studies, it does have a few limitations that must be overcome in order for it to be a stand-alone metabolomic tool. These include the inability to discriminate between isomers, and a lower mass limit of approximately 100 Da. These limitations can be dealt with through the use of a targeted mass spectrometry platform, such as a liquid chromatography tandem mass spectrometer (LC MS/MS), which can be optimized to detect lower weight masses and discriminate between isomers.

2.3 Methods for the analysis of multivariate data

Large-scale biological datasets are often enormous and likely not easily comprehensible in their raw form. The most effective method for dealing with such data is with the application of statistical approaches. Through the use of statistics it is possible to discover naturally occurring groupings in the data, as well as to compress very large datasets into smaller, more discernable, informative datasets (Kristal, 2002). There are two types of commonly used

statistical approaches for mining multivariate data; supervised and unsupervised. Supervised methods are used to find features that fit a predetermined pattern, whereas unsupervised methods characterize the dataset without any prior input or knowledge (Butte, 2002). Unsupervised statistical approaches are very useful when attempting to reduce the complexity of metabolomics data and to visualize patterns of metabolite expression in samples. There are many different unsupervised statistical techniques including principal component analysis, nearest neighbour clustering, self-organizing maps, *k*-means clustering, and hierarchical clustering (Butte, 2002). Hierarchical clustering and principal component analyses are particularly useful in the simplification and visualization of metabolomic datasets, and are used repeatedly throughout this thesis.

Hierarchical cluster analyses (HCA) use algorithms to reduce the complexity of datasets and organize the data into natural groupings, or clusters, based on expression patterns. Dendrograms are used to visually represent the clusters identified through the hierarchical cluster analysis. The dendrogram is organized like a tree, with branches of varying lengths connected to all of the features in a dataset. The length of each of the branches corresponds to the similarity between the features, or other branches (Butte, 2002). The shorter the branch, the more similar the expression patterns are between the features or other branches of features. This type of analysis generates small organized clusters, which can be useful in determining how groups of features are responding to a system. The hierarchical clustering used throughout this thesis utilized a Pearson correlation coefficient, which clusters metabolites with similar signal-to-noise (S/N) patterns across multiple samples. This method is ideal for MS-generated metabolomic data because of the arbitrary intensities of different molecules.

Principal Component Analysis (PCA), also known as an Eigenvector analysis, is a statistical technique that can be used to determine linear combinations of features that account for maximal variation in a dataset (Kristal, 2002). PCA is a key statistical application for the visualization of large complicated datasets, and is therefore suitable for reducing the dimensionality of large metabolomics datasets. PCA is a linear transformation that converts the data to a new coordinate system such that the greatest variance within the data comes to lie on the first coordinate (called the first principal component), the second greatest variance on the second coordinate, etc. Principal components are sets of vectors that decreasingly capture that variation in a dataset (Butte, 2002). The first principal component will capture more variation

than the second principal component, and so on. The great strength of a PCA is that it provides a rapid, and powerful view of a dataset that is simplified into a two or three dimensional graph (Kristal, 2002). In the case of a metabolomic analysis, samples with similar metabolite profiles will group closely on the PCA graph; whereas those with different metabolite profiles will cluster separately on the plot. The distance that the samples are separated on the plot is directly proportional to the differences between the metabolic profiles of the samples. Metabolites responsible for the separation between clusters can then be determined and further characterized.

A movement has begun in the science community towards the use of systems biology approaches in biological research. Integrating all available molecular-biological and phenotypic knowledge will provide a far more comprehensive picture of a system of interest. Determining the molecular differences between a normal and tumour cell or tissue is a crucial step in understanding cancer and in the development of anticancer therapies (Fan *et al.*, 2004). Although a complete understanding of cancer is not yet realistic, the use of systems approaches, in combination with mathematical modeling and advancements in bioinformatics, will continue to increase our understanding of cancer. The systematic analysis of cancer is well on its way due to the availability of high-throughput genomic and proteomic technologies. However, little has been reported on the comprehensive chemical composition of cancer cells, primarily due to the lack of adequate technology.

2.4 Understanding Cancer through the Study of Model Systems

According to the Canadian Cancer Society, 173,800 new cases of cancer, and 76,200 deaths due to cancer, will occur in Canada in 2010 (www.cancer.ca, 2010). Although research is continually adding to our understanding of how cancer develops, the ability to diagnose, treat and prevent the disease remains limited. Cancer, generally regarded as a genetic disease, can arise from a variety of alterations at the genetic, epigenetic and chromosomal levels (Khalil and Hill, 2005). The majority of research efforts have focused directly on genes and signalling pathways that lead to genetic alterations (Fan *et al.*, 2004). In a recent paper published in Nature Reviews Cancer, it was reported that there were precisely 291 genes which are implicated in cancer development (Futreal *et al.*, 2004)! The genomes of cancer cells acquire mutant alleles of oncogenes, tumour suppressor genes and other genes that play roles in cell

proliferation (Hahn and Weinberg, 2002). The pathways in which the products of these 'cancer genes' act have also been highly investigated, resulting in the realization that signalling does not necessarily occur in a linear pathway, but rather a complex web of interacting pathways (Hornberg *et al.*, 2006). In addition, it is also well established that environment, such as diet and lifestyle, play a large role in the risk of developing cancer.

The goal of this thesis was to use a comprehensive metabolomic approach to investigate phenotype changes in key cellular processes that are fundamental to cancer development and progression. There are currently many different cancer model systems used in research. These systems allow researchers to focus on a particular aspect of cancer development through a cell line, or animal model, which express the mutation or tumour of interest. Division, growth and differentiation are fundamental cellular processes (Sulic *et al.*, 2005). These, along with the alterations in a cell that collectively influence malignant growth, are commonly the focus in many cancer model systems. To date, very few reports have been published that examine the metabolic changes that accompany these processes. Developing a thorough understanding of the basic cellular mechanisms that drive a cell into malignancy is a fundamental step in cancer research. This project focused on the application of comprehensive metabolomic analyses on three cell based model systems, including transformation, differentiation and cell cycle progression.

2.4.1 The Role of Cell Cycle and Differentiation in Cancer

Hanahan and Weinberg suggest that there are six essential alterations in cell physiology that lead to transformation and tumorigenesis in nearly all cancers: self-sufficiency in growth signals, insensitivity to growth-inhibitory signals, evasion of apoptosis, limitless replicative potential, sustained angiogenesis, and tissue invasion and metastasis (Hanahan and Weinberg, 2000).

In addition to these six hallmarks, it is believed that aerobic glycolysis, also commonly referred to as the Warburg effect, should be considered the seventh hallmark of cancer, as it was one of the first biochemical alterations detected in cancer (Hsu and Sabatini, 2008; Yeung *et al.*, 2008). Nutrients, energy and biosynthetic activity are all required for a cell to proliferate successfully. It is a massive energetic undertaking for a cell to double all of its biomass (for example proteins, lipids and nucleic acids) during a cell division. Metabolism in highly

proliferative cells, such as cancer cells, differs significantly from those that are quiescent. In 1926 Warburg proposed a model of tumourigenesis involving altered energy production in tumours. This model, which is now known as the Warburg hypothesis, or effect, states that cancer cells shift to a high level of aerobic glycolysis, even in the presence of oxygen, and low respiration to metabolize glucose (Figure 2.3) (Warburg *et al.*, 1927). Under normal physiological conditions, cellular energy metabolism is preferentially based on oxidative phosphorylation, which is considerably more efficient than glycolysis (Warburg *et al.*, 1927) . Warburg hypothesized an alternative state of energy metabolism in cancer systems, which included an impaired mitochondrial function and increased dependence on glycolysis as a source of energy, even under aerobic conditions (Warburg, 1956). According to this hypothesis, the ability of cancer cells to generate ATP via mitochondrial respiration is impaired, which likely triggers alternative metabolic pathways by the over-expression of glycolytic enzymes (Warburg, 1956). This alternative method of energy production may be a response, or perhaps a requirement, due to the rapid growth of cancer cells and consequently the expansion of a tumour mass which may result in an insufficient supply of blood to the tissue. This would create a hypoxic environment with limited mitochondrial respiration, causing cancer cells to utilize the glycolytic pathway as their main source of energy (Xu *et al.*, 2005). This way, if the cancer cells automatically switch to glycolysis, rather than respiration, as a source of energy, then a lack of oxygen will not prevent the cells from growing.

Recent findings in cancer research have rekindled interest in Warburg's theory, including an observation that, during tumourigenesis, an increase in glucose uptake and lactate production occurs and that the fully transformed state is most dependent on glycolysis and minimally dependent on the mitochondria for ATP synthesis (Ramanathan *et al.*, 2005). The increase in glucose uptake in malignant cells has been clearly linked to the increased and deregulated expression of glucose transporter proteins, in particular GLUT1 and GLUT3 (Macheda *et al.*, 2005). There have also been reports that increased GLUT expression directly correlates to increased tumour aggressiveness and inversely correlates to patient survival (Kawamura *et al.*, 2001). The strong correlation between the rate of aerobic glycolysis and the aggressiveness of the cancer likely indicates that the glycolytic phenotype offers a significant proliferative advantage and may be a crucial component of the malignant phenotype (Gatenby and Gillies, 2004). The glycolytic phenotype suppresses apoptosis and the by-products of

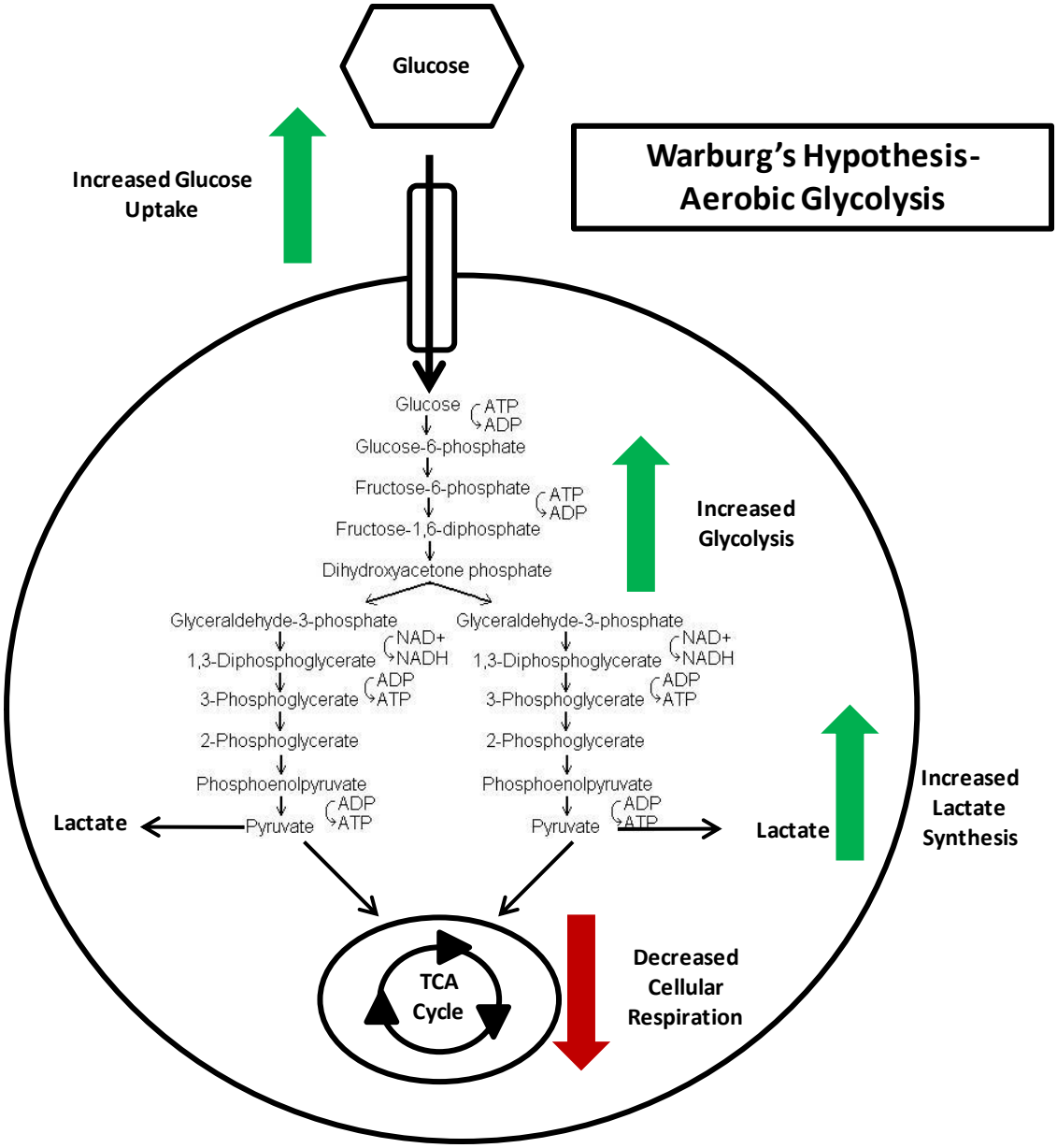

Figure 2.3 Otto Warburg's hypothesis- aerobic glycolysis in cancer.
This model, which is now known as the Warburg hypothesis, states that cancer cells shift to a high level of aerobic glycolysis (green arrows), even in the presence of oxygen, and low respiration (red arrow) to metabolize glucose. Warburg also suggested that the elevated levels of lactate in cancer cells are a direct effect of aerobic glycolysis.

glycolysis contribute to the degradation of the extracellular matrix, thus increasing cell mobility and metastatic potential (Bonnet *et al.*, 2007). Another possible advantage for a cancer cell to shift to glycolysis is to provide a source of acetyl CoA for the mitochondrial synthesis of citrate, which in turn provides the source for cytosolic acetyl CoA (Costello LC, 2005). Cytosolic acetyl CoA is the essential precursor molecule for the synthesis of fatty acids, which in turn are the major building blocks for lipid molecules. The following section 2.5 will provide further detail on lipid synthesis and classification.

There have also been many connections made between cancer-causing genes and glucose metabolism, including the AKT family of proteins, also known as protein kinase B, which has been found to stimulate glucose metabolism in cancer cells, as well as AMP-activated protein kinase, which links glucose metabolism and cell cycle (Langbein *et al.*, 2006). Reports have also showed that mitochondria in rapidly growing tumour cells are generally smaller and show less cristae than mitochondria from normal tissues, and also that the actual number of mitochondria in tumour cells is reduced (Ristow, 2006). It is still unknown whether this is due to the reduced mitochondrial activity, or rather that the mitochondria activity is reduced due to the increased glycolytic activity. Despite numerous reports by many different scientists whose research complements, or supports, Warburg's theory, the underlying cause of the effect is still not well understood. It is also unknown if the same causes always underlie this effect in cancers, or if genetic influences play any part (Unwin *et al.*, 2003).

Cell cycle regulation and cellular differentiation are two fundamental cellular processes that are lost during cancer development and progression. There has been a direct link made between the deregulation of the cell cycle components and cancer (Sulic *et al.*, 2005). The cell cycle is a highly organized, tightly regulated series of events in eukaryotic cells. The cycle can be divided into four phases; G1, S, G2 and M. The G1, or gap1, phase of the cycle is where cell growth primarily occurs, and it is also the portion of the cycle where cells decide to replicate and divide or to exit the cell cycle into a quiescent state (G0). The S phase, or synthesis phase, is the point in the cell cycle in which DNA replication occurs. During the second gap phase, G2, the integrity of the DNA replication is confirmed, and the cell prepares for cell division in the M phase. The M phase, or mitotic phase, of the cell cycle is the point in which nuclear division and cytokinesis takes place, and two new identical daughter cells are produced. Few cells exit the cell cycle during the early developmental stages of an organism;

however, once an adult stage is reached the majority of cells enter a quiescent state, G0, in which they will no longer divide (Malumbres and Barbacid, 2001), or they enter into a differentiation program (Deane *et al.*, 2005). However, upon stimulation by growth factors, most quiescent cells are capable of re-entering the cell cycle, unless they have reached a state of terminal differentiation (Sherr, 2000).

The activation of cell cycle promoting factors (oncogenes) or inactivation of cycle inhibiting factors (tumour suppressors) can lead to the deregulation of cell proliferation and often malignancy (Tessema *et al.*, 2004). This imbalance of growth-inhibiting and growth-promoting factors greatly influences the cell cycle and the development of cancer (Deane *et al.*, 2005). Defects in the G1 and G2 checkpoints, including the inactivation of the checkpoint regulatory proteins Rb and p53, can also lead to uncontrolled proliferation and potentially result in the development of cancer (Tessema *et al.*, 2004; Deane *et al.*, 2005). These checkpoints ensure that the cells are large enough, that the environment is suitable and that there has not been any damage to the cell structure or the genetic material: defects in any one of which would preclude successful division. The checkpoint in late G1 portion of the cell cycle is particularly important for tumour development as this is where the DNA is assessed for damage. Under normal cell conditions, DNA found to be intact will continue through to the synthesis phase of the cycle, whereas those with irreparable damage will undergo apoptosis (Seville *et al.*, 2005). However, through the deregulation of the checkpoints, cancer cells are able to continue dividing without regard to any DNA damage that the cells may contain (Seville *et al.*, 2005).

Any meaningful study of the cell cycle in an *in vitro* system requires a population of synchronized cells. One of the most common methods of synchronization is through serum starvation (Winkles, 1998; Cheong *et al.*, 2003; Liu *et al.*, 2004b; Memili *et al.*, 2004). In order to proliferate in culture, normal fibroblasts require growth factors, typically supplied in the form of foetal calf serum in the cell media. If the growth factors are removed, or more typically greatly diminished, normal fibroblasts enter into the quiescent state G0 of the cell cycle (Iyer *et al.*, 1999). In one study of goat fibroblasts, serum starvation yielded a synchronized population of G0 cells, which made the transition into *bona fide* G1 stage cells five hours after serum stimulation (Memili *et al.*, 2004). This serum deprivation model

provides a system to analyze the molecular changes that occur as quiescent cells re-enter the cell cycle and progress through G1, S, G2 and mitosis.

Differentiation is the process in which pluripotent stem cells, or multipotent progenitor cells, irreversibly mature into specialized cell types. For example hematopoietic stem cells from the bone marrow differentiate into white and red blood cells as well as platelets, whereas mesenchymal stem cells in the bone marrow differentiate into stromal cells and fat cells (Verhoeckx *et al.*, 2004). A number of mechanisms have been identified by which transcription factors regulate differentiation, including: auto regulation (factors that positively regulate their own expression), activation of lineage-specific genes, inhibition of alternative pathways, and inhibition of proliferation (Tenen, 2003). In addition to the loss of cell cycle control, the loss of cellular differentiation is another common feature in many different types of human cancer. It has been hypothesized that disruptions in the cell cycle may be the cause for the loss of differentiation, or that differentiation mechanisms are affected as secondary effects of carcinogenesis (Tenen, 2003). It is also possible that the expression of oncogenes and inhibition of tumour suppressors directly impacts both the cell cycle and the differentiation process. To date the mechanism in which the neoplastic cells are able to block differentiation is still not completely understood.

The human promyelomonocytic leukemic cell line, U937, is a well established model system for studying monocyte-macrophage differentiation (Piquemal *et al.*, 2002). Under normal conditions the process of monocyte to macrophage differentiation occurs once the monocyte arrives at the target tissue, where differentiation stimuli activate the differentiation process (Gonzalez-Mejia and Doseff, 2009). In Acute Myeloid Leukemia the transcription factors that are crucial for the differentiation of monocytes are disrupted, either through mutations or chromosomal translocations (Tenen, 2003). The U937 cell line originated from the pleural fluid of a patient diagnosed with acute promyelocytic lymphoma (Harris and Ralph, 1985). Treatment of U937 cells with phorbol 12-myristate 13-acetate (PMA), a protein kinase C activator, induces maturation from a monocytic cell into a macrophage (Kitamura *et al.*, 2004). A number of phenotypic changes occur during this process, including adherence to the plate surface, gain of macrophage characteristics (phagocytosis, antibody-dependent cellular cytotoxicity, antigen presentation and chemotaxis), and the loss of proliferative potential (Kwon and Kim, 2003; Verhoeckx *et al.*, 2004). To date, numerous types of analyses have

been performed on this cell line, including gene expression (Tamayo *et al.*, 1999; Piquemal *et al.*, 2002; Kitamura *et al.*, 2004), and proteomics (Verhoeckx *et al.*, 2004) in an attempt to understand the process of differentiation. Major gene expression changes occurring during differentiation have been reported, and involve genes associated with transcription and translation, as well as cytoskeleton and macrophage associated functions (Piquemal *et al.*, 2002). Proteomic analysis of differentiating U937 cells revealed 226 proteins which were found to be significantly ($p<0.05$) up-regulated and largely involved with immune response, chemotaxis, cell growth, transport, cell adhesion, signal transduction and differentiation (Verhoeckx *et al.*, 2004). However, there is not a single report to date showing metabolic changes that are associated with this process.

2.5 The Role of Lipids in Cellular Processes

Cellular growth and maintenance in normal tissue is tightly regulated by the availability of nutrients and a balance of glycolysis and fatty acid synthesis, whereas tumour cells are able to bypass these regulatory checks and balances of lipogenesis to meet the high energy demands of increased proliferation and metabolism (Little and Kridel, 2008). Lipogenesis has been recognized as one of the metabolic hallmarks of a tumour cell (Kuhajda, 2000).

Lipids are a class of biological molecules that are typically hydrophobic in nature and soluble in organic solvents such as methanol, acetone, benzene and chloroform but only sparingly, if at all, in water (Fahy *et al.*, 2005). In general, there are three biological roles of lipids; they act as (a) storage molecules, (b) structural components of cellular membranes, and (c) cofactors and signalling molecules (van Meer, 2005; Watson, 2006). Lipids are divided into eight distinct categories; fatty acids, glycerolipids, glycerophospholipids, sphingolipids, sterol lipids, prenol lipids, saccharolipids and polyketides (Fahy *et al.*, 2005).

Fatty acids are carboxylic acids with long-chain hydrocarbon side groups, which can either be saturated or unsaturated. Fatty acids are rarely found to be free in nature; rather they are typically in an esterified form as the major lipid building block of complex lipids (such as glycerolipids and glycerophospholipids) (Fahy *et al.*, 2005). There are two sources of fatty acids for animal metabolism; they can be exogenously derived and attained through diet, or they can be endogenously synthesized by the animal (Menendez and Lupu, 2007). The *de novo* synthesis of fatty acids mainly occurs in the liver or adipose tissue in humans. Pyruvate, the

end-product of glycolysis, is transported into mitochondria where it is converted into acetyl-CoA by pyruvate dehydrogenase. Acetyl-CoA is then condensed with oxaloacetate by citrate synthase to produce citrate. Citrate molecules are then exported out of the mitochondria and into the cytosol, via the tricarboxylate transport system, where they are broken down into acetyl-CoA and oxaloacetate by ATP citrate lyase. The oxaloacetate that is produced is converted by malate dehydrogenase back into malate, which in turn can either be transported back into the mitochondria or can be oxidatively decarboxylated to pyruvate by malic enzyme and then be returned to the mitochondria in this molecular form.

Cytosolic acetyl-CoA and malonyl-CoA are then utilized in the synthesis of fatty acids in seven enzymatic reactions carried out by fatty acid synthase (FASN). FASN is a 250-270kD multifunctional homodimeric polypeptide, comprised of seven separate functional domains; it is the sole protein that is capable of *de novo* synthesis of long-chain fatty acids from acetyl-CoA, malonyl-CoA and nicotinamide adenine dinucleotide phosphate (NADPH) (Menendez *et al.*, 2005; Kuhajda, 2006). In healthy, well nourished individuals sufficient levels of fatty acids are acquired from dietary fat, which results in decreased demand for endogenous fatty acid synthesis (Menendez and Lupu, 2007).

De novo fatty acid synthesis is active during embryogenesis, in foetal lung cells, and in hormone-sensitive cells where it is regulated by progesterone and oestradiol (Menendez and Lupu, 2007). Over-expression and increased activity of FASN occurs during tumour development and progression, and is considered to be one of the most frequent phenotypic alterations to occur in carcinogenic cells (Kuhajda, 2000; Menendez *et al.*, 2005). FASN expression has been correlated with poor prognosis in numerous types of cancer (Little and Kridel, 2008). In both breast and prostate cancer high levels of FASN expression have been associated with increased chance of recurrence and increased risk of death (Kuhajda, 2006). The endogenous *de novo* synthesis of fatty acids occurs in cancer cells regardless of the levels of exogenous lipids. In fact, almost all esterified fatty acids in tumour cells are endogenously derived (Menendez and Lupu, 2007). Growth factors and growth factor receptors have been identified as key players in the over-expression of FASN in cancer cells (Menendez and Lupu, 2007).

The discovery of the activation of FASN in tumours has led many researchers to focus their work on discovering methods of inhibiting the activity of the enzyme and many have had

success with small molecule inhibitors of FASN (Little and Kridel, 2008). FASN inhibition in cancer cells results in a decline of endogenous fatty acids as well as a decrease in cell proliferation, which is typically followed by apoptosis (Menendez and Lupu, 2007). This inhibition of growth suggests that FASN may regulate metabolism, proliferation and survival in cancer cells.

Fatty acids, either endogenously or exogenously synthesized, typically have two fates depending on the organism's metabolic needs. During periods of rapid cellular growth the fatty acids are often incorporated into phospholipids, which are utilized in the synthesis of cellular membranes (van Meer *et al.*, 2008). When the organism is not actively growing, the fatty acids are incorporated into glycerolipids, in particular triacylglycerols, for the storage of energy (Fahy *et al.*, 2005).

The generalized pathway illustrated in Figure 2.4 can be used as a reference for the following explanation of lipid synthesis in mammalian cells. Glycerolipids and phospholipids are synthesized from the same precursor metabolites, glycerol-3-phosphate and fatty acyl-CoA (activated fatty acid), and initially the same biosynthesis pathway. The majority of glycerol-3-phosphate is synthesized in the glycolytic pathway through the action of glycerol-3-phosphate dehydrogenase using dihydroxyacetone phosphate as a precursor (Bell and Coleman, 1980). The activation of a fatty acid to fatty acyl-CoA, by fatty acyl-CoA synthetase, is a requirement for nearly all of the metabolic fates of fatty acids in eukaryotes (Bell and Coleman, 1980). Glycerol-3-phosphate acyltransferase (GPAT) and acyl-glycerol-3-phosphate acyltransferase (AGPAT) transfer fatty acyl groups to glycerol-3-phosphate (Fagone and Jackowski, 2009). The acylation of glycerol-3-phosphate yield a molecule of phosphatidic acid, or diacylgycerol phosphate, an important intermediate in lipid synthesis (Fagone and Jackowski, 2009). Both GPAT and AGPAT have been isolated from the endoplasmic reticulum (ER) and the mitochondria (Fagone and Jackowski, 2009). If there is only one acylation of glycerol-3-phosphate or hydrolysis of phosphatidic acid by phospholipase A_2, the result is lysophosphatidic acid (LPA). LPA was originally thought to merely be an intermediate in lipid metabolism, however, more recently it has been determined that LPA stimulates cell proliferation, migration and survival and in some cell types LPA is a lipid mediator that promotes growth-factor-like responses (Mills and Moolenaar, 2003). Due to LPA's role in cell

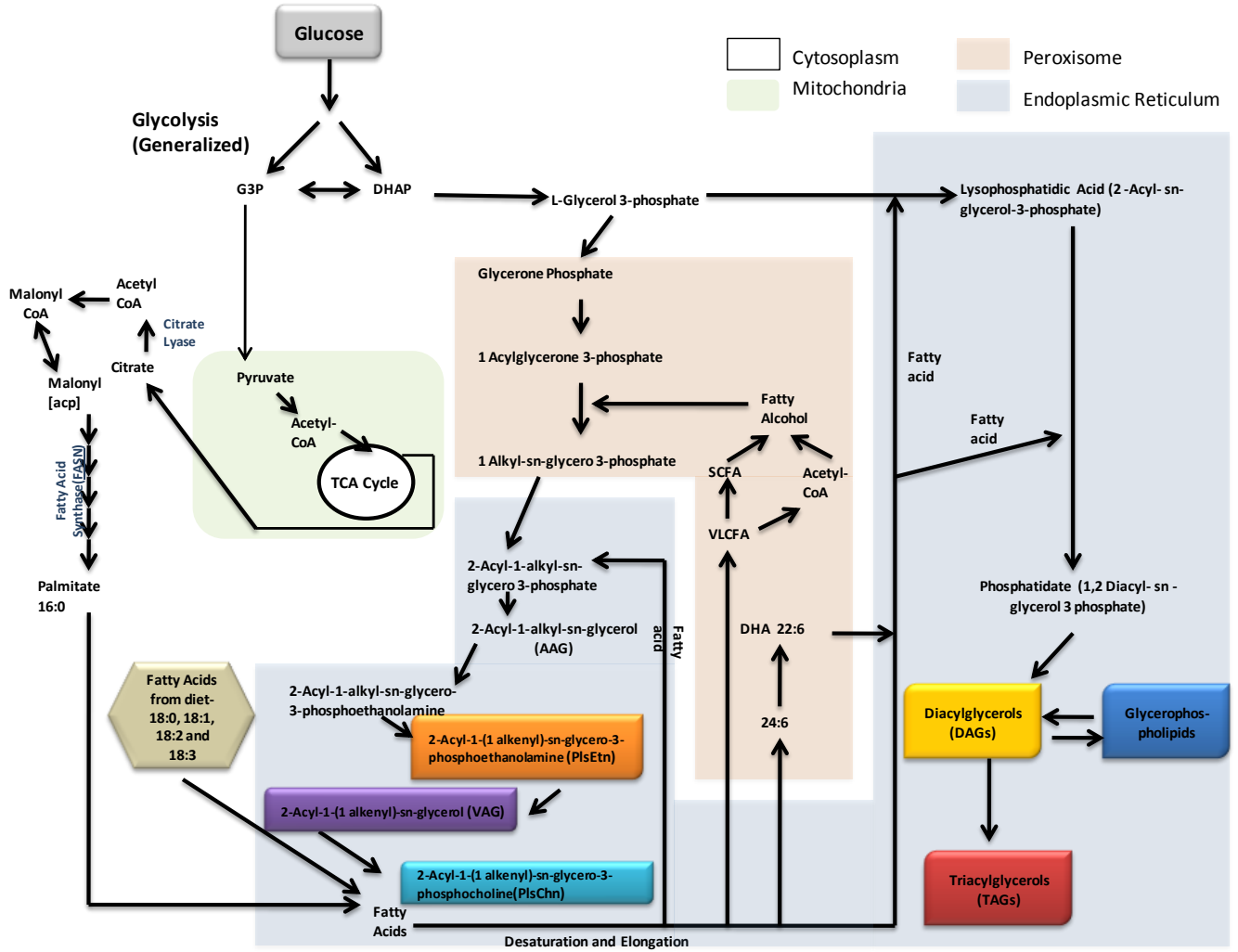

Figure 2.4 The synthesis pathways of fatty acids, glycerolipids, glycerophospholipids, and ether lipids.
This figure summarizes how and where lipids are synthesized in cells. The pathway initiates with the transport of glucose into the cell, after which it continues through the glycolytic pathway and the TCA cycle in the mitochondria. Citrate that is synthesized in the mitochondria is exported out into the cytosol where it is used in the synthesis of fatty acids. The fatty acids are transported to the endoplasmic reticulum for desaturation and elongation. Glycerolipids and glycerophospholipids are synthesized in the endoplasmic reticulum. The first two steps in the synthesis of ether lipids occur in the peroxisome, and are completed in the endoplasmic reticulum.

proliferation and migration it has become a target molecule of interest to cancer researchers, especially since the discovery that LPA is a key contributor to the metastasis in cancer (Mills and Moolenaar, 2003). The next step in the lipid synthesis pathway is the dephosphorylation of phosphatidic acid by phosphatidic acid phosphatase, yielding 1,2-diacylglycerol. Diacylglycerols play many different functional roles in the cell, not only are they the precursor molecules for many classes of lipids (including triacylglycerols, phosphatidylcholines and phosphatidylethanolamines), but they also function as secondary messengers that are required for the activation protein kinase C (PKC) (Bell and Coleman, 1980).

The structure of the major lipid classes in mammalian cells is illustrated in Figure 2.5. A description of each of these classes is detailed in the following paragraphs. The sn-1, sn-2 and sn-3 positions, which denote the first, second and third carbon atoms of the glycerol in a glycerol containing metabolite respectively, are labelled on the diacylglycerol structure. The "sn" stands for stereospecifical or stereoselective numbering and indicates that only compounds with S configuration for glycerol are known to exist in living systems. The polar head group of a phospholipid is located at the sn-3 position. The vinyl ether bond at the sn-1 position of ether lipids has also shown on the plasmenylethanolamine (ethanolamine plasmalogen) structure.

A major component of eukaryotic cells are glycerolipids, in particular triacylglycerols, making up 10 to 90% of the dry weight of the cell depending on the cell type (Bell and Coleman, 1980). Triacylglycerols, also known as triglycerides or neutral fats, are composed of three fatty acids each in ester linkage to a single glycerol (Turkish and Sturley, 2007). In most eukaryotic cells triacylglycerols form oily droplets in the cytosol, which are available as metabolic fuel when energy is required (Turkish and Sturley, 2007). In most vertebrates triacylglycerols are actually stored in specialized fat cells, called adipocytes, in the form of fat droplets (Bell and Coleman, 1980). These fat cells contain enzymes, called lipases, that catalyze the hydrolysis of the triacylglycerols releasing the fatty acids when the organism requires them for energy (Bell and Coleman, 1980).

Glycerophospholipids are the major structural lipids in eukaryotic membranes, and include: phosphatidylcholine (PtdCho), phosphatidylethanolamine (PtdEtn), phosphatidylserine (PtdSer) and phosphatidylinositol (PtdIns) (van Meer *et al.*, 2008). PtdCho is the most abundant phospholipid in mammalian membranes, accounting for more than 50% of the lipid species in the membrane (van Meer *et al.*, 2008; Fagone and Jackowski, 2009).

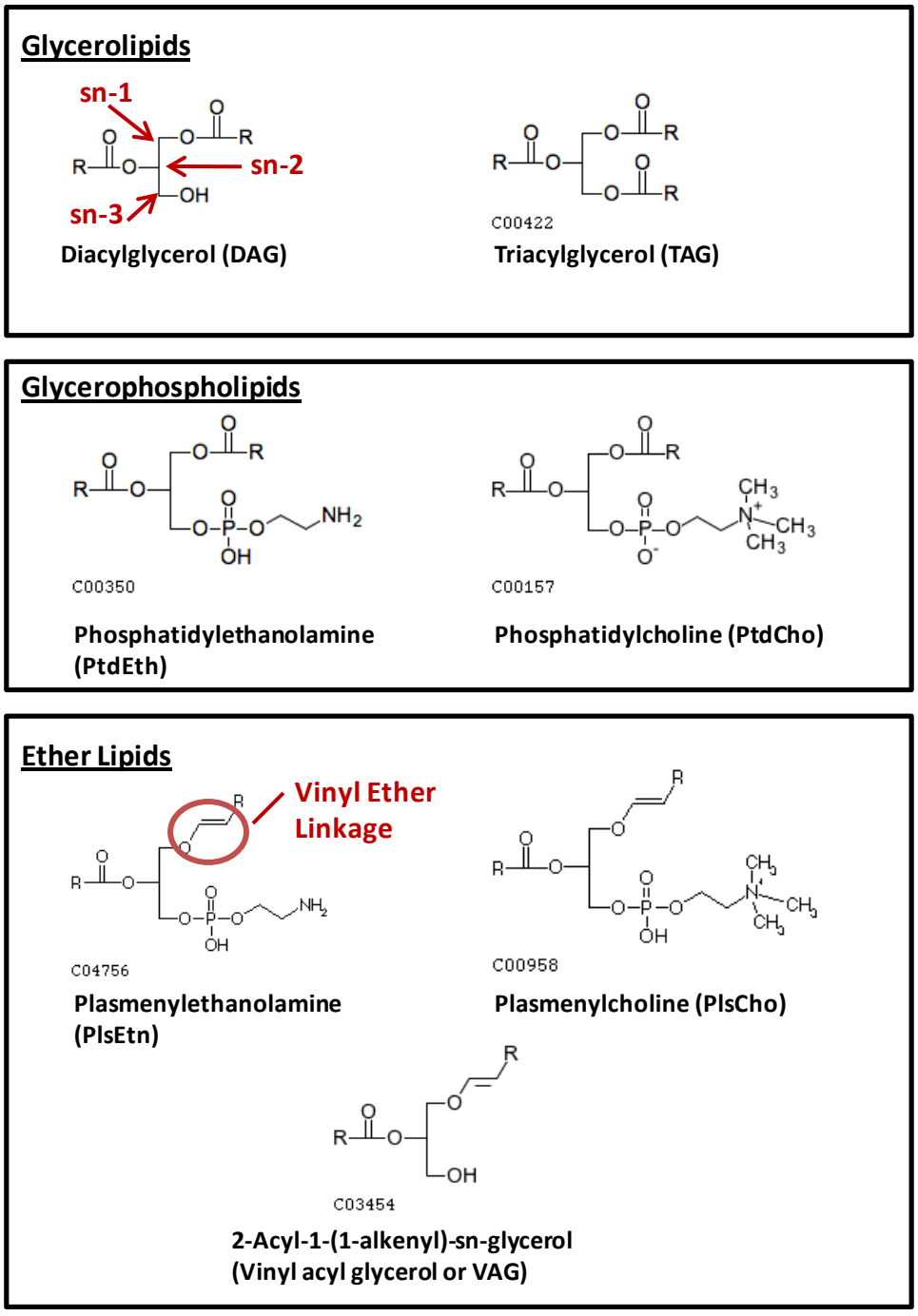

Figure 2.5 The structures of glycerolipids, glycerophospholipids and ether lipids. The 'R' in the structures represents a fatty acid side chain. The carbon atoms of the glycerol backbone in lipids are labelled as sn-1, sn-2 and sn-3. The polar head groups of phospholipids are located at sn-3 position of the glycerol backbone and the vinyl-ether bond in ether lipids is located at sn-1. Structures of these lipids were obtained from the Kyoto Encyclopedia of Genes and Genomes (KEGG) (*www.genome.jp/kegg).*

Glycerophospholipids are amphipathic lipids, consisting of two hydrophobic, non-polar, hydrocarbon chains and a hydrophilic phosphorylated polar head group (Fagone and Jackowski, 2009). When exposed to water the glycerophospholipids can arrange into a lipid bilayer with the hydrophobic tails pointing towards the center of the bilayer and the polar head group facing out, creating a membrane (van Meer *et al.*, 2008). Cellular membranes are required for segregation and protection from the environment, cell-cell interactions, compartmentalization, storage, protein synthesis and secretion, phagocytosis and movement (Fagone and Jackowski, 2009). The synthesis of PtdCho and PtdEtn requires the activation of choline, or ethanolamine, to CDP-choline and CDP-ethanolamine before the attachment of the head group to the diacylglycerol (Bell and Coleman, 1980). The addition of the choline head group to diacylglycerol, to yield PtdCho, is facilitated by diacylglycerol cholinephosphotransferase, and ethanolaminephosphotransferase facilitates the addition of the ethanolamine head group to form PtdEtn (Bell and Coleman, 1980).

PtdCho is synthesized in the endoplasmic reticulum (ER) and the Golgi apparatus, and PtdEtn is synthesized in the ER (van Meer *et al.*, 2008). Another important class of lipids are the ether-phospholipids, a special type of phospholipid characterized by the presence of ether linkage at the sn-1 position of the glycerol backbone, as compared to the ester bond present at the sn-1 position in diacylglycerophospholipids (Brites *et al.*, 2004). Two main types of ether bonds exist in nature: the ether bond found in platelet activating factor (PAF), and the vinyl-ether bond that is found in plasmalogens (Brites *et al.*, 2004). Plasmalogens represent one in every five lipids in the human body (Nagan and Zoeller, 2001).

Plasmalogens are not only structural components in the membrane, but they also play many other key roles in the cell. Plasmalogens affect membrane dynamics, such as fusion and ion transport, they are also reservoirs for polyunsaturated fatty acids, and they are involved in intracellular signalling and may serve in a protective role during periods of oxidative stress (Farooqui and Horrocks, 2001; Nagan and Zoeller, 2001). The vinyl-ether bond that is present in plasmalogens contains a *cis* double bond, adjacent to the ether bond, on the alkyl chain at the sn-1 position of the lipid (Nagan and Zoeller, 2001). The first step in the biosynthesis of plasmalogens requires dihydroxyacetone phosphate acyltransferase (DHAP-AT), which carries out the esterification of the free hydroxyl group of dihydroxyacetone phosphate (DHAP) with a long-chain acyl-CoA ester (Figure 2.6) (Brites *et al.*, 2004). The second step in the

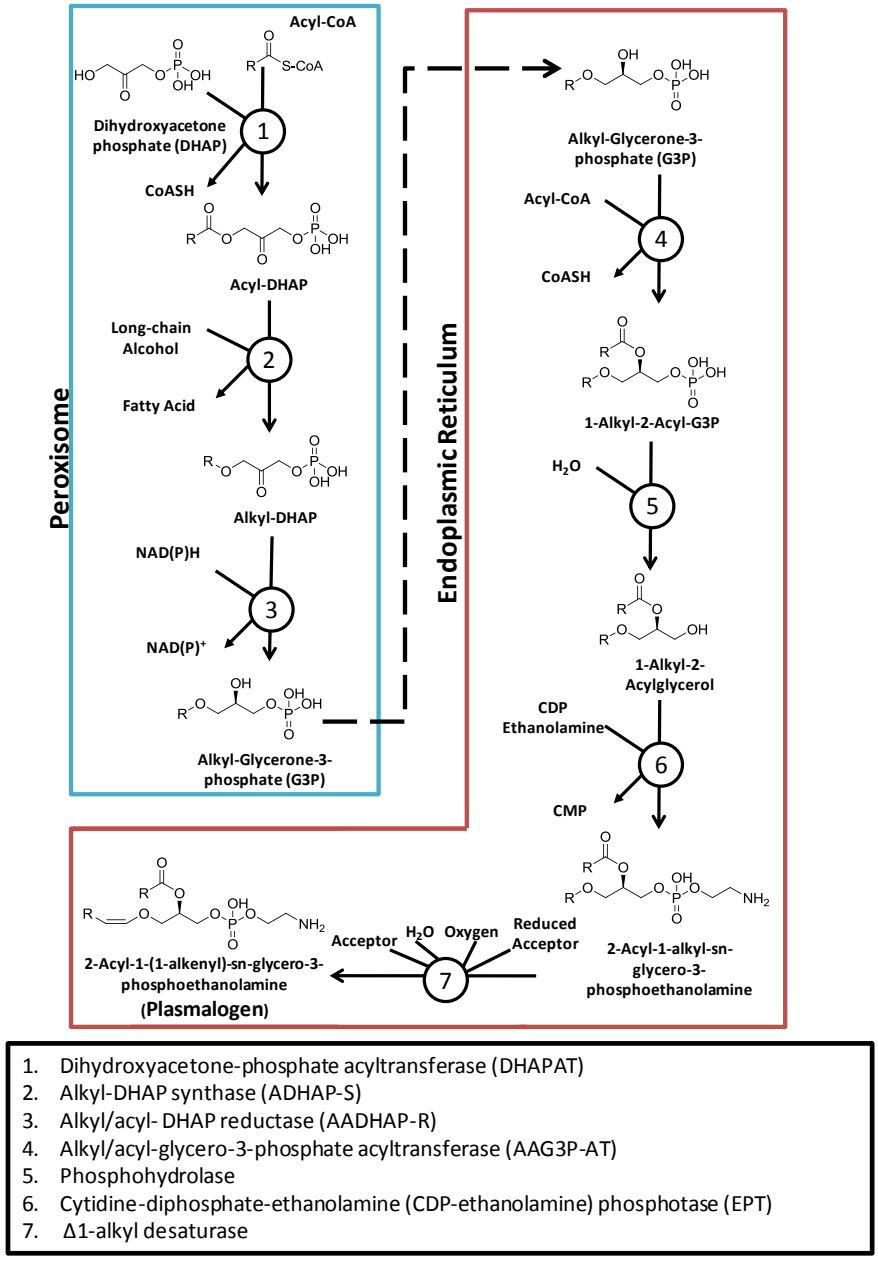

1. Dihydroxyacetone-phosphate acyltransferase (DHAPAT)
2. Alkyl-DHAP synthase (ADHAP-S)
3. Alkyl/acyl- DHAP reductase (AADHAP-R)
4. Alkyl/acyl-glycero-3-phosphate acyltransferase (AAG3P-AT)
5. Phosphohydrolase
6. Cytidine-diphosphate-ethanolamine (CDP-ethanolamine) phosphotase (EPT)
7. Δ1-alkyl desaturase

Figure 2.6 Ether lipid synthesis.
Ether lipid synthesis begins in the peroxisome with the esterification of DHAP by DHAPAT. The second step of the pathway is the addition of the ether bond at sn-1, which is catalyzed by ADHAP-S. The third reaction is the reduction of the ketone group at sn-2, producing alkyl-glycerone-3-phosphate (1-alkyl-G3P). 1-alkyl-G3P is then transported to the endoplasmic reticulum where it is acylated by AAG3P-AT in the fourth reaction. The fifth reaction is the removal of the phosphate group by a phosphohydrolase, producing 1-alkyl-2-acyl-sn-glycerol. The sixth reaction involves the addition of the ethanolamine head group by EPT, resulting in the synthesis of alkylacyl-GPE. The final step of the pathway is the desaturation of alkylacyl-GPE, which results in the synthesis of an ethanolamine plasmalogen. Adapted from http://www.peroxisomedb.org

plasmalogen synthesis pathway creates the ether bond at the sn-1 position. The reaction is catalyzed by alkyl-dihydroxyacetone phosphate synthase (ADHAP-S), and results in the replacement of the fatty acid at sn-1 with a long-chain fatty alcohol (Nagan and Zoeller, 2001; Brites *et al.*, 2004). These first two reactions in the synthesis of plasmalogens take place exclusively in the peroxisomes of the cell (Nagan and Zoeller, 2001). Acyl/alkyl-dihydroxyacetone phosphate reductase (AADHAP-R) catalyses the third reaction, which is the reduction of the ketone group at the sn-2 position of 1-alkyl-DHAP resulting in the formation of 1-alkyl-sn-glycero-3-phosphate (1-alkyl-G3P) (Brites *et al.*, 2004). Researchers have discovered that AADHAP-R is utilized in both the ether-lipid and diacyl-phospholipid pathways, and is therefore located in the peroxisome as well in the ER (Nagan and Zoeller, 2001). The fourth reaction involves the acylation of 1-alkyl-G3P by alkyl/acyl-glycero-3-phosphate acyltransferase (AAG3P-AT), resulting in 1-alkyl-2-acyl-glycero-3-phosphate (Brites *et al*., 2004). When the phosphate group is removed from 1-alkyl-2-acyl-G3P by phosphohydrolase, 1-alkyl-2-acyl-sn-glycerol is formed (Brites *et al.*, 2004). At this point cytidine-diphosphate-ethanolamine (CDP-ethanolamine) phosphotransferase (EPT) catalyzes the attachment of the phosphoethanolamine head group to the lipid, resulting in 1-alkyl-2-acyl-sn-glycero-3-phosphoethanolamine (alkylacyl-GPE) (Nagan and Zoeller, 2001). The final step in the synthesis of an ethanolamine plasmalogen is the desaturation carried out by a cytochrome b5-dependent microsomal electron transport system and a Δ1-alkyl desaturase, resulting in 1-alk-1-enyl-2-acyl-GPE (PE-plasmalogen) (Brites *et al.*, 2004). The choline plasmalogens (1-alk-1-enyl-2-acyl-GPC) are typically formed from PE-plasmalogens with a polar-head group modification executed by a transferase. Another type of ether lipid that can be synthesized in this pathway is 2-acyl-1(1-alkenyl)-sn-glycerol, a diacyl-ether lipid. This type of ether lipid results from either the action of phospholipase C on ethanolamine plasmalogens or the phosphate removal from plasmenic acid by a hydrolase enzyme (Brites *et al.*, 2004).

Ether lipids, including plasmalogens, are probably one of the least known classes of lipids, likely due to the difficult process required to isolate them from cells (Nagan and Zoeller, 2001). A couple of decades ago many scientists would likely not have been familiar with ether lipids. However, there has been a renewed interest in these lipids, likely inspired by the implication of plasmalogen deficiencies in various degenerative diseases, such as Zellweger's Syndrome (Schutgens *et al.*, 1985), and Alzheimer's disease (Goodenowe *et al.*, 2007). With

the progress and ingenuity of scientific research today, in combination with the advancements made in technology, the isolation and analysis of these lipids is achievable and their importance in mammalian cells and systems has become more evident.

The objective of this thesis was to investigate phenotypic changes in key cellular processes that are fundamental to cancer development and progression, using FTICR-MS, and to generate a data-driven hypothesis regarding how the metabolome of the cell is altered during the processes studied.

The specific objectives were to characterize metabolic changes associated with:

a) Cell-cycle progression;
b) Differentiation;
c) Oncogenic transformation.

3 MATERIALS AND METHODS

3.1 Materials

3.1.1 Cell Lines

CNA14 cells are derived from a parental rat fibroblast cell line, Rat2, and contain a temperature-sensitive mutation of the oncogene p130gag-fps. P130gag-fps is the product of the Fujinami sarcoma virus (FSV) (Park and Seo, 1995). The parental Rat2 cell line was transfected with wild type FSV cDNA producing the NW16 cell line, and with the AX9m mutant FSV (which contains an insertion N-terminal to the kinase domain) which produced the NA9 line (Sadowski *et al.*, 1986). It was determined that the AX9m mutant cDNA could not transform the Rat2 cells; however, once the AX9m mutant gene was introduced into chicken cells, transformation occurred in a temperature-dependent manner (Sadowski *et al.*, 1986). These results suggested that the chicken cells possess a cellular factor which allows the mutant FSV protein to transform the cells. It was then discovered that transfection of the NA9 line with DNA from chicken cells gave rise to the CNA14 line, which was transformed at 34ºC but not at 39ºC. CNA14 cells have a normal phenotype at 39ºC but are tumourigenic at 34ºC, due to the apparent incompatibility between a temperature-sensitive version of the oncogene p130gag-fps of FSV(functional at 34ºC, but not at 39ºC) and wild type p53 (expressed at 39ºC, but not at 34ºC) (Sadowski *et al.*, 1986). This model system allows comparisons to be made between normal and cancer cells with not only essentially 'isogenic' cells, but also with a well characterized oncogene.

Two cell lines were used as controls; Rat2 and NW16 cells. The Rat2 cell line is the parental rat fibroblast cell line from which the CNA14 cells were derived, and the NW16 cells are a fibroblast cell line that constitutively expresses the wild type form of oncogene p130gag-fps. A mouse embryo cell line (10T1/2) was also used as a control cell line in the temperature shift experiments. The CNA14, NW16 and Rat2 cells were supplied by Dr. Lambert Loh (University of Saskatchewan), and the 10T1/2 cells were purchased from ATCC (CCL-226,

Manassas, VA, USA). Human promyelomonocytic leukemic U937 cells were used as a model system for the differentiation of monocytes into macrophages. These cells were derived by Sundstrom and Nilsson in 1974 from malignant cells obtained from the pleural effusion of a patient with histiocytic lymphoma (Sundstrom, 1976). The treatment of U937 cells with phorbol 12-myristate 13-acetate (PMA) induces them to undergo monocytic differentiation. These cells were obtained from ATCC (CRL-1593.2; Manassas, VA, USA).

MRC5 cells, low-passage human lung fibroblasts (Jacobs *et al.*, 1970), were used for the metabolomic analysis of cell cycle progression. When human cells, such as MRC5 cells, are grown in media containing low serum levels (0.1%) for 48 hours the cells arrest in the G0 phase of the cell cycle (Schorl and Sedivy, 2007). After the starvation period the low serum media is replaced with media containing normal serum levels (10%) and the cells re-enter the cell cycle where they complete one complete growth cycle as a synchronous population (Schorl and Sedivy, 2007). MRC5 cells were obtained from ATCC (CCL-171; Manassas, VA, USA).

3.1.2 Reagents and Supplies

All chemicals, media and enzymes used were of analytical grade or higher, and were purchased from Sigma, Invitrogen or VWR unless otherwise stated. RNA purification kits and Atlas Plastic Rat 4K microarray were purchased from BD Biosciences Clontech.

3.2 Methods

3.2.1 Tissue Culture Media and Techniques

3.2.1.1 Cell Culture

CNA14, Rat2, NW16, 10T1/2 and MRC5 cells were cultured in HyQ Dulbecco's modified Eagles medium (DMEM)/ High Glucose media, supplemented with 10% Fetalclone II serum (HyClone Laboratories, Logan, Utah, U.S.A), 100 U/mL penicillin and 100 µg/mL streptomycin (Gibco). U937 cells were cultured in HyQ RPMI-1640 media, supplemented with 10% Fetalclone II serum or Bovine Calf Serum (HyClone Laboratories, Logan, Utah, USA), 100 U/mL penicillin and 100 µg/mL streptomycin (Gibco), 4.5 g/L of glucose and 10 mM Hepes. Cultures of U937 and MRC5 were maintained at 37˚C with 5% CO_2 and 100%

relative humidity. CNA14, Rat2, NW16 and 10T1/2 cells were grown at 37˚C, 34˚C and 39˚C with 5% CO_2 and 100% relative humidity.

To harvest adherent cells, the existing media was removed and cells were covered in a Dulbecco's Phosphate buffered saline (DPBS) solution containing 0.25% (w/v) trypsin-EDTA ($4Na^+$) (Gibco) for 5 minutes, or until the cells began to lift off the plate. To block the proteolytic action of the trypsin-EDTA, an excess of media containing serum was added. The cells were resuspended and transferred to a 15 mL conical centrifuge tube for pelleting by centrifugation at 450 X g for 5 minutes. Cell pellets were re-suspended in complete media and an aliquot of the cells was seeded into a new plate containing complete media.

Cells used for mass spectrometry or microarray analysis were harvested as described above. However, after the removal of the media, cells were rinsed three times with 5 mL of DPBS and on the final centrifugation the cells were spun at 500 X g for five minutes. The DPBS was removed and the pellets were stored at -80°C until extraction could be completed.

The storage of cells for later use were generated as follows: cells in 150 x 25 mm plates of approximately 80% confluence (log-phase growth) were harvested, as described above, and resuspended in 5 mL complete media with 10% (v/v) dimethyl sulfoxide (DMSO). Approximately 1.5 mL of cell suspension (10^6 cells/mL) was added to 1.8 mL Cryotube™ vials (NUNC Brand Products), and the tubes were immediately placed at –80°C, and if required, transferred to liquid nitrogen for long-term storage.

3.2.1.2 Temperature Shift Experiments

The CNA14 cells were initially grown at 34˚C and 39˚C on 25 cm^2 plates until they reached 50-60% confluence. They were then shifted to the alternative temperatures (i.e. 34˚C to 39˚C and 39˚C to 34˚C), and samples were then collected at 0, 8, 16, 24, 48, 72 and 96 hours for analysis. Along with the CNA14 cells, Rat2, 10T1/2 and NW16 cells were also cultured and grown at 34˚C, 39˚C and 37˚C to ensure that any metabolic changes observed were due to the oncogene expression and not merely due to the different growth conditions. All harvested cells were extracted (protocol explained below) and analyzed by FTICR-MS.

3.2.1.3 Differentiation Experiment

The treatment of U937 cells with phorbol 12-myristate 13-acetate (PMA) induces them to undergo monocytic differentiation (Harris and Ralph, 1985). The cells were seeded at a density of 20 x 10^6/ 30 mL 16 hours before PMA treatment. A PMA stock was prepared by dissolving 1mg PMA in 1 mL DMSO (Sigma Aldrich, Oakville, ON). The cells were treated with PMA (10 ng/mL) for 0, 1, 3, 6, 12, 24, 48, 72 and 96 hours. Differentiated cells that had attached to the plate surface were detached from the plates with Trypsin/EDTA, they were then rinsed with PBS and immediately frozen at -80°C until extraction. Untreated U937 cells (monocytes that grow in suspension) were also grown and harvested for use as a control.

3.2.1.4 Cell Cycle Experiment

Serum starvation was used in order to synchronize the cell populations for cell cycle analyses on the FTICR-MS. MRC5 cells were grown to about 60% confluence in 150 cm Petri dishes. The cells were then washed three times with HyQ Dulbecco's modified Eagle's medium (DMEM)/ High Glucose media (without serum), and then low serum media (0.1% foetal calf serum) was added to the plates. The cells were incubated in the low serum media for a period of 48 hours, after which time the media was replaced with normal serum media (10%). Cells were harvested at 0, 30 min, 2 hours, 6 hours, 12 hours, 24 hours and 48 hours. Cells that were not serum starved, and will be referred to as -48 hour timepoint, were also harvested. Cell counts were completed using trypan blue stain and a haemocytometer to ensure that the same number of cells was harvested at each of the time points. The cells were analyzed by flow cytometry, to determine the stage of the cell cycle the cells were in at each time point, and FTICR-MS to identify global metabolic changes that occur during the cell cycle (see method below).

3.2.1.5 1,2,3-Benzene Tricarboxylic Acid (BTA) Treatment

1,2,3-Benzentricarboxylic acid (BTA) is used to inhibit the export of citrate out of the mitochondria, which in turn inhibits the *de novo* synthesis of lipids (Kajimoto *et al.*, 2005). BTA was dissolved in ethanol to make a 0.5 M stock solution (Sigma Aldrich, Oakville, ON). U937 cells were treated with the BTA (5 mM) for three hours prior to the addition of PMA in

order to inhibit fatty acid synthesis prior to the initiation of differentiation. After the 3 hours of pre-treatment with the BTA the PMA was added to the cells for 24 and 48 hours. Some of the cells that were treated with both BTA and PMA for 24 hours were re-plated in fresh media after being rinsed with PBS, and left to grow for 24 and 48 hours after the re-plating. The cells were counted before harvesting to ensure that 6 million cells were harvested from of each plate for metabolomics analysis. The re-plated samples only had 2 million cells total to harvest, so metabolomics data has been adjusted three fold to account for the cell number difference.

3.2.2 Fourier Transform Ion Cyclotron Resonance Mass Spectrometry (FTICR-MS)

3.2.2.1 Metabolite Extraction

Cell pellets were initially extracted with 0.5 mL of 1% ammonium hydroxide and 4 x 2.5 mL of ethyl acetate. Samples were sonicated for 20 seconds, then centrifuged at 4˚C for 10 minutes at 1000 X g. An additional 1.5 mL of 1% formic acid was added to each sample and the aqueous fraction was transferred to a new tube. A portion (5 mL) of the ethyl acetate fraction was removed and evaporated to dryness, then reconstituted in 1mL of butanol. All fractions were stored at -80˚C until needed for analysis.

The extracted sample fractions were diluted prior to analysis using methanol: 0.1% (v/v) ammonium hydroxide (50: 50, v/v) for the negative ionization modes and methanol: 0.1% (v/v) formic acid (50: 50, v/v) for the positive ionization modes. An internal standard mixture, which included; serine, tetra-alanine, reserpine, Hewlett-Packard tuning mix and the adrenocorticotrophic hormone fragment 4-10, was also added to each sample for the internal calibration of each sample spectrum (Aharoni *et al.*, 2002).

3.2.2.2 Sample Analysis

The mass spectrometry analyses were performed on a Bruker Daltonics APEX III Fourier Transform Ion Cyclotron Resonance Mass Spectrometer that contains a 7.0 Tesla actively shielded superconducting magnet (Bruker Daltonics, Billerica, MA). The organic and aqueous sample fractions were directly injected into an electrospray ionization (ESI) or atmospheric pressure chemical ionization (APCI) source in both positive and negative ionization modes (Gray, 2005). Table 3.1 lists each of the analyses that were completed on the

Table 3.1 The different types of analyses completed on the FTICR-MS.
Phenomenome Discoveries completes six analyses on each sample to ensure that as many metabolites are detected as possible. Organic and aqueous extracts are collected from the sample. Using an electrospray ionization source (ESI), both the organic and aqueous extracts are analyzed using positive and negative ionization. The atmospheric pressure chemical ionization source (APCI) is used to analyze an organic extract of the sample, and both positive and negative ionization are applied.

Ionization	Source	Extract
Positive	ESI	Aqueous
Negative	ESI	Aqueous
Positive	ESI	Organic (butanol)
Negative	ESI	Organic (butanol)
Positive	APCI	Organic (Ethyl Acetate)
Negative	APCI	Organic (Ethyl Acetate)

FTICR-MS. The instrument conditions were tuned and optimized for ion intensity and broadband accumulation for a mass range between 100-1,000 accurate mass units (amu) (Aharoni *et al.*, 2002).

3.2.2.3 XMASS Peak Picking

XMASS software (Bruker Daltonics) was used to acquire 1 megaword data files, which were then zero-filled to 2 megawords, and transformed prior to Fourier transformation and magnitude calculations (Aharoni *et al.*, 2002; Gray, 2005). The result is a complex mass spectrum of highly resolved mass-to-charge ratios. The spectra from each of the samples was then put through a combination of automated and manual peak picking processes, selecting only sample specific compounds in the range of 100-2000 m/z. Once all of the modes had been analyzed, the files were merged and converted into a form that could be viewed using Phenomenome Discoveries DISCOVAmetrics^{TM} bioinformatics software. The software creates an array that allows multiple samples to be easily compared and mined for both known and novel metabolites.

3.2.2.4 DISCOVAmetrics^{TM} Data Mining and Statistics

DISCOVAmetrics^{TM} software was used to generate two-dimensional (mass vs. sample intensity) arrays and for statistical analyses of the datasets. Each row in the array contains the data for a unique mass, and each column is for an individual sample. Unsupervised statistical techniques were used in order to identify significant metabolic changes between each of the samples, these approaches included; hierarchical clustering and principal component analysis (PCA). These statistical strategies allow groups of similarly expressed metabolites to be identified and the visualization of the samples with similar, or dramatically different, metabolic profiles. An explanation of these approaches can be found in the literature review of this thesis. Hierarchical cluster analyses (HCA) and principal component analyses (PCA) were completed on the complete data sets in order to visualize them as a whole, and to determine if any masses were specific to specific samples or treatments. The data was then analyzed with a two-tailed Student's *t*-test to identify the metabolites with the most significant intensity changes between samples, and those with a $p<0.05$ were deemed statistically significant. Both HCA and PCA were completed on the data with $p<0.05$ (in some cases more stringent cut–offs

were used). Each dataset was also normalized to the control samples in order to determine metabolic changes that were due to treatment or growth condition. Student's *t*-tests were also used to filter out the significant changes between specific samples.

Once the key masses had been identified through the different statistical analyses, a putative molecular formula and corresponding metabolite name were assigned to each of the masses.

3.2.3 Multiple Reaction Monitoring (MRM) Triple Quadrupole Method

All of the MRM triple quadrupole analyses were performed according to previously published methods (Goodenowe *et al.*, 2007; Pastural *et al.*, 2009). The high-throughput screening of the lipids of interest was performed with a linear ion-trap mass spectrometer (4000 Q Trap: Applied Biosystems) coupled with the Agilent 1100 LC system. The sample was prepared by adding 15 µL of internal standard (5 µg/mL of [24-^{13}C]-cholic acid (Cambridge Isotopes Laboratories, Andover, MA) in methanol) to 120 µL of the ethyl acetate fraction of each of the samples. 100 µL of the sample was injected by flow injection analysis, and monitored under negative atmospheric pressure chemical ionization (APCI) mode. The method was based on multiple reaction monitoring of one parent/fragment for each metabolite of interest and (24-^{13}C)-cholic acid. Each transition was scanned for 70 ms. The mobile phase was made up of 10% ethyl acetate in methanol at a flow rate of 360 µL/min. The source parameters were set as follows: curtain gas (CUR): 10.0, collision-activated dissociation gas (CAD): 8, nebulizing current (NC): -4.0, temperature: 400, ion source gas 1: 30, ion source gas 2: 50, interface heater: on. The compound parameters were set as follows: declustering potential: -120, entrance potential: -10, NC: -4.0, collision energy (CE): -40, collision cell exit potential (CXP): -15. The transitions that were used in these analyse are listed in Table 3.2. Standard curves were generated for all of the analytes to verify instrument linearity by serial dilution of a healthy normal serum extract, or a cell pellet extract, with a constant concentration of (24- ^{13}C)-cholic acid. All samples were analyzed in a randomized blinded manner and were bracketed by known standard dilutions. All standard curves had R^2 values more than 0.98.

Table 3.2(a-d). Molecular formulae and MS/MS transitions for lipids analysed with the high-throughput Multiple Reaction Monitoring (MRM) Triple Quadrupole Method.
a. Phosphatidylethanolamines (PtdEtn) and Ethanolamine Plasmalogens (PlsEtn), **b.** Phosphatidylcholine (PtdCho) and Choline Plasmalogens (PlsCho), **c.** Diacylglycerols (DAGs) and Triacylglycerols (TAGs) and **d.** Vinyl acylglycerols (VAGs) (b, c and d on following pages).

a. Phosphatidylethanolamines and ethanolamine plasmalogens

Metabolite Name	Molecular Formula	Parent Mass	M-H Mass	Diagnostic Fragment Mass	MS/MS Transition
PtdEtn 16:0/18:0	C39H78N1O8P1	719.54648	718.5	R1 (C16H31O2) - 255	718.5 / 255.2
PtdEtn 16:0/18:1	C39H76N1O8P1	717.53083	716.5	R1 (C16H31O2) - 255	716.5 / 255.2
PtdEtn 16:0/18:2	C39H74N1O8P1	715.51518	714.5	R1 (C16H31O2) - 255	714.5 / 255.2
PtdEtn 16:0/18:3	C39H72N1O8P1	713.49953	712.5	R1 (C16H31O2) - 255	712.5 / 255.2
PtdEtn 16:0/20:4	C41H74N1O8P1	739.51518	738.5	R1 (C16H31O2) - 255	738.5 / 255.2
PtdEtn 16:0/22:6	C43H74N1O8P1	763.51518	762.5	R1 (C16H31O2) - 255	762.5 / 255.2
PtdEtn 18:0/18:1	C41H80N1O8P1	745.56213	744.5	R1 (C18H35O2) - 283	744.5 / 283.2
PtdEtn 18:0/18:2	C41H78N1O8P1	743.54648	742.5	R1 (C18H35O2) - 283	742.5 / 283.2
PtdEtn 18:0/18:3	C41H76N1O8P1	741.53083	740.5	R1 (C18H35O2) - 283	740.5 / 283.2
PtdEtn 18:0/20:4	C43H78N1O8P1	767.54648	766.5	R1 (C18H35O2) - 283	766.5 / 283.2
PtdEtn 18:0/22:6	C45H78N1O8P1	791.54648	790.5	R1 (C18H35O2) - 283	790.5 / 283.2
PlsEtn 16:0/18:1	C39H76N1O7P1	701.53591	700.5	R2 (C18H33O2) - 281	700.5 / 281.2
PlsEtn 16:0/18:2	C39H74N1O7P1	699.52026	698.5	R2 (C18H31O2) - 279	698.5 / 279.2
PlsEtn 16:0/18:3	C39H72N1O7P1	697.50461	696.5	R2 (C18H29O2) - 277	696.5 / 277.2
PlsEtn 16:0/20:4	C41H74N1O7P1	723.52026	722.5	R2 (C20H31O2) - 303	722.5 / 303.2
PlsEtn 16:0/22:6	C43H74N1O7P1	747.52026	746.5	R2 (C22H31O2) - 327	746.5 / 327.2
PlsEtn 18:0/18:1	C41H80N1O7P1	729.56721	728.5	R2 (C18H33O2) - 281	728.5 / 281.2
PlsEtn 18:0/18:2	C41H78N1O7P1	727.55156	726.5	R2 (C18H31O2) - 279	726.5 / 279.2
PlsEtn 18:0/18:3	C41H76N1O7P1	725.53591	724.5	R2 (C18H29O2) - 277	724.5 / 277.2
PlsEtn 18:0/20:4	C43H78N1O7P1	751.55156	750.5	R2 (C20H31O2) - 303	750.6 / 303.2
PlsEtn 18:0/22:6	C45H78N1O7P1	775.55156	774.5	R2 (C22H31O2) - 327	774.5 / 327.2
PtdEtn 18:1/18:1	C41H78N1O8P1	743.54651	742.5	R1 (C18H33O2) - 281.2	742.5 / 281.2
PtdEtn 18:1/18:2	C41H76N1O8P1	741.53086	740.5	R1 (C18H33O2) - 281.2	740.5 / 281.2
PtdEtn 18:1/18:3	C41H74N1O8P1	739.51521	738.5	R1 (C18H33O2) - 281.2	738.5 / 281.2
PtdEtn 18:1/20:4	C43H76N1O8P1	765.53086	764.5	R1 (C18H33O2) - 281.2	764.5 / 281.2
PtdEtn 18:1/22:6	C45H76N1O8P1	789.53086	788.5	R1 (C18H33O2) - 281.2	788.5 / 281.2
PlsEtn 18:1/18:1	C41H78N1O7P1	727.55159	726.5	R2 (C18H33O2) - 281	726.5 / 281.2
PlsEtn 18:1/18:2	C41H76N1O7P1	725.53594	724.5	R2 (C18H31O2) - 279	724.5 / 279.2
PlsEtn 18:1/18:3	C41H74N1O7P1	723.52029	722.5	R2 (C18H29O2) - 277	722.5 / 277.2
PlsEtn 18:1/20:4	C43H76N1O7P1	749.53594	748.5	R2 (C20H31O2) - 303	748.5 / 303.2
PlsEtn 18:1/22:6	C45H76N1O7P1	773.53594	772.5	R2 (C22H31O2) - 327	772.5 / 327.2
Free 22:6	C22H32O2	328.24022	327.2	283	327.2 / 283.2
Free 20:4	C20H32O2	304.24022	303.2	259	303.2 / 259.2

b. Phosphatidylcholines and choline plasmalogens

Metabolite Name	Molecular Formula	Parent Mass	M+H Mass	Diagnostic Fragment Mass	Transition
PtdCh 16:0/18:0	C42H84NO8P	761.5935	762.6	R1 (C16H31O2) - 255.2	762.6 / 184.2
PtdCho 16:0/18:1	C42H82N1O8P1	759.5778	760.6	R1 (C16H31O2) - 255	760.6 / 184.2
PtdCho 16:0/18:2	C42H80N1O8P1	757.5621	758.6	R1 (C16H31O2) - 255	758.6 / 184.2
PtdCho 16:0/18:3	C42H78N1O8P1	755.5464	756.5	R1 (C16H31O2) - 255	756.5 / 184.2
PtdCho 16:0/20:4	C44H80N1O8P1	781.5600	782.6	R1 (C16H31O2) - 255	782.6 / 184.2
PtdCho 16:0/22:6	C46H80N1O8P1	805.5622	806.6	R1 (C16H31O2) - 255	806.6 / 184.2
PtdCho 18:0/18:1	C44H86N1O8P1	787.6090	788.6	R1 (C16H31O2) - 255	788.6 / 184.2
PtdCho 18:0/18:2	C44H84N1O8P1	785.5900	786.6	R1 (C16H31O2) - 255	786.6 / 184.2
PtdCho 18:0/18:3	C44H82N1O8P1	783.5778	784.6	R1 (C16H31O2) - 255	784.6 / 184.2
PtdCho 18:0/20:4	C46H84N1O8P1	809.5930	810.6	R1 (C16H31O2) - 255	810.6 / 184.2
PtdCho 18:0/22:6	C48H84N1O8P1	833.5930	834.6	R1 (C16H31O2) - 255	834.6 / 184.2
PlsCho 16:0/18:1	C42H84N1O7P1	745.5985	746.6	R2 (C18H33O2) - 281	746.6 / 184.2
PlsCho 16:0/18:2	C42H82N1O7P1	743.5829	744.6	R2 (C18H31O2) - 279	744.6 / 184.2
PlsCho 16:0/18:3	C42H80N1O7P1	741.5672	742.6	R2 (C18H29O2) - 277	742.6 / 184.2
PlsCho 16:0/20:4	C44H82N1O7P1	767.5829	768.6	R2 (C20H31O2) - 303	768.6 / 184.2
PlsCho 16:0/22:6	C46H82N1O7P1	791.5829	792.6	R2 (C22H31O2) - 327	792.6 / 184.2
PlsCho 18:0/18:1	C44H88N1O7P1	773.6298	774.6	R2 (C18H33O2) - 281	774.6 / 184.2
PlsCho 18:0/18:2	C44H86N1O7P1	771.6141	772.6	R2 (C18H31O2) - 279	772.6 / 184.2
PlsCho 18:0/18:3	C44H84N1O7P1	769.5985	770.6	R2 (C18H29O2) - 277	770.6 / 184.2
PlsCho 18:0/20:4	C46H86N1O7P1	795.6142	796.6	R2 (C20H31O2) - 303	796.6 / 184.2
PlsCho 18:0/22:6	C48H86N1O7P1	819.6142	820.6	R2 (C22H31O2) - 327	820.6 / 184.2
PtdCho 18:1/18:1	C44H84N1O8P1	785.5934	786.6	R1 (C16H31O2) - 255	786.6 / 184.2
PtdCho 18:1/18:2	C44H82N1O8P1	783.5778	784.6	R1 (C16H31O2) - 255	784.6 / 184.2
PtdCho 18:1/18:3	C44H80N1O8P1	781.5621	782.6	R1 (C16H31O2) - 255	782.6 / 184.2
PtdCho 18:1/20:4	C46H82N1O8P1	807.5770	808.6	R1 (C16H31O2) - 255	808.6 / 184.2
PtdCho 18:1/22:6	C48H82N1O8P1	831.5778	832.6	R1 (C16H31O2) - 255	832.6 / 184.2
PlsCho 18:1/18:1	C44H86N1O7P1	771.6142	772.6	R2 (C18H33O2) - 281	772.6 / 184.2
PlsCho 18:1/18:2	C44H84N1O7P1	769.5985	770.6	R2 (C18H31O2) - 279	770.6 / 184.2
PlsCho 18:1/18:3	C44H82N1O7P1	767.5828	768.6	R2 (C18H29O2) - 277	768.6 / 184.2
PlsCho 18:1/20:4	C46H84N1O7P1	793.5985	794.6	R2 (C20H31O2) - 303	794.6 / 184.2
PlsCho 18:1/22:6	C48H84N1O7P1	817.5985	818.6	R2 (C22H31O2) - 327	818.6 / 184.2

c. Diacylglycerols and triacylglycerols

Metabolite Name	Molecular Formula	Parent Mass	M+H Mass	Diagnostic Fragment Mass (Intensity %)		MS/MS Transition
				R1	R2	
TAG 16:0/14:0	$C_{53}H_{96}O_6$	828.7561	829.8	(C16H31O) - 239.2 (10%)	(C14H27O) - 211.2 (8%)	829.8 / 239.2
TAG 16:0/14:0	$C_{53}H_{96}O_6$	828.7561	829.8	(C16H31O) - 239.2 (10%)	(C14H27O) - 211.2 (8%)	829.8 / 211.2
TAG 16:0/18:1	$C_{53}H_{98}O_6$	830.7876	831.8	(C16H31O) - 239.2 (22%)	(C18H33O) - 265.2 (27.8%)	831.8 / 239.2
TAG 16:0/18:1	$C_{53}H_{98}O_6$	830.7876	831.8	(C16H31O) - 239.2 (22%)	(C18H33O) - 265.2 (27.8%)	831.8 / 265.2
TAG 16:1/18:1	$C_{53}H_{100}O_6$	832.8206	833.8	(C16H29O) - 237.2 (50%)	(C18H33O) - 265.2 (50%)	833.8 / 237.2
TAG 16:1/18:1	$C_{53}H_{100}O_6$	832.8206	833.8	(C16H29O) - 237.2 (50%)	(C18H33O) - 265.2 (50%)	833.8 / 265.2
TAG 16:0/18:2	$C_{55}H_{100}O_6$	856.7900	857.8	(C16H31O) - 239.2 (5.5%)	(C18H31O) - 263.2 (4%)	857.8 / 239.2
TAG 16:0/18:2	$C_{55}H_{100}O_6$	856.7900	857.8	(C16H31O) - 239.2 (5.5%)	(C18H31O) - 263.2 (4%)	857.8 / 263.2
TAG 16:0/18:1	$C_{55}H_{102}O_6$	858.8197	859.8	(C16H31O) - 239.2 (5%)	(C18H33O) - 265.2 (5%)	859.8 / 239.2
TAG 16:0/18:1	$C_{55}H_{102}O_6$	858.8197	859.8	(C16H31O) - 239.2 (5%)	(C18H33O) - 265.2 (5%)	859.8 / 265.2
DAG 18:0/18:1	$C_{39}H_{74}O_5$	622.5536	623.5	(C18H35O) - 267.2	R2 (C18H33O) - 265.2	623.5 / 267.2
DAG 18:0/18:2	$C_{39}H_{72}O_5$	620.5379	621.5	(C18H35O) - 267.2	R2 (C18H31O) - 263.2	621.5 / 267.2
DAG 18:1/18:1	$C_{39}H_{72}O_5$	620.5379	621.5	(C18H33O) - 265.2	R2 (C18H33O) - 265.2	621.5 / 265.2
DAG 18:1/18:2	$C_{39}H_{70}O_5$	618.5223	619.5	(C18H33O) - 265.2	R2 (C18H31O) - 263.2	619.5 / 265.2
DAG 18:1/18:3	$C_{39}H_{68}O_5$	616.5066	617.5	(C18H33O) - 265.2	R2 (C18H29O) - 261.2	617.5 / 265.2
DAG 18:1/20:4	$C_{41}H_{70}O_5$	642.5223	643.5	(C18H33O) - 265.2	R2 (C20H31O) - 287.2	643.5 / 265.2
DAG 16:0/18:3	$C_{37}H_{66}O_5$	590.4910	591.5	(C16H31O) - 239.2	R2 (C18H29O) - 261.2	591.5 / 239.2
DAG 16:1/18:2	$C_{37}H_{66}O_5$	590.4910	591.5	R1 (C16H29O) - 237.2	R2 (C18H31O) - 263.2	591.5 / 237.2
DAG 18:0/18:3	$C_{39}H_{70}O_5$	618.5223	619.5	(C18H35O) - 267.2	R2 (C18H29O) - 261.2	619.5 / 267.2
DAG 18:0/20:4	$C_{41}H_{72}O_5$	644.5379	645.5	(C18H35O) - 267.2	R2 (C20H31O) - 287.2	645.5 / 267.2
DAG 18:0/22:6	$C_{43}H_{72}O_5$	668.5379	669.5	(C18H35O) - 267.2	R2 (C22H31O) - 311.2	669.5 / 267.2
DAG 18:1/22:6	$C_{43}H_{70}O_5$	666.5223	667.5	(C18H33O) - 265.2	R2 (C22H31O) - 311.2	667.5 / 265.2
DAG 16:0/18:1	$C_{37}H_{70}O_5$	594.5223	595.5	(C16H31O) - 239.2	R2 (C18H33O) - 265.2	595.5 / 239.2
DAG 16:0/18:2	$C_{37}H_{68}O_5$	592.5066	593.5	(C16H31O) - 239.2	R2 (C18H31O) - 263.2	593.5 / 239.2
DAG 16:0/20:4	$C_{39}H_{68}O_5$	616.5066	617.5	(C16H31O) - 239.2	R2 (C20H31O) - 287.2	617.5 / 239.2
DAG M16:0/22:6	$C_{41}H_{68}O_5$	640.5066	641.5	(C16H31O) - 239.2	R2 (C22H31O) - 311.2	641.5 / 239.2
DAG 16:1/18:1	$C_{37}H_{68}O_5$	592.5067	593.5	R1 (C16H29O) - 237.2	R2 (C18H33O) - 265.2	593.5 / 237.2
DAG 16:1/18:3	$C_{37}H_{64}O_5$	588.4753	589.5	R1 (C16H29O) - 237.2	R2 (C18H29O) - 261.2	589.5 / 237.2
DAG 16:1/20:4	$C_{39}H_{66}O_5$	614.4910	615.5	R1 (C16H29O) - 237.2	R2 (C20H31O) - 287.2	615.5 / 237.2
DAG 16:1/22:6	$C_{41}H_{66}O_5$	638.4910	639.5	R1 (C16H29O) - 237.2	R2 (C22H31O) - 311.2	639.5 / 237.2

d. Vinylacyl glycerols (2-Acyl-1-(1-alkenyl)-sn-glycerols

Metabolite Name	Molecular Formula	Parent Mass	M+H Mass	Diagnostic Fragment Mass (Intensity %)		MS/MS Transition
				R1	R2	
VAG 18:0/18:1	$C_{39}H_{74}O_4$	606.5587	607.5	(C18H35O) - 267.2	R2 (C18H35O) - 267.2	607.5 / 267.2
VAG 18:0/18:2	$C_{39}H_{72}O_4$	604.543	605.5	(C18H35O) - 267.2	R2 (C18H33O) - 265.2	605.5 / 267.2
VAG 18:0/18:3	$C_{39}H_{70}O_4$	602.5274	603.5	(C18H35O) - 267.2	R2 (C18H31O) - 263.2	603.5 / 267.2
VAG 18:0/20:4	$C_{41}H_{72}O_4$	628.543	629.5	(C18H35O) - 267.2	R2 (C20H33O) - 289.2	629.5 / 267.2
VAG 18:0/22:6	$C_{43}H_{72}O_4$	652.543	653.5	(C18H35O) - 267.2	R2 (C22H33O) - 313.2	653.5 / 267.2
VAG 18:1/18:1	$C_{39}H_{72}O_4$	604.543	605.5	(C18H33O) - 265.2	R2 (C18H35O) - 267.2	605.5 / 265.2
VAG 18:1/18:2	$C_{39}H_{70}O_4$	602.5274	603.5	(C18H33O) - 265.2	R2 (C18H33O) - 265.2	603.5 / 265.2
VAG 18:1/18:3	$C_{39}H_{68}O_4$	600.5117	601.5	(C18H33O) - 265.2	R2 (C18H31O) - 263.2	601.5 / 265.2
VAG 18:1/20:4	$C_{41}H_{70}O_4$	626.5274	627.5	(C18H33O) - 265.2	R2 (C20H33O) - 289.2	627.5 / 265.2
VAG 18:1/22:6	$C_{43}H_{70}O_4$	650.5274	651.5	(C18H33O) - 265.2	R2 (C22H33O) - 313.2	651.5 / 265.2
VAG 16:0/18:1	$C_{37}H_{70}O_4$	578.5274	579.5	(C16H31O) - 239.2	R2 (C18H35O) - 267.2	579.5 / 239.2
VAG 16:0/18:2	$C_{37}H_{68}O_4$	576.5117	577.5	(C16H31O) - 239.2	R2 (C18H33O) - 265.2	577.5 / 239.2
VAG 16:0/18:3	$C_{37}H_{66}O_4$	574.4961	575.5	(C16H31O) - 239.2	R2 (C18H31O) 18- 263.2	575.5 / 239.2
VAG 16:0/20:4	$C_{39}H_{68}O_4$	600.5117	601.5	(C16H31O) - 239.2	R2 (C20H33O) - 289.2	601.5 / 239.2
VAG 16:0/22:6	$C_{41}H_{68}O_4$	624.5117	625.5	(C16H31O) - 239.2	R2 (C22H33O) - 313.2	625.5 / 239.2
VAG 16:1/18:1	$C_{37}H_{68}O_4$	576.5118	577.5	(C16H29O) - 237.2	R2 (C18H35O) - 267.2	577.5 / 237.2
VAG 16:1/18:2	$C_{37}H_{66}O_4$	574.4961	575.5	(C16H29O) - 237.2	R2 (C18H33O) - 265.2	575.5 / 237.2
VAG 16:1/18:3	$C_{37}H_{64}O_4$	572.4804	573.5	(C16H29O) - 237.2	R2 (C18H31O) - 263.2	573.5 / 237.2
VAG 16:1/20:4	$C_{39}H_{66}O_4$	598.4961	599.5	(C16H29O) - 237.2	R2 (C20H33O) - 289.2	599.5 / 237.2
VAG 16:1/22:6	$C_{41}H_{66}O_4$	622.4961	623.5	(C16H29O) - 237.2	R2 (C22H33O) - 313.2	623.5 / 237.2
VAG 14:0/18:1	$C_{35}H_{66}O_4$	550.4961	551.5	(C14H27O) - 211.2	R2 (C18H35O) - 267.2	551.5 / 211.1
VAG 14:0/18:2	$C_{35}H_{64}O_4$	548.4805	549.5	(C14H27O) - 211.2	R2 (C18H33O) - 265.2	549.5 / 211.1
VAG 14:0/18:3	$C_{35}H_{62}O_4$	546.4846	547.5	(C14H27O) - 211.2	R2 (C18H31O) - 263.2	547.5 / 211.1
VAG 14:0/20:4	$C_{37}H_{64}O_4$	572.4804	573.5	(C14H27O) - 211.2	R2 (C20H33O) - 289.2	573.5 / 211.1
VAG 14:0/22:6	$C_{39}H_{64}O_4$	596.4805	597.5	(C14H27O) - 211.2	R2 (C22H33O) - 313.2	597.5 / 211.1
VAG 12:0/18:2	$C_{33}H_{60}O_4$	520.4492	521.4	(C12H23O) - 183.2	R2 (C18H33O) - 265.2	521.4 / 183.2
VAG 12:0/2:0	$C_{17}H_{32}O_4$	300.23	301.2	(C12H23O) - 183.2		301.2 / 183.2

3.2.4 Real Time-Polymerase Chain Reaction (RT-PCR)

Total RNA was isolated from cell pellets using the Qiagen RNeasy Mini Kit as per manufacturer's instruction. The RNA pellets were resuspended in 50 µL of DEPC-treated water and stored at -80°C. RNA concentration and purity were determined by spectrophotometry at 260 nm (DNA) and 280 nm (protein) repectively. Reverse transcription was performed using qScript cDNA super mix (Quanta Biosciences) on an Applied Biosystems Step one Plus Real-time PCR system. The real-time PCR primers that were used are listed in Table 3.3.

3.2.5 Gene Expression of CNA14 Cells at 34ºC and 39ºC

3.2.5.1 RNA Isolation

Total RNA was isolated using a Nucleospin RNA II Kit (BD Biosciences). Cells were grown to approximately 80% confluency in complete media in a 15 cm^2 plate as described above. The media was removed from the plate and the cells were rinsed with phosphate-buffered saline (PBS). Total RNA was isolated according to the manufacturer's instructions for RNA isolation from cultured cells. The mRNA was isolated from the total RNA using BD Biosciences NucleoTrap Nucleic Acid Kit, following the manufacture's protocol for mRNA purification. The poly $(A)^+$ mRNA was concentrated using a protocol obtained from Protocol-online.org. One tenth volume of 3 M NaAc (pH 5.2) and 2.5 volumes of 100% ethanol were added to the mRNA pellet. The pellet was mixed and incubated at -20°C overnight. The tube was then centrifuged at 15,000 X g for 20 minutes at 4°C. The pellet was washed twice with 80% ethanol and then air dried. The pellet was re-suspended in RNAse-DNAse free water, and then stored at -80°C until needed. RNA concentrations and purity were determined by measuring the absorbance of the RNA samples at wavelengths of 260 and 280 nm using a spectrophotometer.

Table 3.3. Real-time polymerase chain reaction (RT-PCR) primers.
The primer sequences used for the quantitative analysis of transcript levels for the following genes: glyceraldehyde 3-phosphate dehydrogenase (GAPDH), fatty acid synthase (FASN), **1-**acylglycerol-3-phosphate O-acyltransferase (AGPAT1 and AGPAT2), glycerol-3-phosphate acyltransferase (GPATM), peroxisomal membrane protein 11a (Pex11A), phospholipase C (PLC).

Gene	Amplicon	Sequences (5' to 3')
GAPDH- Forward	226 bp	GAAGGTGAAGGTCGGAGTC
GAPDH- Reverse		GAAGATGGTGATGGGATTTC
FASN- Forward	156 bp	GAGAGCCTCTTCTCCAGGGT
FASN- Reverse		CTTCAGAGACTCCACCCAGC
AGPAT1- Forward	191 bp	CATCAGGTGCTGCACTCACT
AGPAT1- Reverse		AGTTGTGGGAACAGGTCTGG
AGPAT2- Forward	192 bp	GTACTTTTACGGGCTCCGCT
AGPAT2- Reverse		AGGTACATGATGAGGCCCAC
GPATM- Forward	183 bp	CCAGCCTGTGCTACCTTCTC
GPATM- Reverse		GAAGCTTCTTGTCCCACTGC
Pex11a- Forward	94 bp	TGGCATCATTGGACTTGGAGGTCT
Pex11a- Reverse		AACACCCTAACGGGTCTTCAGCTT
PLC-b1-Forward	194 bp	CGTGGCTTTCCAAGAAGAAG
PLC-b1-Reverse		GCTTCCGATCTGCTGAAAAC
PLC-g2-Forward	208bp	CCTGTCCATTGAGGACCACT
PLC-g2-Reverse		CATGGATGTAGGCACCTCCT
PLC-d1-Forward	123bp	ACAAGATCATCCACCACTCAGGCT
PLC-d1-Reverse		TCTGCAGCTCCTTGAAGCTCATCT
PLC-e1-Forward	194pb	AATGATGCTGAAGAACGCCAGCC
PLC-e1-Reverse		AGCAAAGGTAGTCGACTGGCAAGA

3.2.5.2 MicroArray Analysis

A BD Atlas™ plastic rat 4K microarray (BD Biosciences Clontech) was used to analyze the gene expression differences between the CNA14 cells grown at 34°C and 39°C. As per manufacturer's directions, cDNA probes were prepared and were purified using column chromatography. The radioactivity of the probe was determined by scintillation spectrometry. The plastic microarray was pre-rinsed and then the cDNA probes were hybridized to the array overnight at 60°C. The next day the microarray was rinsed and air dried completely. Once it had dried, the microarray was exposed to a ^{33}P Phosphorimaging screen for 48 hours. However, after this period it was determined a longer exposure was necessary, so it was left for a period of 10 days. The phosphorimaging screen was scanned and analyzed at the Saskatoon Cancer Center. Quantity-One software (Bio-Rad) was used to visualize and analyze the microarray.

3.2.6 Cell Cycle Analysis

3.2.6.1 Flow Cytometry

Harvested cells were re-suspended in 1% (vol/vol) of formaldehyde, and left for 15 minutes at room temperature. The cells were then centrifuged at 500 X g for 5 minutes in order to remove the formaldehyde from the cells. The pellets were resuspended in ice-cold ethanol (70%). After a 12 hour fixation period at -20°C the samples were centrifuged at 500 X g for 5 minutes and then resuspended in PBS containing 18 µg/mL propidium iodide and 40 µg/mL heat-treated pancreatic ribonuclease A for 20 min at room temperature. The cells were then kept on ice and shielded from light. The flow cytometry work was completed on an EPICS XL flow cytometer (Coulter Electronics, Miami, FL) at the Saskatoon Cancer Center.

3.2.7 Western Blot Analysis

The Western blot analysis was completed under the supervision and direction of Dr. Gerald Davies of Phenomenome Discoveries. The differentiated (attached) U937 cells were removed from tissue culture dishes using with Versene and TrypLE Express (Invitrogen), and rinsed with PBS three times. The cells that were growing in suspension were pelleted by

centrifugation at 1000 X g to remove the media, and where then rinsed with PBS three times. The cells were pelleted by chilled (4°C) centrifugation at 1000 X g and the pellets resuspended in ice-cold lysis buffer (20 mM HEPES (pH 7.5), 50 mM KCl, 10% glycerol, 0.5 mM EDTA, 0.1 mM EGTA, 1 mM DTT plus 1X mammalian cell anti-protease cocktail (Sigma-Aldrich Ltd). The cells were lysed using multiple freeze-thaw cycles followed by pulse sonication and centrifugation at 1000 X g to remove cell debris. Western blot analysis of these protein lysates was performed as previously described (Davies *et al.*, 2005). Briefly, equivalent amounts of protein (assessed by Bradford protein assay (Bradford, 1976) using BioRad Protein Reagent) were resolved by 10% sodium dodecyl sulfate–polyacrylamide gel electrophoresis (SDS-PAGE). Following electrophoresis the proteins were trans-blotted onto nitrocellulose membranes (Pall-VWR). The membranes were blocked overnight at 4°C on a gyratory plate with 5% molecular grade skim milk powder (BioRad Laboratories Ltd.) in phosphate-buffered saline (PBS) containing 0.1% Tween-20 (PBST). Primary and secondary antibody incubations and subsequent washes were carried out in the same buffer. Primary antibodies were obtained from Santa Cruz Biotechnology. The primary antibody for GAPDH was purchased from Sigma-Aldrich Ltd.. Secondary HRP-conjugated antibodies were purchased from BioRad Laboratories Ltd.. Blots were immunoprobed overnight with primary antibodies at a 1:1000 dilution. Secondary antibodies were applied at room temperature on a gyratory plate at a concentration of 1:10,000 for 30 min. Following multiple washes, an enhanced chemiluminescence detection system (Dupont-NEN) was used to detect the target antigen/antibody complexes. Blots were then stripped at 50°C for 30 minutes in a Tris-buffered 20% SDS/1% 2-mercaptoethanol stripping solution, washed and re-probed with GAPDH to verify protein loading equivalency.

4 RESULTS

4.1 Metabolic Alterations Associated with Cell Cycle Progression

4.1.1 Flow Cytometry

Serum starvation of low passage MRC5 cells, a human fibroblast cell line, was used as a model system for studying metabolic alterations associated with cell cycle progression. Reduction of serum levels in the media to 0.1% for 48 hours forced the MRC5 cells into the G0 stage, or quiescent state, of the cell cycle. Once normal levels of serum were returned to the media, cells re-entered the cell cycle and continued to grow as a synchronous population for one complete cell cycle. Cells were collected before, during and after the serum starvation to ensure that populations of cells at each of the stages in the cell cycle were captured.

Flow cytometry is a method used to distinguish cells in different phases of the cell cycle. Flow cytometry can be used to quantitatively measure the DNA content in the cells. The DNA in a cell doubles during the synthesis phase (S phase) of the cell cycle, therefore it is possible to determine whether cells are in the G0 phase and G1 phase (prior to DNA doubling), or in the G2/M stage (after the DNA doubling) solely based on DNA content. The results of our flow cytometry analysis of the MRC5 cells suggest that the cells were synchronized in the G0 phase of the cell cycle after the serum starvation (Figure 4.1).

The control cells, those growing asynchronously, appear to be mostly in the G0 or G1 stage of the cell cycle. The broadness of the peak suggests that cells are in various stages of the cell cycle. The analysis of the 0 hour time point, which was collected immediately following the 48 hour serum starvation, revealed that the cells were in the G0/G1 phase of the cell cycle. The more defined peak shape suggests that the cells appear to be synchronized in G0. Very few changes in DNA content were observed in the cells collected up to 12 hours after the synchronization. It is likely that the cells have entered the G1 stage of the cycle within 6 hours, which is the stage when cells are doubling all cellular components except DNA.

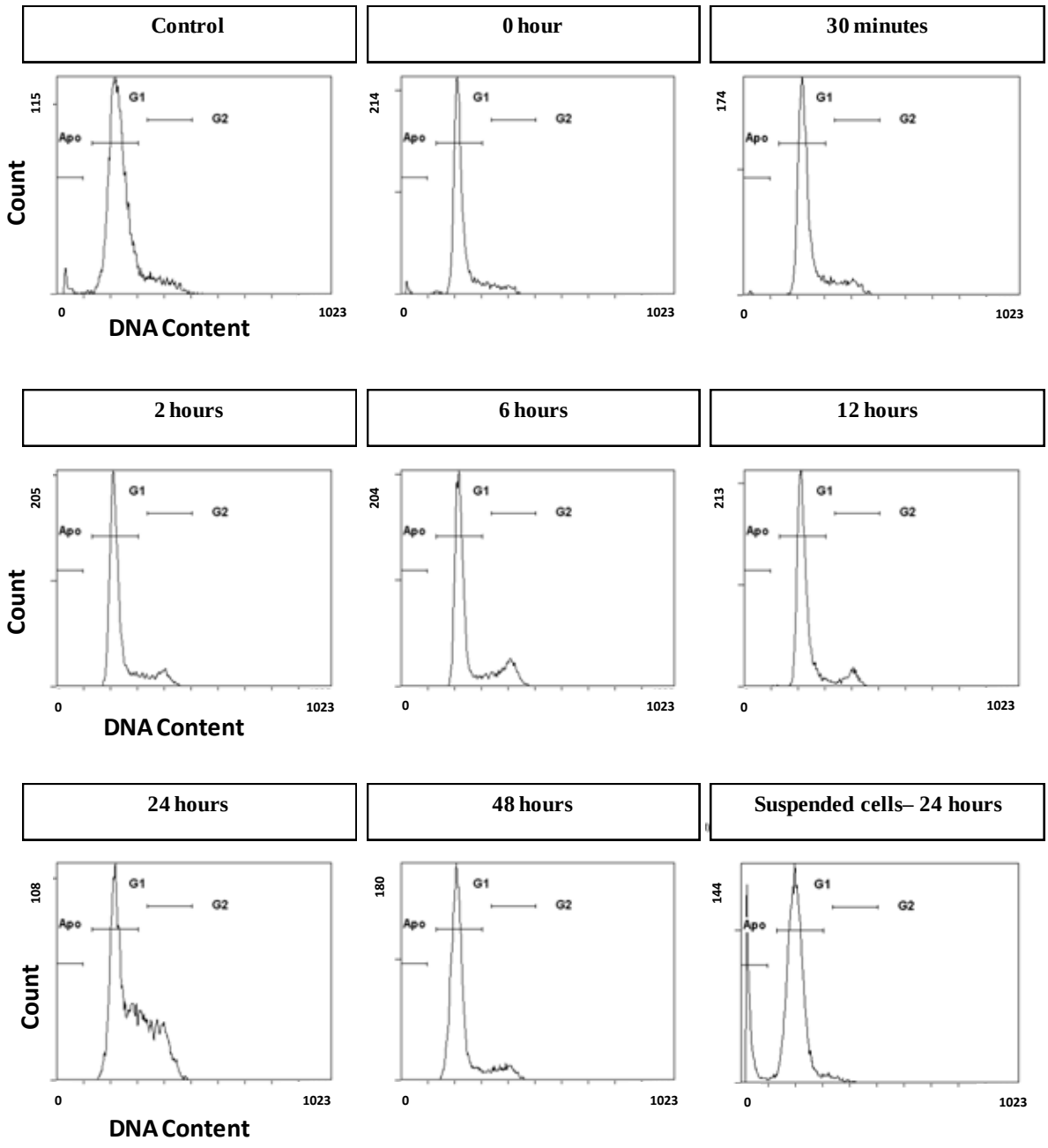

Figure 4.1. Flow cytometry analysis of MRC5 cells (low passage human fibroblasts) as they progress through the cell cycle.

Flow cytometry was employed to determine which stage of the cell cycle each collection was at. The cell count for each sample is listed on the Y axis of each plot, and the DNA content on the X axis. It is not possible to discriminate between G1 and G0 using flow cytometry as the DNA content at the two stages will be the same. The cells that have entered into the G2 phase of the cell cycle have twice the amount of DNA content as they have completed the synthesis (S) phase of the cell cycle.

As expected, 24 hours after the starvation period I see a large increase of cells in the S phase of the cell cycle. All cells appeared to have completed one cell cycle by 24 hours and were more than 100% confluent. Consequently, there were also numerous suspended cells in these plates, which were not observed in any of the other time points. The flow cytometry analysis revealed that the attached cells had likely arrested in G1, or into G0 probably due to contact inhibition, whereas the suspended cells were mostly apoptotic, or arrested in G1/G0.

4.1.2 Data Alignment and Array Generation

Samples at corresponding time points were extracted into aqueous and organic phases, as described in the materials and methods section, and then analyzed of the FTICR-MS using both electrospray ionization and atmospheric pressure chemical ionization. Accurate masses for 1075 compounds were detected in the analysis. The resulting spectra were aligned and a two dimensional array was created, allowing the visualization of the FTICR-MS analysis (Figure 4.2). Each column in the array represents a sample, and each row represents a unique mass. The samples are ordered with the control samples at the left hand side followed by the 0 hour time point (samples collected after the 48 hour serum starvation), then the 30 min, 2 hours, 6 hours, 12 hours, 24 hours and 48 hours samples. Duplicate samples were collected at each time point. Reproducibility of the mass spectrometry analyses was determined for each of the replicates by plotting the $\log_2$ intensity of the replicates and calculating the R^2 values (Pearson correlation coefficient) (Figure 4.3). The R^2 value for the entire experiment was found to be 0.88, suggesting good reproducibility in the experiment.

4.1.3 Unsupervised Statistical Analyses

Masses with p-value less than 0.001 (292 masses) were further selected and statistical analyses were performed. The principal component analysis (PCA) plot indicates that synchronization of the cells by serum starvation alone results in a substantial metabolic shift (Figure 4.4). The difference between the location of the control samples and the cluster of samples containing the 0, 30 min and 2 hour time points indicate metabolic changes occur after the cells have gone through serum starvation. There is then a significant separation between the early time point cluster (up to 2 hours after serum re-introduction to the starved cells) and the 6, 12 and 24 hour time points. The later time points cluster on the opposite side

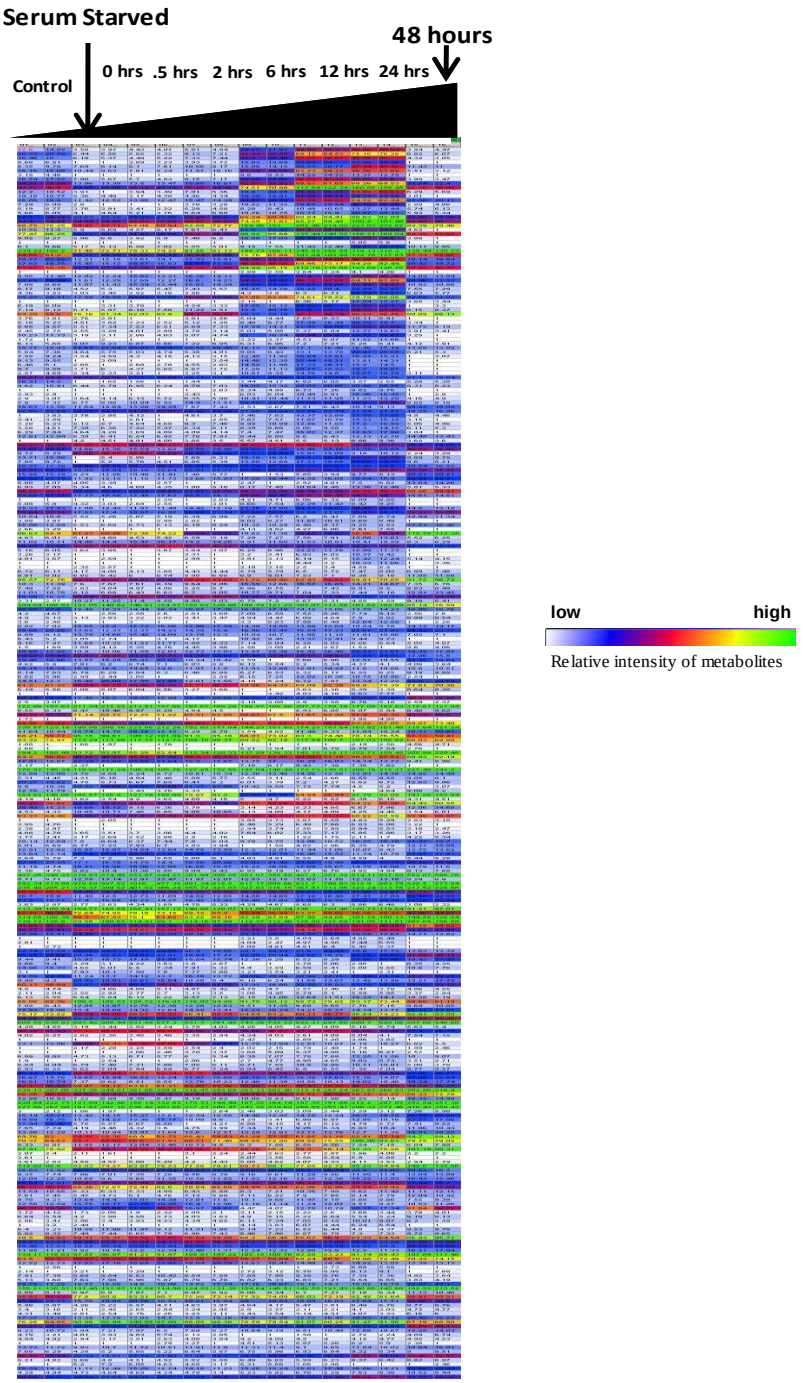

Figure 4.2 Metabolite array of all metabolites detected in MRC5 cells as they progress through the cell cycle.

A two dimensional array of masses detected in the analysis of MRC5 cells as they progress through the cell cycle ($p<0.001$). Each sample is in duplicate. Each column is 1 sample, and each row is 1 metabolite. The colour of each cell in the array represents the relative intensity of the metabolite in each sample. The samples are ordered from asynchronous population (control), then the 0 hour time point (after the 48 hour serum starvation), 30 min, 2 hr, 6 hr, 12 hr, 24 hr and 48 hr post serum reintroduction (left to right).

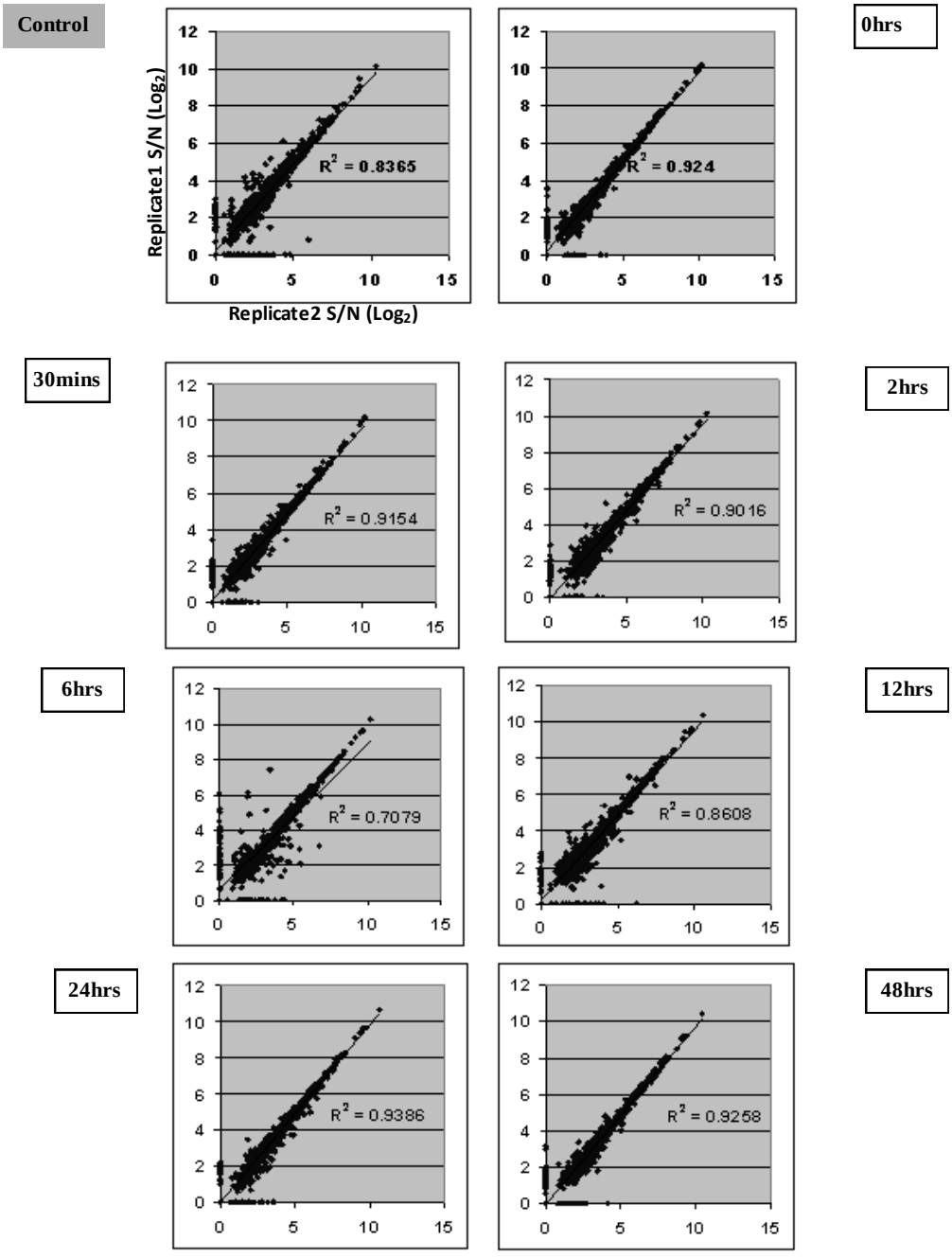

Figure 4.3 Quality assurance and quality control (QAQC) results from the cell cycle experiment.

Correlation plots for each of the replicates of each time point collected. The analytical reproducibility was monitored by analyzing the replicate samples. Each of the replicate profiles was compared to each other by plotting the $\log_2$ relative intensities of the replicates. The closer the R^2 value is to 1, the more reproducible the experiment was.

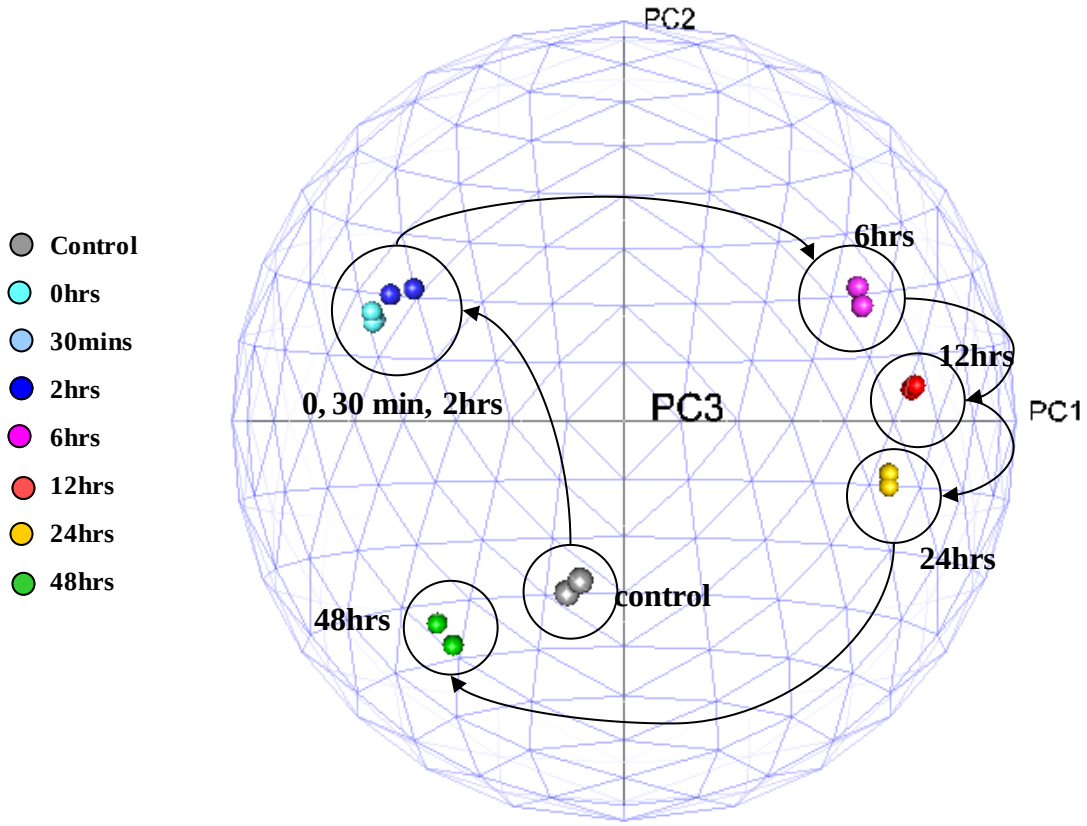

Figure 4.4 Principal component analysis of metabolites ($p<0.001$) detected in cells as they progress through the cell cycle.
PCA is a linear transformation that converts data to a new coordinate system such that the greatest variance within the data comes to lie on the first coordinate (called the first principal component, PC1), the second greatest variance on the second coordinate (PC2), and so on. The closer the samples cluster together in a PCA plot the more metabolically similar they are, and likewise the further the samples separate from each other along the more metabolically distinct they are. The 0, 30 min and 2 hr time points cluster together on the left hand side of principal component 1 (PC1). The 6, 12 and 24 hr time cluster at coordinates different from the rest of the samples on the right hand side of PC1. The control and 48 hr time points localize to the same region of the PCA.

of PC1 as opposed to the earlier time points, signifying a dramatic difference in their metabolic profiles. The separation of these samples suggests that a metabolic shift takes place between 2 and 6 hours after the re-introduction of serum. Interestingly, the 48 hour time point clusters most closely to the control samples. This may be due to the fact that the samples are no longer synchronized and are possibly metabolically similar to the control population that is also an unsynchronized population.

It is also important to note that by 48 hours the cells had become slightly overgrown, and so metabolic differences may be due to non-adherent cells or cells becoming apoptotic due to lack of space. Overall the result of this analysis demonstrated that the largest metabolic change which occurred during the cell cycle took place between two and six hours following the addition of serum to the synchronized cells. The masses that are responsible for the separation of the control, 30 minute and 2 hour samples from the 6, 12 and 24 samples along PC1 are listed in Table 4.1. The masses that are elevated in the later time points, resulting in a positive loadings score, were all detected in the same analysis mode 1203 (organic fraction, positive ionization, APCI source) and are all quite large in size (Table 4.1). The masses with a negative loadings score along PC1 were mostly detected in the analysis modes 1101 and 1102 (aqueous fraction, positive and negative ionization respectively, ESI source). The masses with the most positive and negative loadings along PC2 separate the control samples from the samples collected after the serum starvation (Table 4.2). The masses that increase after synchronization, which therefore have a positive loadings score, were detected in modes 1101 (aqueous fraction, positive ionization, ESI source) and 1203 (organic fraction, positive ionization, APCI source). The masses with negative loadings, which decrease after synchronization, are detected in all different analysis modes (1203, 1101, 1102 and 1201).

The hierarchical cluster analysis, using a Pearson correlation with complete linkage, of the cell cycle dataset ($p<0.0001$, $\log_2$ normalized) identified clusters of metabolites showing slightly different patterns of expression over the cell cycle period (Figure 4.5). Each of these clusters contains metabolites that have similar expression patterns as the MRC5 progressed through the cell cycle, and in this case there appears to be four overall distinct clusters of metabolites.

The first step in identifying the metabolites in each of the clusters of the analysis is to screen the masses for known metabolites in Phenomenome Discoveries' metabolite database.

Table 4.1 Masses responsible for the separation of the MRC5 samples along principal component 1 (PC1) in the principal component analysis (PCA).

The masses listed in these tables are responsible for the separation of the samples along PC1. Masses that increase 6 hours after the synchronization period are listed in the first table on the left (positive loadings score, highlighted green), and the masses that decrease 6 hours after synchronization are listed in the table on the right (negative loadings score, highlighted red). The first column in each table contains the detected mass. The second column lists the analysis mode that the mass was detected in (1101- positive ESI aqueous, 1102- negative ESI aqueous, 1201- positive ESI organic butanol, 1202- negative ESI organic butanol, 1203- positive APCI organic ethyl acetate and 1204- negative APCI organic ethyl acetate). The third column contains the PC1 loadings score from the PCA. The last column lists the p-value of the mass.

	Detected Mass	Analysis Mode	PC1-loadings score	P_Value
1	885.7864	1203	0.1577	3.13E-05
2	882.7678	1203	0.1547	1.19E-09
3	884.7827	1203	0.1546	0.0002
4	881.7562	1203	0.1496	0.0001
5	883.7714	1203	0.1464	1.47E-09
6	886.7939	1203	0.1464	0.0007
7	880.7523	1203	0.146	2.06E-08
8	565.515	1203	0.1446	0.0001
9	878.738	1203	0.1415	0.0001
10	879.7417	1203	0.1383	0.0006
11	909.7878	1203	0.1375	0.0007
12	828.7222	1203	0.1367	2.55E-05
13	907.7727	1203	0.1353	0.0001
14	908.7837	1203	0.133	7.25E-07
15	852.7199	1203	0.1318	0.0007
16	906.7684	1203	0.1312	1.37E-07
17	910.7991	1203	0.1269	0.0006
18	912.8166	1203	0.1245	0.001
19	536.5163	1203	0.1233	3.19E-05
20	631.5623	1203	0.1216	0.0003
21	492.3814	1203	0.1202	1.48E-07
22	598.4584	1203	0.1177	0.0003
23	580.5348	1203	0.1156	0.0005
24	853.7244	1203	0.1156	0.0002
25	934.799	1203	0.1143	2.30E-06
26	911.8037	1203	0.1139	0.0009
27	564.5507	1203	0.1131	0.0001
28	830.737	1203	0.1127	0.0004
29	466.3651	1203	0.1099	0.0004
30	935.8016	1203	0.1083	0.0007
31	829.7263	1203	0.1077	4.10E-07
32	932.7821	1203	0.1069	0.0005
33	887.8029	1203	0.105	0.0007
34	930.7679	1203	0.1034	0.0003
35	937.819	1203	0.1023	7.37E-10
36	936.8133	1203	0.0952	0.0008
37	578.5278	1203	0.093	3.57E-08
38	579.5314	1203	0.0929	1.86E-07
39	591.5697	1203	0.0903	0.0004
40	600.5128	1203	0.0882	7.66E-09

	Detected Mass	Analysis Mode	PC1-loadings score	P_Value
1	704.5183	1201	-0.0394	0.0002
2	329.0658	1101	-0.0396	4.37E-09
3	369.0451	1101	-0.0421	0.0007
4	677.4993	1201	-0.0431	1.35E-05
5	257.1028	1101	-0.0445	0.0002
6	651.1128	1102	-0.0452	2.56E-05
7	153.0385	1101	-0.046	2.22E-05
8	614.1486	1102	-0.0492	4.53E-06
9	613.1584	1102	-0.0498	1.02E-07
10	330.0691	1101	-0.0499	4.73E-08
11	367.0216	1101	-0.0509	1.03E-05
12	307.0838	1101	-0.0521	1.86E-06
13	678.5029	1201	-0.0542	0.0001
14	672.0897	1102	-0.0551	0.0001
15	612.1554	1102	-0.0578	1.17E-06
16	295.0586	1101	-0.0582	5.36E-06
17	347.0625	1102	-0.0619	0.0006
18	650.1103	1102	-0.0642	9.44E-06
19	404.9776	1101	-0.0703	0.0001
20	345.0399	1101	-0.0723	9.08E-06

Table 4.2 Masses responsible for the separation of the MRC5 samples along principal component 2 (PC2) in the principal component analysis (PCA).
The masses listed in these tables are responsible for the separation of the samples along PC2. These are masses that separate the control samples from the samples collected after the synchronization period. Masses that increase after the synchronization period are listed at the top of the table (positive loadings score, highlighted green), and the masses that decreased after synchronization are listed at the bottom of the table (negative loadings score, highlighted red). The first column in the table contains the detected mass. The second column lists the analysis mode that the mass was detected in (1101- positive ESI aqueous, 1102- negative ESI aqueous, 1201- positive ESI organic butanol, 1202- negative ESI organic butanol, 1203- positive APCI organic ethyl acetate and 1204- negative APCI organic ethyl acetate). The third column contains the PC2 loadings score from the PCA. The last column lists the p-value of the mass detected.

	Detected Mass	Analysis Mode	PC2-loadings score	P_Value
1	279.0847	1101	0.2581	1.97E-07
2	257.1028	1101	0.2275	0.0002
3	303.9936	1101	0.1745	0.0004
4	295.0586	1101	0.1657	5.36E-06
5	438.2485	1101	0.1581	0.0005
6	934.799	1203	0.1079	2.30E-06
7	910.7991	1203	0.0812	0.0006
8	909.7878	1203	0.0768	0.0007
9	878.738	1203	0.0765	0.0001
10	930.7679	1203	0.0746	0.0003
1	241.0927	1201	-0.217	0.001
2	650.1103	1102	-0.151	9.44E-06
3	607.0814	1102	-0.149	0.0001
4	564.5507	1203	-0.133	0.0001
5	345.0399	1101	-0.129	9.08E-06
6	672.0897	1102	-0.124	0.0001
7	612.1554	1102	-0.123	1.17E-06
8	613.1584	1102	-0.103	1.02E-07
9	614.1486	1102	-0.102	4.53E-06
10	619.5256	1203	-0.098	1.46E-05

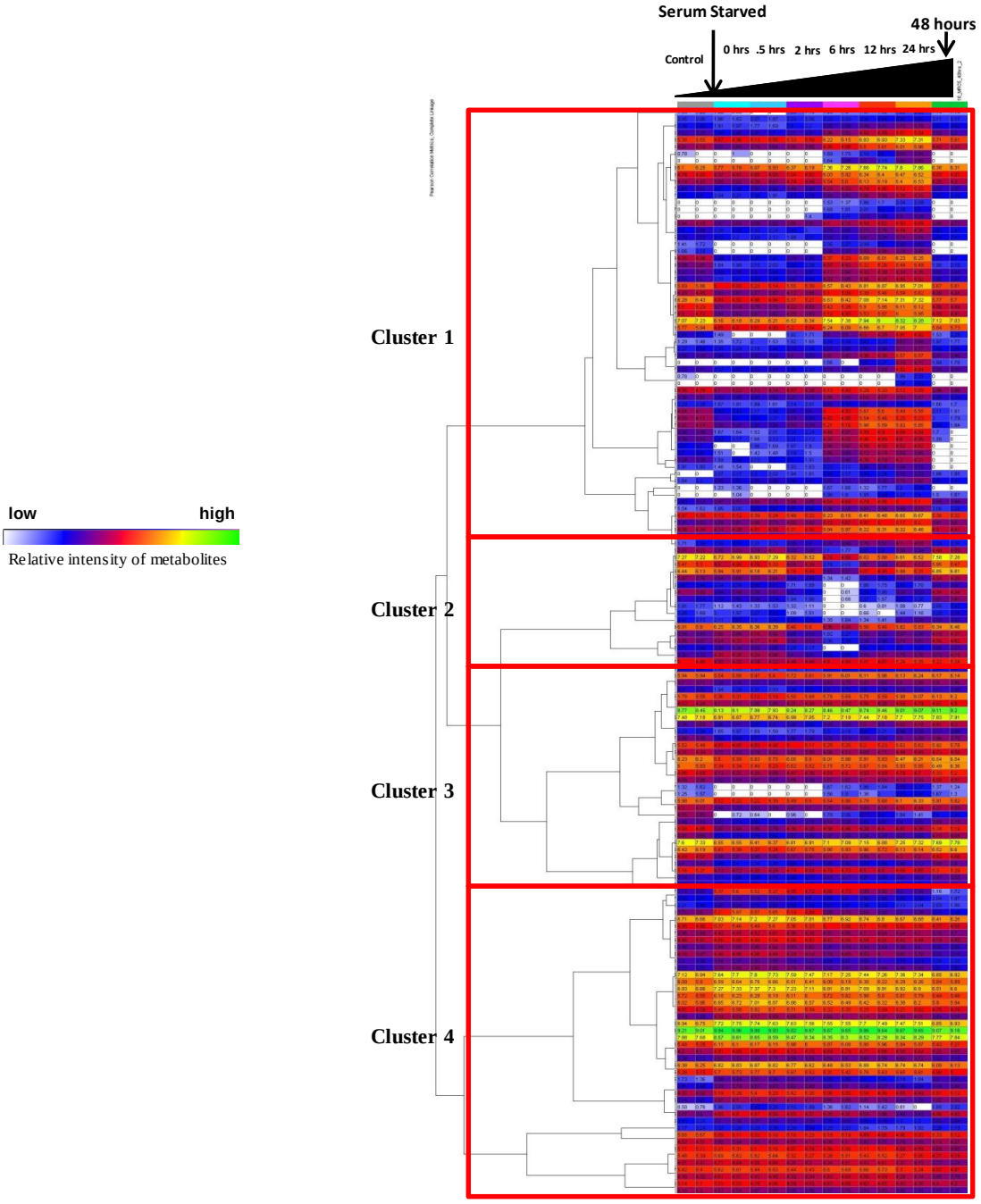

Figure 4.5 Hierarchical cluster analysis (HCA) of metabolites (p<0.001) detected in MRC5 cells as they progress through the cell cycle.

Masses deemed significant (p<0.001) were hierarchically clustered using a Pearson correlation. Using this type of analysis will cluster together masses with similar changes in S/N across the samples. Each sample is in duplicate. Each column is one sample, and each row is one metabolite. The colour of each cell in the array represents the relative intensity of the metabolite in each sample. The samples are ordered from asynchronous population (control, -48 hours)), then the 0 hour time point (after the 48 hour serum starvation), 30 min, 2 hr, 6 hr, 12 hr, 24 hr and 48 hr (left to right).

This will typically result in the identification of about 30-50% of the masses detected in the analysis. The remaining masses that did not match any of the known metabolites have to be identified one at a time with a molecular formula calculator. The molecular calculator determines all of the possible combinations of elements that will result in the mass detected. Depending on the mass, the calculator may only find a single formula match or it may find hundreds of potential matches. Once the list of possible formulas is determined the next step is to establish which of them are actually probable (taking the extract type and analysis mode into consideration). Another consideration that has to be made is whether the mass detected is a parent mass or an adduct form of a metabolite (i.e. a sodium or potassium adduct).

It was quickly realized that a large percentage of the metabolites detected in these analyses were lipids, and it was therefore necessary to determine formulae for as many of the lipid classes as possible. The main groups of lipids that were detected in this analysis were triacylglycerols, phospholipids, 2-acyl-1-(1-alkenyl)-sn-glycerols and plasmalogens. The masses and formulas were determined for each of these classes of lipids, including all possible combinations of fatty acid side chains.

In order to visualize the expression patterns in each of the clusters, the average log2 signal to noise of the masses were plotted (Figure 4.6). Beside each graph there is a pie chart that shows the different classes of metabolites identified in each of the clusters, and the proportions of each class in the cluster. The first cluster was mainly composed of triacylglycerols and 2-acyl-1-alkyl-sn-glycerols (a precursor molecule of plasmalogens) (Figure 4.6A). These metabolites began to accumulate 6 hours after serum reintroduction. The increase of these metabolites continues until the 24 hour time point, and then at 48 hours they decrease to the levels they were at in the control cells. The majority of the masses in this cluster (67%) have been putatively identified as vinyl acylglycerols (VAGs, also known as 2-Acyl-1-(1-alkenyl)-sn-glycerols) and triacylglycerols (TAGs). The second cluster contained reduced and oxidized glutathione, which both showed dramatic decreases 6 hours after serum reintroduction and returning back to the levels detected in the control cells after 24 hours (Figure 4.6B). The last two clusters were largely made up of phospholipids and plasmalogens, and the levels of these metabolites changed very little during the course of the experiment (Figure 4.6C,D).

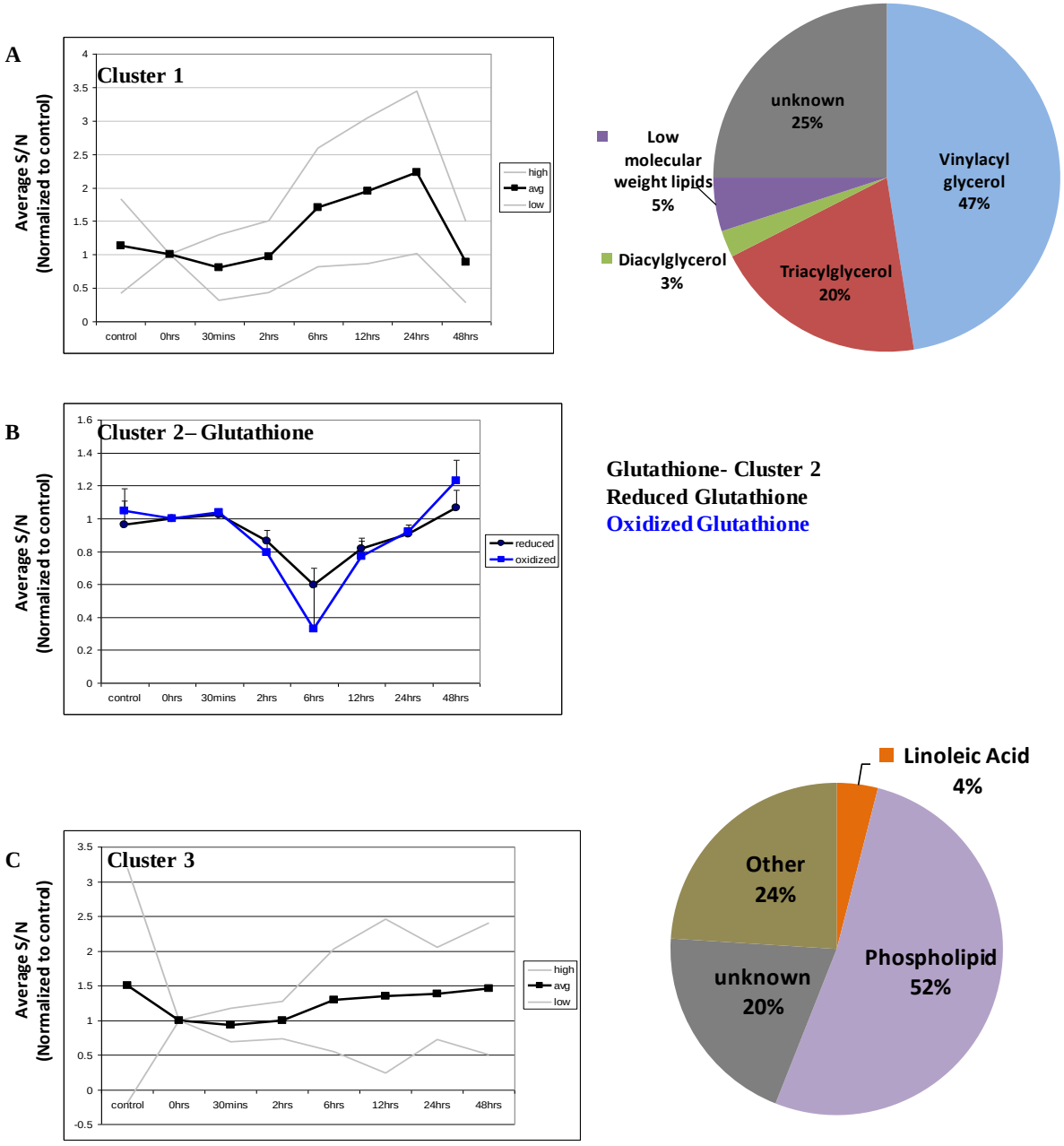

Figure 4.6(A-C) A graphical representation of the pattern of expression and class of metabolites clustered together in a hierarchical clustering analysis (Pearson correlation with complete linkage) of the cell cycle data.

The average of the control normalized S/N of the masses in each of the clusters has been graphed in a line plot on the left hand side. The grey lines above and below the average S/N represents the standard deviation between masses within the cluster. The pie charts on the right hand side of the figure show the putatively identified metabolite classes of each cluster, as well as the percentage of each class that was identified. Figures continued on next page.

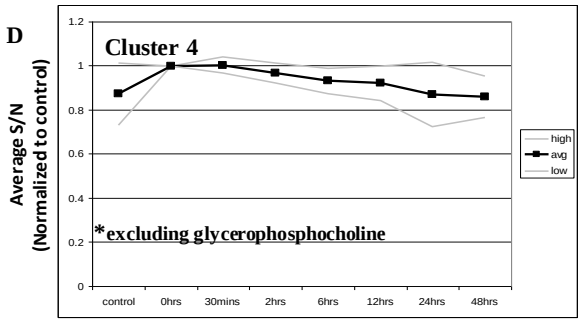

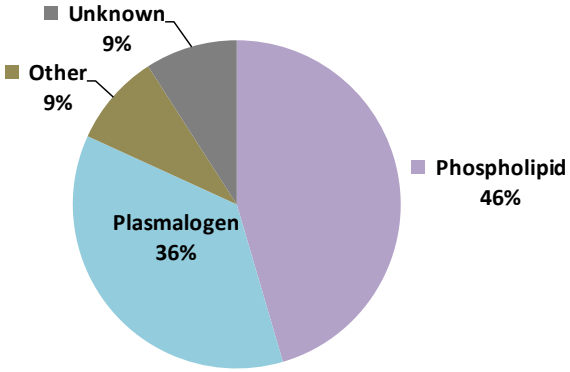

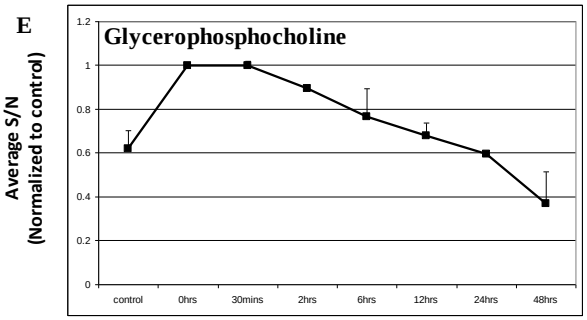

Glycerophosphocholine (Located within cluster 4)

Figure 4-6 (D,E). A graphical representation of the pattern of expression, and class of metabolites, clustered together in a hierarchical clustering analysis (Pearson correlation with complete linkage) of the Cell Cycle data.

The metabolites in the third cluster slightly decreased after the serum starvation, whereas the metabolites in the fourth cluster slightly increased with the starvation and returned back to the levels detected in the control cells after 24 hours. Glycerophosphocholine was detected at increased levels after the serum starvation, and then steadily decreased after the serum was reintroduced (Figure 4.6E).

Major metabolic changes occurred in MRC5 cells during the cell cycle (Figure 4.7). The 2-acyl-1-(1-alkenyl)-sn-glycerols (VAGs) and triacylgycerols (TAGs) follow a very similar expression pattern with a drop in levels after synchronization, then an increase at 6 hours followed by a drop again at 48 hours. Glycerophosphocholine increased with synchronization and then slowly decreased until the 48 hour time point where it was virtually absent. Glutathione levels decreased at 6 hours, but then by 12 hours the level began to increase and by 48 hours it had reached levels similar to what was measured in the control sample. Phosphatidylcholine levels increased upon synchronization and remained at constant levels across all samples. Lastly, the phosphatidylethanolamine plasmalogens also appeared to stay at quite constant levels across all of the time points. These results implicate several classes of lipids in the progression of the cell cycle, in particular TAGs and VAGs.

4.1.4 Confirmation of Metabolite Identifications using High Throughput Triple Quadrupole Analysis

A high-throughput method was developed on a Multiple Reaction Monitoring (MRM) Triple Quadrupole (TQ-MRM) to analyze 2-Acyl-1-(1-alkenyl)-sn-glycerols (VAGs) and Triacylglycerols (TAGs) levels in the MRC5 cell extracts (Figure 4.8). This high throughput approach is based on the analysis of parent-daughter fragmentation (MRM) for the quantification of specific analytes of interest. Using a targeted method to measure the levels of VAGs and TAGs will determine if the metabolite identifications that were made from the FTICR-MS data are correct. High-throughput TQ-MRM analysis of the MRC5 cell extracts (triplicate samples for each time point) showed similar results to those found with the initial FTICR-MS analysis; increases in both VAGs and TAGs when the cells re-enter the cell cycle after the serum starvation (Figure 4.8). The TAGs significantly ($p<0.05$) increased in the cells 12 hours after the serum levels were returned to normal, whereas the VAGs were detected at significantly ($p<0.05$) elevated levels 6 hours after the serum starvation. These results were

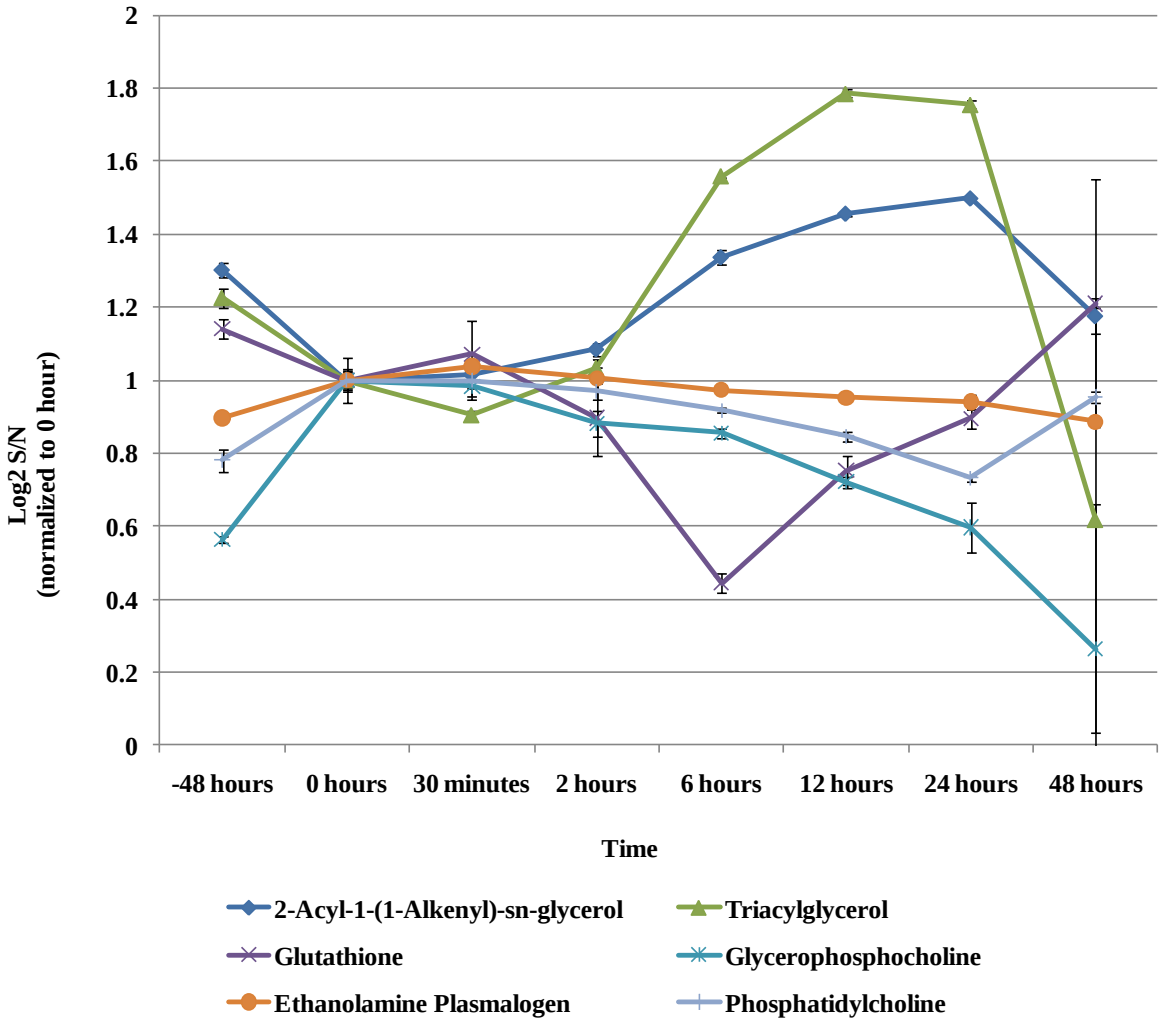

Figure 4.7 The relative intensities (log2, normalized to the 0 hour sample) of seven metabolites that show the most change during the progression of MRC5 cells through the cell cycle.

Relative levels of 2-Acyl-1-(1-alkenyl)-sn-glycerols (VAGs), Triacylglycerols (TAGs), glycerophosphocholine, ethanolamine plasmalogens and phosphatidylcholines as MRC5 cells progress through the cell cycle. Data has been normalized to the 0 hour time point. The -48 hour time point was collected 48 hours prior to serum starvation; the cells were therefore not a synchronously growing population. All of the masses have $p<0.001$ as assessed by Student's *t*-test. Error bars represent the standard deviation between replicate samples.

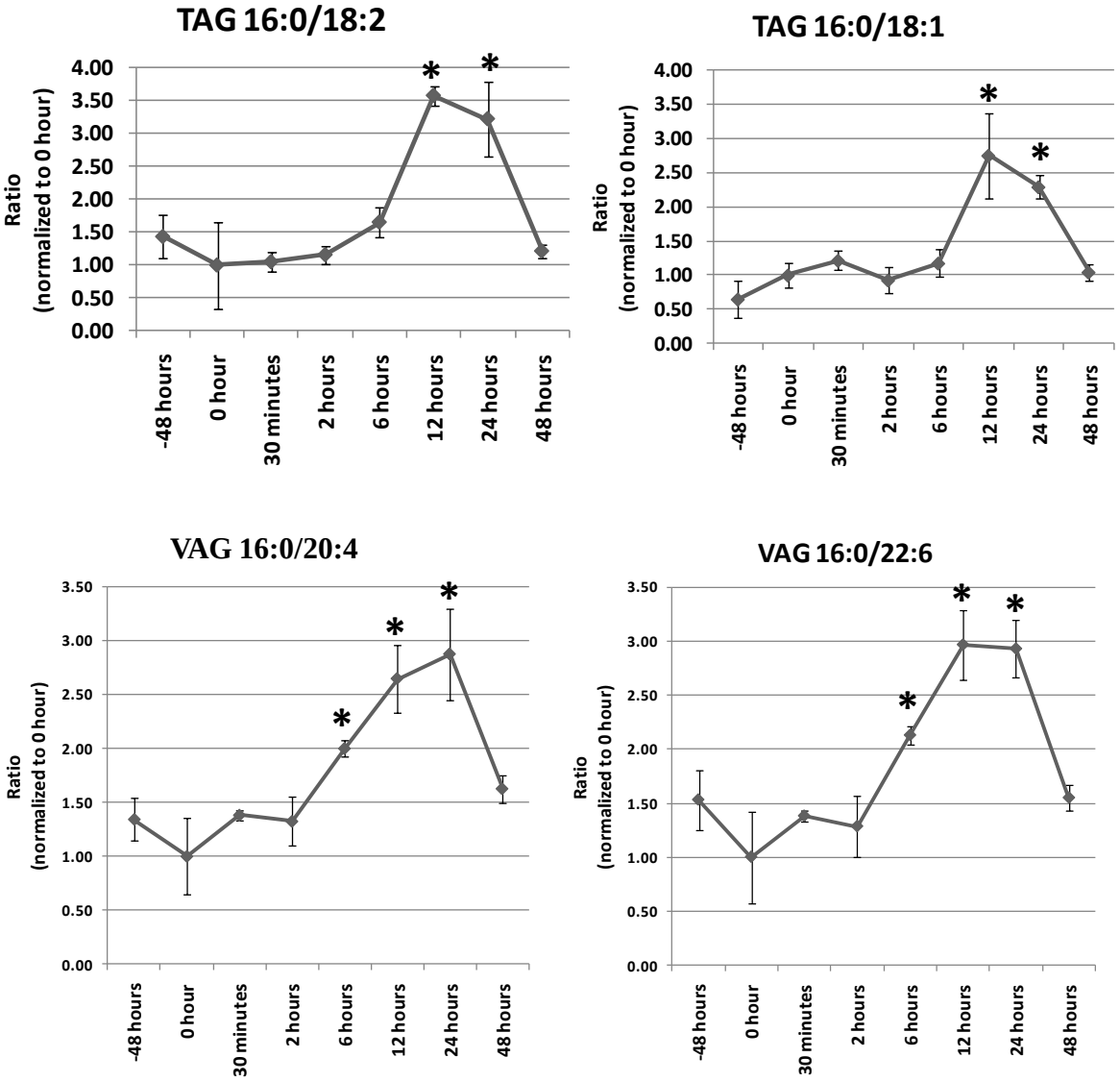

Figure 4.8 High-throughput analyses of 2-acyl-1-(1-alkenyl)-sn-glycerols (VAGs) and triacylglycerols (TAGs) in MRC5 cells as they progress through the cell cycle.
Cell extracts were analyzed with a high throughput analysis (MRM- triple quadrupole method) to confirm the putative identifications made from the FTICR-MS analysis. The four plots show the increase of VAGs and TAGs within 12 hours of treatment. * $p<0.05$ relative to the 0 hour time point. Error bars represent the standard deviation between replicate samples.

consistent with the FTICR-MS data.

4.1.5 Real Time Polymerase Chain Reaction of MRC5 Cells

2-Acyl-1-(1-alkenyl)-sn-glycerols and diacylglycerols are both generated by Phospholipase C (PLC)-mediated cleavage of ethanolamine plasmalogens and phospholipids respectively. PLC enzymes cleave the polar head group from phospholipids at the phosphate group located at the sn3 position of the lipid (Katan, 2005). There are six different families of PLC enzymes; γ, ε, β, η, ζ and δ, and within each family there are multiple isoforms (Katan, 2005). A recent publication has demonstrated that diacylglycerols that are derived from plasma membrane phospholipids, through the action of PLC, are mainly used for triacylglycerol synthesis (Igal *et al.*, 2001). It was therefore decided to examine PLC transcript levels in the MRC5 cells as they progressed through the cell cycle (Figure 4.9). A selection of four PLC isoforms: γ2, ε1, β1, and δ4 were analyzed. PLCβ and PLCδ have both been found to localize in the cleavage furrow during cytokinesis (Naito *et al.*, 2006), and were therefore selected for analysis. I also selected PLCγ and ε as they are regulated differently than the other PLC isoforms. Most of the PLC isoforms are regulated by the GTP-binding subunits of G-proteins, interestingly PLCγ is regulated through receptor and non-receptor tyrosine kinases and PLCε is regulated directly by GTPases from the Ras family (Katan, 2005). PLCβ1 mRNA levels did not significantly change as the cells progressed through the cell cycle (Figure 4.9). PLCγ2 and ε had similar mRNA expression patterns, showing increases following synchronization (when the cells are in G0) and again 12hr after the serum had been added back into the media (possibly corresponding to the G1-S transition) (Figure 4.9). PLCδ4 showed an increase in mRNA following synchronization and then steadily decreased as the cells progressed through the cell cycle (Figure 4.9). The corresponding increase of PLC γ, ε, and δ gene expression to the induction of VAGs and TAGs, suggests that these genes may be involved in the metabolic shift that occurs 12 hours after synchronization.

4.1.6 Discussion

As far as I am aware, the work presented in this section is the first non-targeted examination of metabolic changes that accompany cell cycle progression. The cell cycle is a

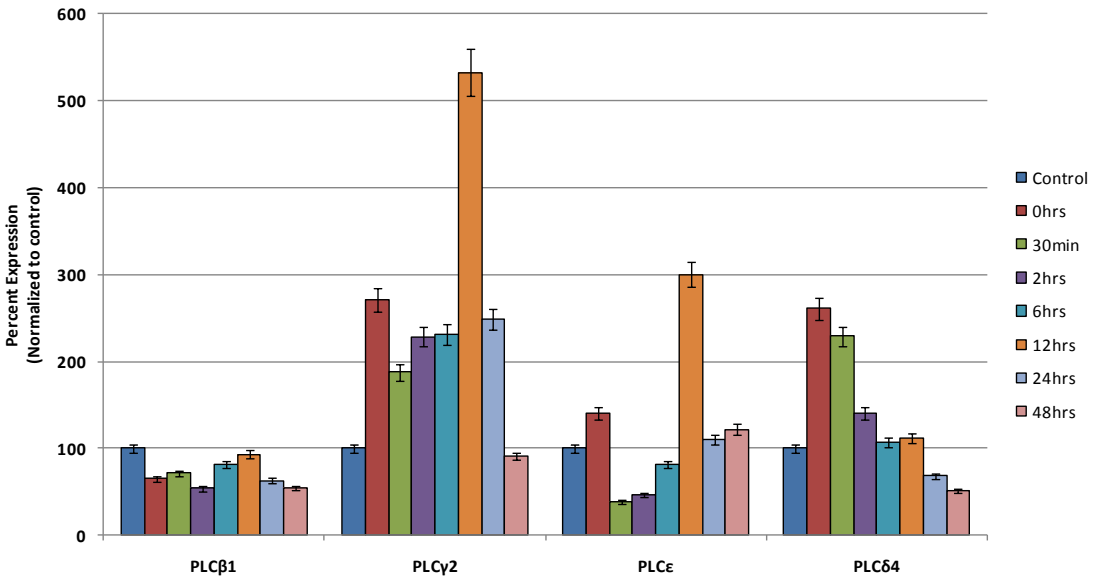

Figure 4.9 Real time PCR analyses of phospholipase-C (PLC)-β, γ, ε, and δ expression in MRC5 cells as they progress through the cell cycle.

Real-time PCR was completed to quantify the expression of PLC in MRC5 cells as they progressed through the cell cycle. Four isoforms of PLC were selected for analysis: PLCβ1, PLCγ2, PLCε, and PLCδ4. All results were normalized to the control cells. Error bars represent the standard deviation between replicate samples.

tightly controlled process, with checkpoints throughout the cycle to insure that errors do not take place, and that damaged cells are not able to divide. The most important checkpoints in the cell cycle are at the G1/S and G2/M transitions, as it is at these points in the cell cycle where cancer related defects can occur (Erson and Petty, 2004). Upon synchronization of the cells, levels of TAGs, VAGs and glutathione slightly decrease, and glycerophosphocholine and phospholipids slightly increase. Our results suggest that there is a robust elevation of triacylglycerols (TAGs) and 2-acyl-1-(1-alkenyl)-sn-glycerols (VAGs) which steadily accumulate up to the point of cell division. It is likely that the MRC5 cells reached the G0/G1 transition within 6 hours following the synchronization (Memili *et al.*, 2004), and the G2/M transition was reached between 12 and 24 hour post synchronization (results collected from flow cytometry analysis). The increase in the TAGs and VAGs may be linked to the checkpoints in the cell cycle.

2-Acyl-1-(1-alkenyl)-sn-glycerols and diacylglycerols (DAGs) are generated by PLC-mediated cleavage of ethanolamine plasmalogens and phospholipids respectively. It has been reported that PLCδ_1 accumulated in the nucleus of cells at the G1/S boundary and the G0 phase of the cell cycle (Stallings *et al.*, 2005). A siRNA knockdown strategy that specifically targeted PLCδ_1 significantly decreased proliferation of rat C6 glioma cells and altered S phase progression in the cell cycle (Stallings *et al.*, 2008). Another group discovered that the interaction of AKT and PLCγ regulates the G2/M transition in the cell cycle, and in fact if this interaction is blocked, the cell arrests in the G2 stage of the cell cycle (Browaeys-Poly *et al.*, 2009).

The elevated transcript levels of PLC γ, ε, and δ in the MRC5 cells as they progress through the cell cycle may be connected to the elevated levels of TAGs and VAGs. Several papers have recently been published linking PLC, AKT, DAGs and plasmalogens to the cell cycle (Sun *et al.*, 1997; Albi *et al.*, 2004; Browaeys-Poly *et al.*, 2009). It has been proven that DAGs are cell cycle regulated, and that they are detected at increased levels at the G2/M transition phase of the cell cycle due to an increase in PLC activity (Sun *et al.*, 1997). The DAGs that are generated by the PLC activity are believed to be responsible for the activation of the nuclear protein kinase C (PKC) during the late G2 phase of the cycle, which is required for the transition into the mitotic phase (Sun *et al.*, 1997). Inhibition of PLC activity halts the cells in the G2 phase of the cell cycle (Sun *et al.*, 1997).

Another interesting observation is that AKT regulates the activity of PLCγ, and if the AKT-PLCγ interaction is disrupted, the entry into the mitotic phase of the cell cycle is expedited in MDA-MB-231 breast cancer cells (Browaeys-Poly *et al.*, 2009). AKT regulates both PLC and Checkpoint with forkhead and ring finger domains (Chfr) through phosphorylation, which in turn allows the release of the G2 checkpoint and the transition into the M phase of the cell cycle (Browaeys-Poly *et al.*, 2009). Chfr plays an important role as a checkpoint protein during the G2/M transition, as its activation holds the cell cycle in prophase by inhibiting the phosphorylation of cell division control protein 2 homolog (CDC2), more commonly known as cyclin dependent kinase 1 (CDK1) (Erson and Petty, 2004). CDK1 forms a complex with cyclin B1, referred to as the maturation promoting factor or the mitosis promoting factor (MPF) (Lindqvist *et al.*, 2009). If the interaction of AKT and PLCγ is inhibited, AKT phosphorylates Chfr, inactivating the checkpoint protein and expediting the transition into the M phase of the cycle (Browaeys-Poly *et al.*, 2009). There have also been recent studies which have identified reduced expression and mutations of Chfr in multiple cancer cell lines (Erson and Petty, 2004). Therefore, it may be interesting to examine cancer cells as they progress through the cell cycle to determine if the reduced regulation of the G1/S and G2/M transitions affects the expression of PLC and the synthesis of lipids (in particular TAGs, DAGs and VAGs).

A research group from Italy has identified plasmalogens as potential regulators of phosphatidylcholine-dependent phospholipase C (PC-PLC) and the cell cycle (Albi *et al.*, 2004). The lipid fraction of chromatin is a minor component; however, it plays an important role in cell proliferation (Albi and Viola Magni, 2004). The chromatin lipids, including phospholipids, cholesterol and plasmalogens, increase during DNA replication and are often localized to newly synthesized RNA in condensed chromatin (Albi and Viola Magni, 2004). The fraction of plasmalogens to diacyl-phospholipids in the chromatin is higher than that present in the homogenate, cytosol and nuclear membranes (Albi *et al.*, 2004). They also discovered that PC-PLC has a higher affinity for ether phospholipids as compared to the diacyl equivalents (Albi *et al.*, 2004). The hypothesis that has resulted from this work is that plasmalogens are transported into the nucleus where they activate PC-PLC to produce alkyl-acyl glycerols, which, in turn, stimulate PKC. The detection of increased VAGs at the G2/M

transition in the MRC5 cells may be linked to the activity of PC-PLC on plasmalogens in the chromatin and cellular membranes.

I was unable to conclude whether the observed induction of lipids is an obligate requirement for cell division, or whether it is simply an associated effect. Initial efforts had examined the possibility of inhibiting Phospholipase C, using an inhibitor for PLC, such as U-73122 (Liu *et al.*, 2004a). I hypothesized that if the results indicated that cells were unable to progress through the cell cycle following addition of the serum in the presence of the PLC inhibitor, then it would be possible to suggest that the changes in the lipid profile would be a requirement for cell cycle progression. However, it became evident that simply inhibiting PLC was not going to provide the targeted inhibition of the synthesis of TAGs and VAGs that I had hoped for. A more specific inhibitor or knock-down system is required to effectively complete this experiment.

4.2 Metabolomic Changes Associated With Differentiation

4.2.1 Data Alignment and Array Generation

Undifferentiated monocytic U937 cells were treated with phorbol 12-myristate 13-acetate (PMA), a protein kinase C activator, which induces maturation from a monocytic cell into a macrophage (Kitamura *et al.*, 2004). The cells begin a number of phenotypic changes during this process, including adherence to the plate surface, gain of macrophage characteristics (phagocytosis, antibody-dependent cellular cytotoxicity, antigen presentation and chemotaxis), and the loss of proliferative potential (Kwon and Kim, 2003; Verhoeckx *et al.*, 2004). Photographs were taken at each time point during the PMA treatment to document the hallmark phenotypic changes that occur during differentiation, such as rapid adherence, followed by the progression into macrophages within 24 hours of treatment (Figure 4.10).

The U937 cells were harvested at various time points throughout the differentiation process and analyzed using flow injection FTICR-MS as described in the previous section. A total of 1,589 masses were detected when the U937 cells were analysed with the FTICR-MS. The complete dataset was subject to a Student's *t*-test, resulting in 386 masses with $p < 0.001$ (Figure 4.11). The resulting spectra were aligned in an array, which is organized with the masses detected, and the analysis modes they were detected in, on the left hand side of the

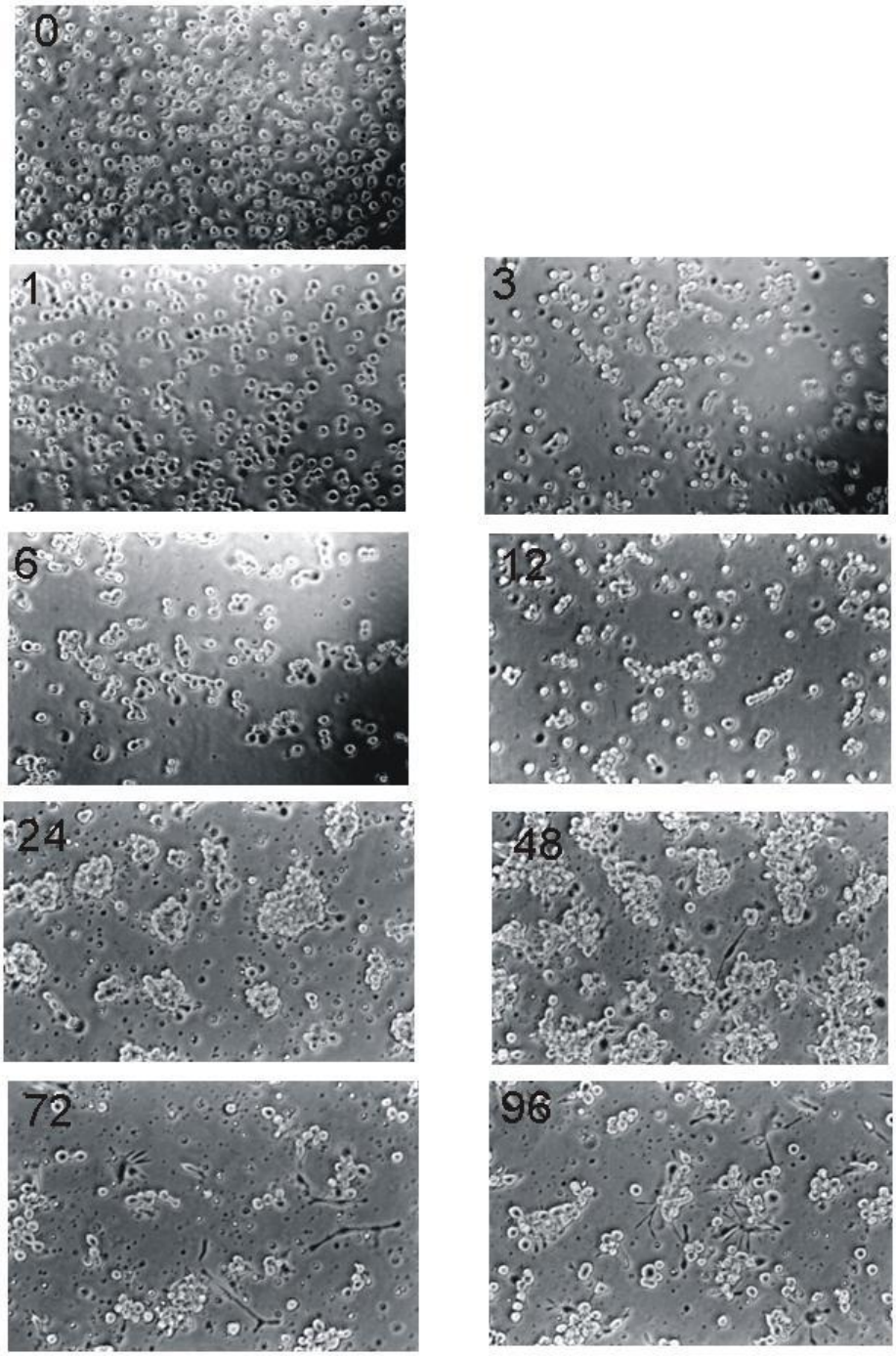

Figure 4.10 Photographs taken from 0 to 96 hours during treatment of U937 cells with phorbol 12-myristate-13-acetate (PMA).
Cells begin to attach after 1 hour of treatment with PMA, a protein kinase C activator. After 48 hours of treatment, cells are beginning to differentiate into macrophages, as evident by the long dark spindle looking cells that can be seen in the pictures taken at 48, 72 and 96 hours.

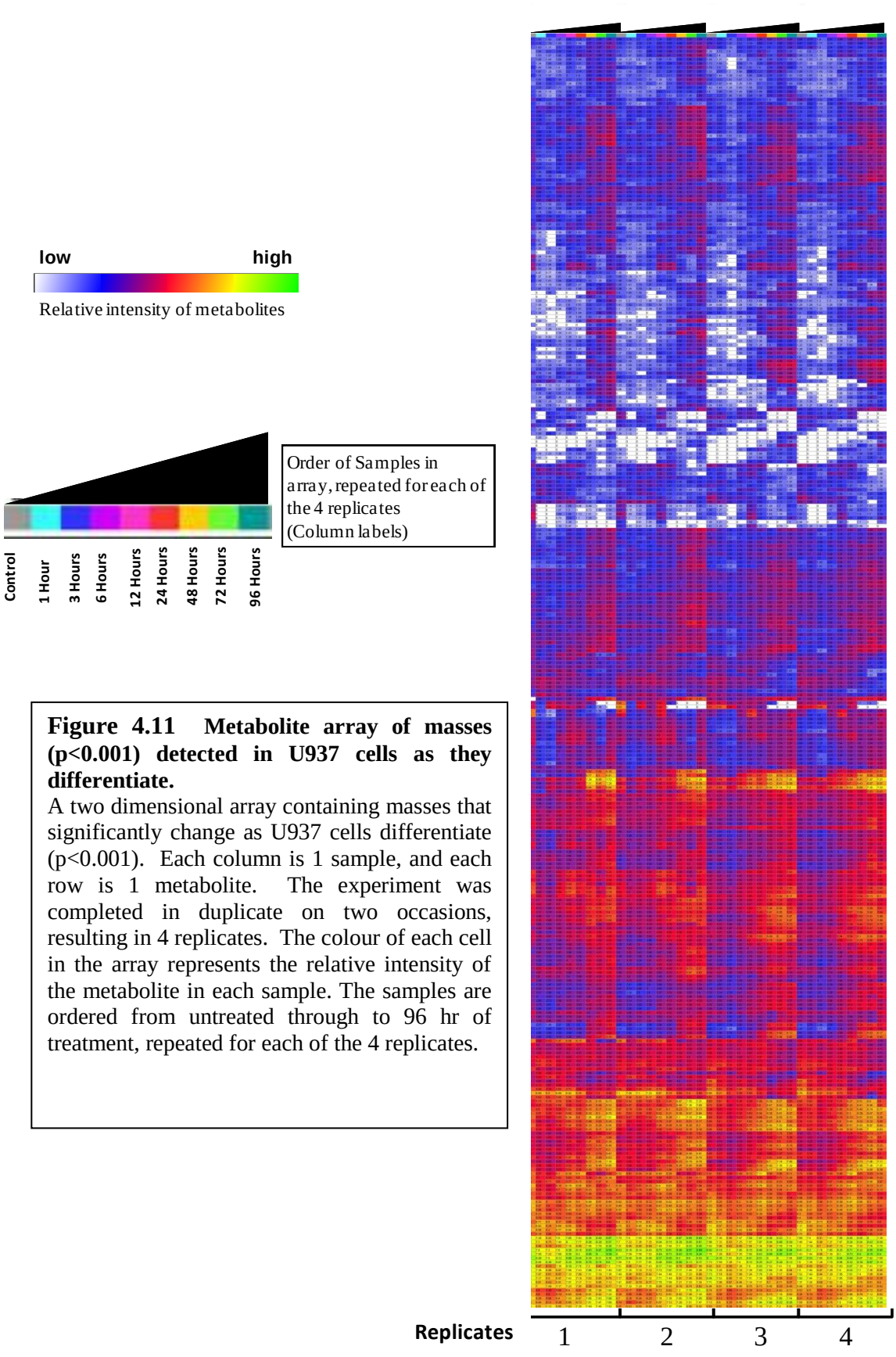

Figure 4.11 Metabolite array of masses ($p<0.001$) detected in U937 cells as they differentiate.
A two dimensional array containing masses that significantly change as U937 cells differentiate ($p<0.001$). Each column is 1 sample, and each row is 1 metabolite. The experiment was completed in duplicate on two occasions, resulting in 4 replicates. The colour of each cell in the array represents the relative intensity of the metabolite in each sample. The samples are ordered from untreated through to 96 hr of treatment, repeated for each of the 4 replicates.

array (coloured grey). Each row in the array contains the data for a single unique mass. Each individual sample is listed along the top of the array, and they have been ordered from the control (monocytes) through to the cells collected at 96 hours (left to right). This is repeated for the other three replicates. The relative intensities (log_2 transformed) of the masses have been coloured according to the scale located to the left of the array. The R^2 value for the entire experiment was found to be 0.78, which is acceptable considering that the two duplicate experiments were performed a few months apart.

4.2.2 Unsupervised Statistical Analyses

The principal component analysis of the dataset ($p<0.001$) showed a clear separation of the samples (Figure 4.12), which suggested changes in the metabolome of the cells as they transition from monocytes into macrophages. The samples collected during the 48, 72 and 96 hour time points clearly separated from the earlier time points, and the 12 and 24 hour samples appear to be in transition between the early and later time points across PC1. This suggested that there were minimal metabolic changes taking place within the first six hours, and that the most dramatic changes occurred between 6 and 48 hours after PMA addition.

The masses responsible for the separation of the samples in the PCA analysis are listed in Table 4.3. These are the masses with the most positive and negative loadings scores from the principal component analysis. The top half of the table contains the masses that increase during differentiation (positive PC1 loadings score, highlighted green). Each mass has been assigned a putative formula and metabolite identification. The last column in the table shows the possible combinations of fatty acid side chains of the identified lipids. From these identifications it appears that an increase in plasmalogens (1-Alkenyl-2-Acyl-plasmenyl phosphatidylethanolamines) occurs in U937 cells as they differentiate into macrophages. Another group of metabolites that increase during differentiation have been identified as 1-alkenyl-2-Acyl-sn-glycerols. These molecules, also known as vinyl acyl glycerols (VAGs), are vinyl ether lipids synthesized in the same metabolic pathway as plasmalogens. The masses that were found to decrease during differentiation are listed in the bottom half of the table (negative PC1 loadings score, highlighted red). There does not seem to be a specific family of metabolites that decrease during differentiation. Adducts of diacyl phospholipids (both

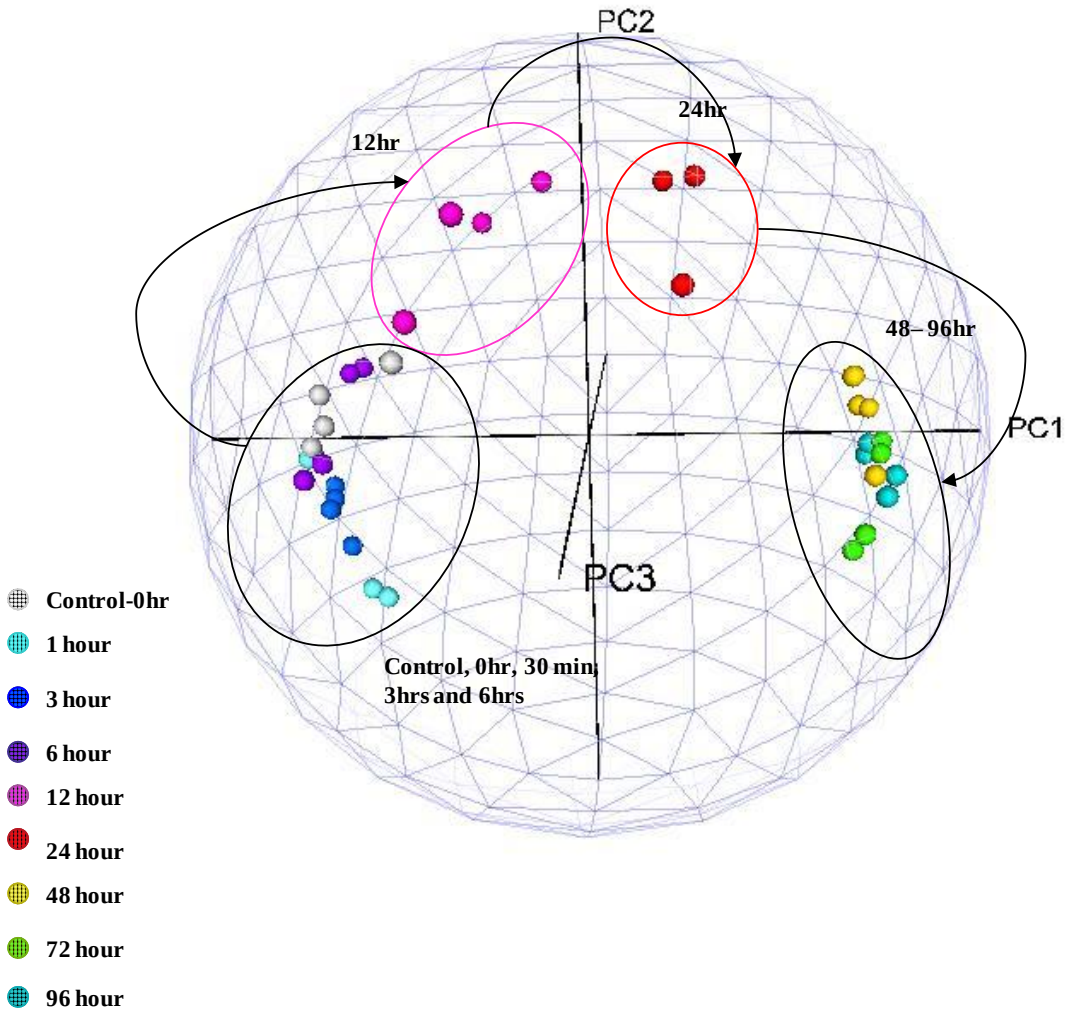

Figure 4.12 Principal component analysis of metabolites ($p<0.001$) detected in U937 cells as they differentiate.

PCA is a linear transformation that converts data to a new coordinate system such that the greatest variance within the data comes to lie on the first coordinate (called the first principal component, PC1), the second greatest variance on the second coordinate (PC2), and so on. The closer the samples cluster together in a PCA plot the more metabolically similar they are. The 48, 72 and 96 hour time points cluster on the right hand side of PC1, separately from the 12 and 24 hour samples which appear to be in a transition between the early time points and the later time points.

Table 4.3 Metabolites responsible for the separation of differentiating U937 samples in the principal component analysis (PCA).

Masses that increase during differentiation are listed in the top portion of the table (positive loadings score, highlighted green), and the masses that decrease during differentiation are at the bottom of the table (negative loadings score, highlighted red). The first column contains the detected mass. The second column lists the analysis mode that the mass was detected in. The third column contains the loadings score from the PCA. The center of the table displays the array, showing the relative intensity of the masses in each of the samples. The last three columns list the putative formula and metabolite identifications.

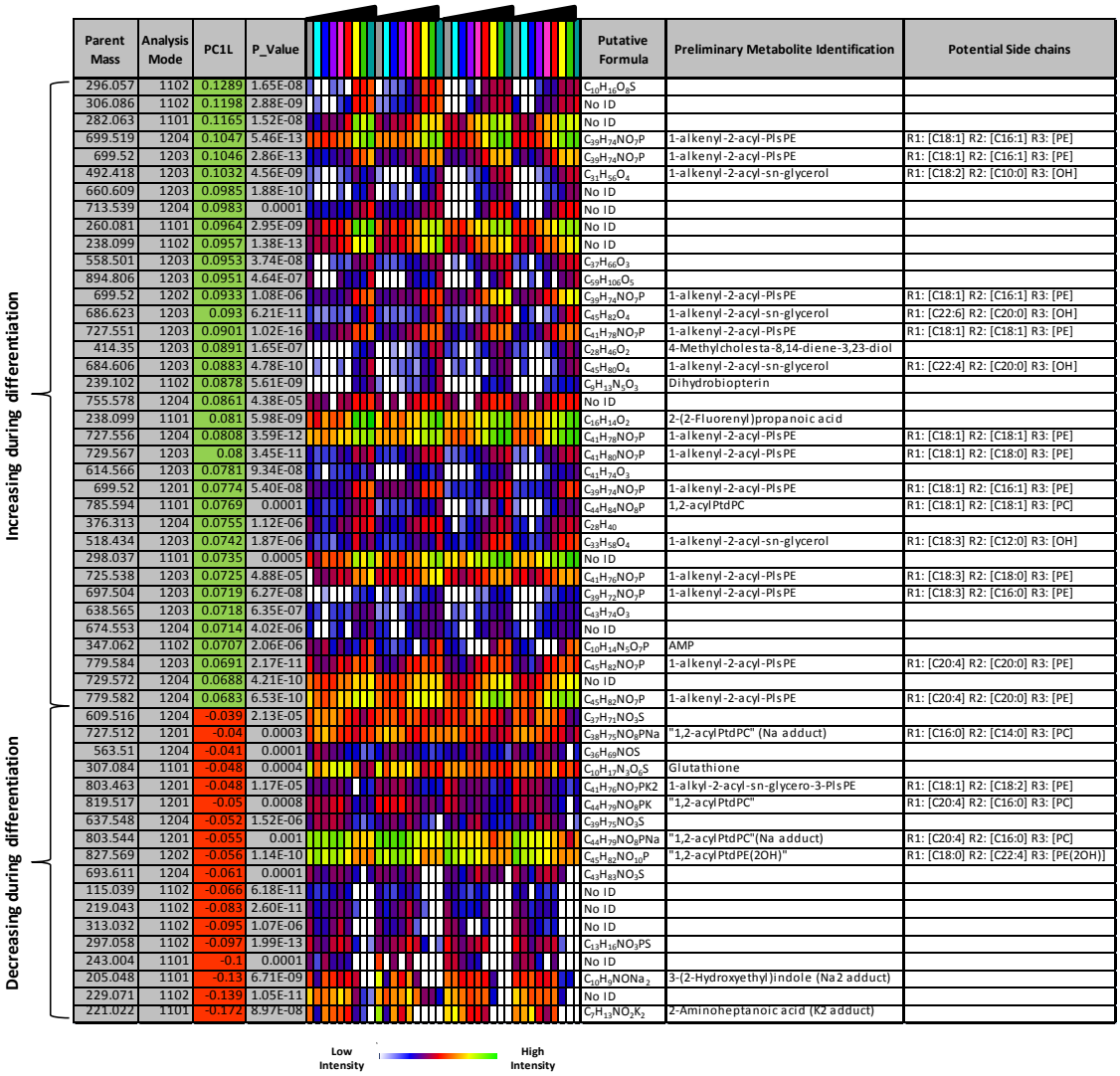

	Parent Mass	Analysis Mode	PC1L	P_Value	Putative Formula	Preliminary Metabolite Identification	Potential Side chains
Increasing during differentiation	296.057	1102	0.1289	1.65E-08	$C_{10}H_{16}O_6S$		
	306.086	1102	0.1198	2.88E-09	No ID		
	282.063	1101	0.1165	1.52E-08	No ID		
	699.519	1204	0.1047	5.46E-13	$C_{39}H_{74}NO_7P$	1-alkenyl-2-acyl-PlsPE	R1: [C18:1] R2: [C16:1] R3: [PE]
	699.52	1203	0.1046	2.86E-13	$C_{39}H_{74}NO_7P$	1-alkenyl-2-acyl-PlsPE	R1: [C18:1] R2: [C16:1] R3: [PE]
	492.418	1203	0.1032	4.56E-09	$C_{31}H_{56}O_4$	1-alkenyl-2-acyl-sn-glycerol	R1: [C18:2] R2: [C10:0] R3: [OH]
	660.609	1203	0.0985	1.88E-10	No ID		
	713.539	1204	0.0983	0.0001	No ID		
	260.081	1101	0.0964	2.95E-09	No ID		
	238.099	1102	0.0957	1.38E-13	No ID		
	558.501	1203	0.0953	3.74E-08	$C_{37}H_{66}O_3$		
	894.806	1203	0.0951	4.64E-07	$C_{59}H_{106}O_5$		
	699.52	1202	0.0933	1.08E-06	$C_{39}H_{74}NO_7P$	1-alkenyl-2-acyl-PlsPE	R1: [C18:1] R2: [C16:1] R3: [PE]
	686.623	1203	0.093	6.21E-11	$C_{45}H_{82}O_4$	1-alkenyl-2-acyl-sn-glycerol	R1: [C22:6] R2: [C20:0] R3: [OH]
	727.551	1203	0.0901	1.02E-16	$C_{41}H_{78}NO_7P$	1-alkenyl-2-acyl-PlsPE	R1: [C18:1] R2: [C18:1] R3: [PE]
	414.35	1203	0.0891	1.65E-07	$C_{28}H_{46}O_2$	4-Methylcholesta-8,14-diene-3,23-diol	
	684.606	1203	0.0883	4.78E-10	$C_{45}H_{80}O_4$	1-alkenyl-2-acyl-sn-glycerol	R1: [C22:4] R2: [C20:0] R3: [OH]
	239.102	1102	0.0878	5.61E-09	$C_5H_{13}N_5O_3$	Dihydrobiopterin	
	755.578	1204	0.0861	4.38E-05	No ID		
	238.099	1101	0.081	5.98E-09	$C_{16}H_{14}O_2$	2-(2-Fluorenyl)propanoic acid	
	727.556	1204	0.0808	3.59E-12	$C_{41}H_{78}NO_7P$	1-alkenyl-2-acyl-PlsPE	R1: [C18:1] R2: [C18:1] R3: [PE]
	729.567	1203	0.08	3.45E-11	$C_{41}H_{80}NO_7P$	1-alkenyl-2-acyl-PlsPE	R1: [C18:1] R2: [C18:0] R3: [PE]
	614.566	1203	0.0781	9.34E-08	$C_{41}H_{74}O_3$		
	699.52	1201	0.0774	5.40E-08	$C_{39}H_{74}NO_7P$	1-alkenyl-2-acyl-PlsPE	R1: [C18:1] R2: [C16:1] R3: [PE]
	785.594	1101	0.0769	0.0001	$C_{44}H_{84}NO_8P$	1,2-acylPtdPC	R1: [C18:1] R2: [C18:1] R3: [PC]
	376.313	1204	0.0755	1.12E-06	$C_{28}H_{40}$		
	518.434	1203	0.0742	1.87E-06	$C_{33}H_{58}O_4$	1-alkenyl-2-acyl-sn-glycerol	R1: [C18:3] R2: [C12:0] R3: [OH]
	298.037	1101	0.0735	0.0005	No ID		
	725.538	1203	0.0725	4.88E-05	$C_{41}H_{76}NO_7P$	1-alkenyl-2-acyl-PlsPE	R1: [C18:3] R2: [C18:0] R3: [PE]
	697.504	1203	0.0719	6.27E-08	$C_{39}H_{72}NO_7P$	1-alkenyl-2-acyl-PlsPE	R1: [C18:3] R2: [C16:0] R3: [PE]
	638.565	1203	0.0718	6.35E-07	$C_{43}H_{74}O_3$		
	674.553	1204	0.0714	4.02E-06	No ID		
	347.062	1102	0.0707	2.06E-06	$C_{10}H_{14}N_5O_7P$	AMP	
	779.584	1203	0.0691	2.17E-11	$C_{45}H_{82}NO_7P$	1-alkenyl-2-acyl-PlsPE	R1: [C20:4] R2: [C20:0] R3: [PE]
	729.572	1204	0.0688	4.21E-10	No ID		
	779.582	1204	0.0683	6.53E-10	$C_{45}H_{82}NO_7P$	1-alkenyl-2-acyl-PlsPE	R1: [C20:4] R2: [C20:0] R3: [PE]
Decreasing during differentiation	609.516	1204	-0.039	2.13E-05	$C_{37}H_{71}NO_3S$		
	727.512	1201	-0.04	0.0003	$C_{38}H_{72}NO_8PNa$	"1,2-acylPtdPC" (Na adduct)	R1: [C16:0] R2: [C14:0] R3: [PC]
	563.51	1204	-0.041	0.0001	$C_{36}H_{69}NOS$		
	307.084	1101	-0.048	0.0004	$C_{10}H_{17}N_3O_6S$	Glutathione	
	803.463	1201	-0.048	1.17E-05	$C_{41}H_{76}NO_7PK2$	1-alkyl-2-acyl-sn-glycero-3-PlsPE	R1: [C18:1] R2: [C18:2] R3: [PE]
	819.517	1201	-0.05	0.0008	$C_{44}H_{79}NO_8PK$	"1,2-acylPtdPC"	R1: [C20:4] R2: [C16:0] R3: [PC]
	637.548	1204	-0.052	1.52E-06	$C_{39}H_{75}NO_3S$		
	803.544	1201	-0.055	0.001	$C_{44}H_{79}NO_8PNa$	"1,2-acylPtdPC"(Na adduct)	R1: [C20:4] R2: [C16:0] R3: [PC]
	827.569	1202	-0.056	1.14E-10	$C_{45}H_{82}NO_{10}P$	"1,2-acylPtdPE(2OH)"	R1: [C18:0] R2: [C22:4] R3: [PE(2OH)]
	693.611	1204	-0.061	0.0001	$C_{43}H_{83}NO_3S$		
	115.039	1102	-0.066	6.18E-11	No ID		
	219.043	1102	-0.083	2.60E-11	No ID		
	313.032	1102	-0.095	1.07E-06	No ID		
	297.058	1102	-0.097	1.99E-13	$C_{13}H_{16}NO_3PS$		
	243.004	1101	-0.1	0.0001	No ID		
	205.048	1101	-0.13	6.71E-09	$C_{10}H_9NONa_2$	3-(2-Hydroxyethyl)indole (Na2 adduct)	
	229.071	1102	-0.139	1.05E-11	No ID		
	221.022	1101	-0.172	8.97E-08	$C_7H_{13}NO_2K_2$	2-Aminoheptanoic acid (K2 adduct)	

Low Intensity — High Intensity

phosphatidylethanolamine and phosphatidylcholine) were putatively identified as metabolites that decrease during differentiation. Glutathione also appears to decrease during differentiation.

When the data set ($p<0.001$, $\log_2$ normalized) was hierarchically clustered, using a Pearson correlation, five distinct groups were revealed (Figure 4.13). The first cluster of metabolites was largely composed of ethanolamine phospholipids and small aqueous molecules (Figure 4.14a). All of the metabolites in cluster 1 slightly decreased in intensity with the addition of PMA, followed by an increase at 6 hours and a decrease after 48 hours. The second, third and fourth clusters contained metabolites that steadily increased 6 hours after the PMA treatment (Figure 4.14b,c,d). A large percentage of these metabolites have been putatively identified as plasmalogens and 2-Acyl-1-(1-alkenyl)-sn-glycerols (diacylglycerol plasmalogens). Interestingly there were not any phospholipids in these three clusters. The final cluster contained a group of metabolites that increased after 48 hours of PMA treatment (Figure 4.14e). This group was largely made up of plasmalogens and choline phospholipids.

The most dramatic metabolic changes that occurred as the cells differentiated were increased levels of plasmalogens (Figure 4.15). The masses began to increase 48 hours after PMA treatment and continued to increase until the last time point collected at 96 hours.

4.2.3 Confirmation of Lipid Changes using High Throughput Triple Quadrupole Analysis

Although the metabolite predictions from the accurate masses allowed for the putative identification of ethanolamine plasmalogens (PlsEtn) as well as potential side-chain speciation, a Multiple Reaction Monitoring (MRM) Triple Quadrupole method was developed to ensure that our preliminary identifications made from the FTICR-MS data were correct. This high throughput approach involves the selection of a specific parent mass, followed by its fragmentation (using collision induced dissociation or CID via an inert gas) into specific daughter ions. This type of analysis is like finding the 'fingerprint' of the molecule; no two molecules will have the same daughter ions. Sample extracts were re-analyzed with this method, which specifically measured phosphatidylethanolamines and ethanolamine plasmalogens. A comparison of the results between the targeted triple quadrupole method and

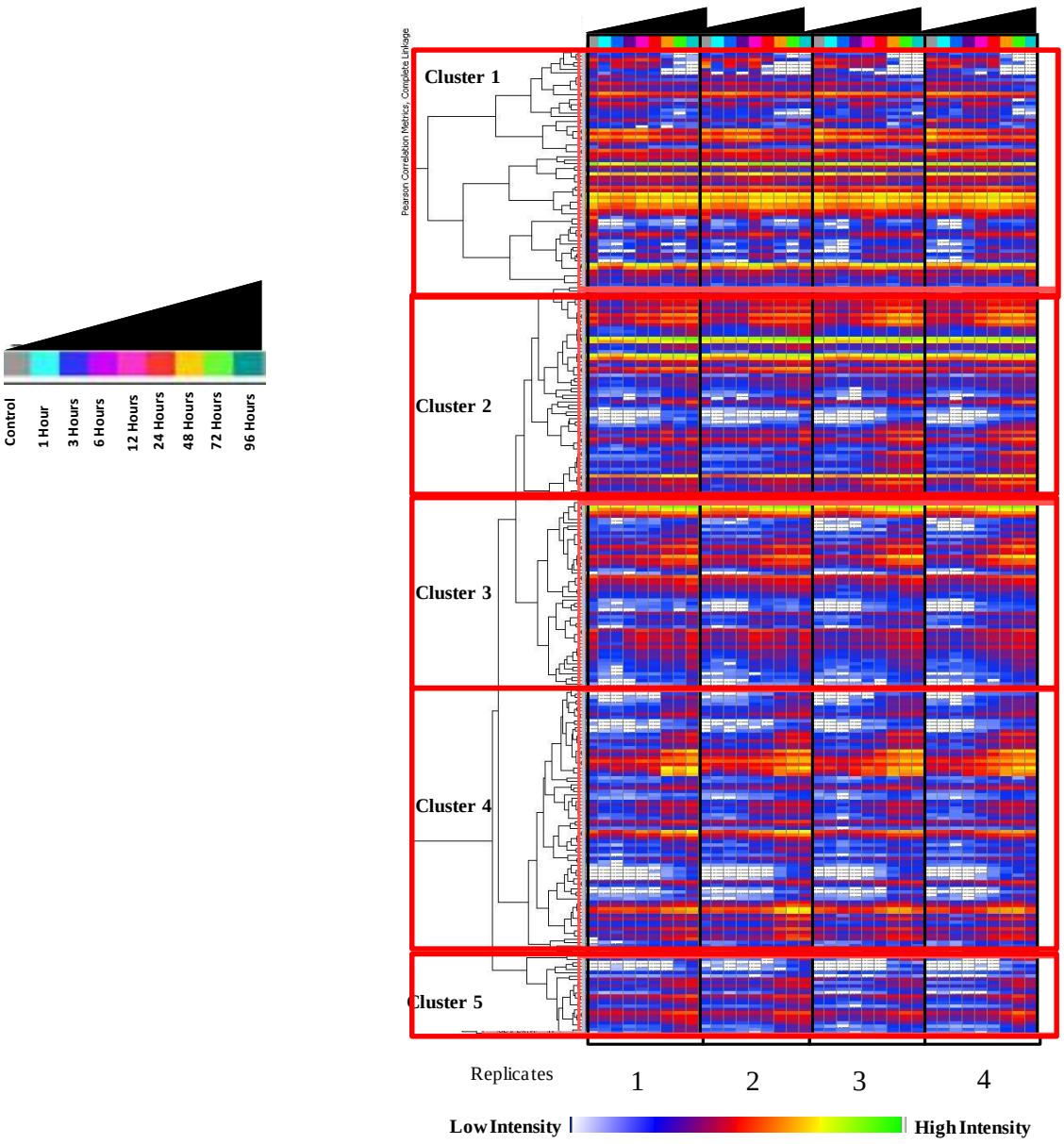

Figure 4.13 Hierarchical cluster analysis (HCA) of metabolites ($p<0.001$) detected in U937 cells as they differentiate.

Masses deemed significant ($p<0.001$) were hierarchically clustered using a Pearson correlation. Using this type of analysis will cluster together masses with similar changes in S/N across the samples. Each column is 1 sample, and each row is 1 metabolite. The color of each cell in the array represents the relative intensity of the metabolite in each sample. The samples are ordered from untreated through to 96 hours of treatment, repeated for each of the 4 replicates. The results of the HCA identified five clusters of masses.

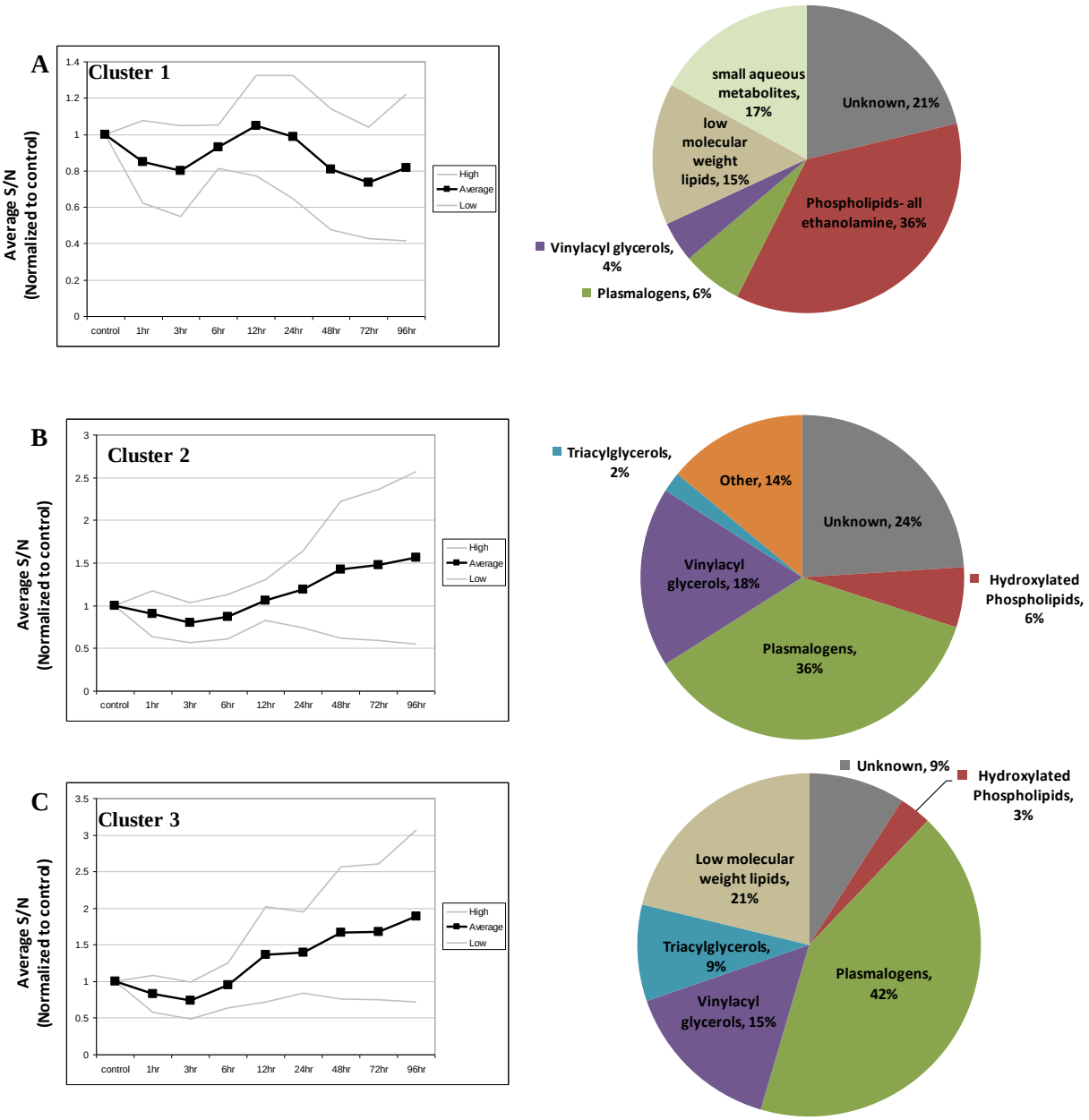

Figure 4.14(a-c) A graphical representation of the pattern of expression and class of metabolites clustered together in a hierarchical clustering analysis (Pearson correlation with complete linkage) of the U937 differentiation data.

The average of the control normalized S/N of the masses in each of the clusters has been graphed in a line plot on the left hand side. The grey lines above and below the average S/N represent the standard deviations between the masses within each cluster. The column graphs on the right hand side of the figure show the putatively identified metabolite classes of each cluster, as well as the percentage that each class contributes to the cluster. Figure continued on next page.

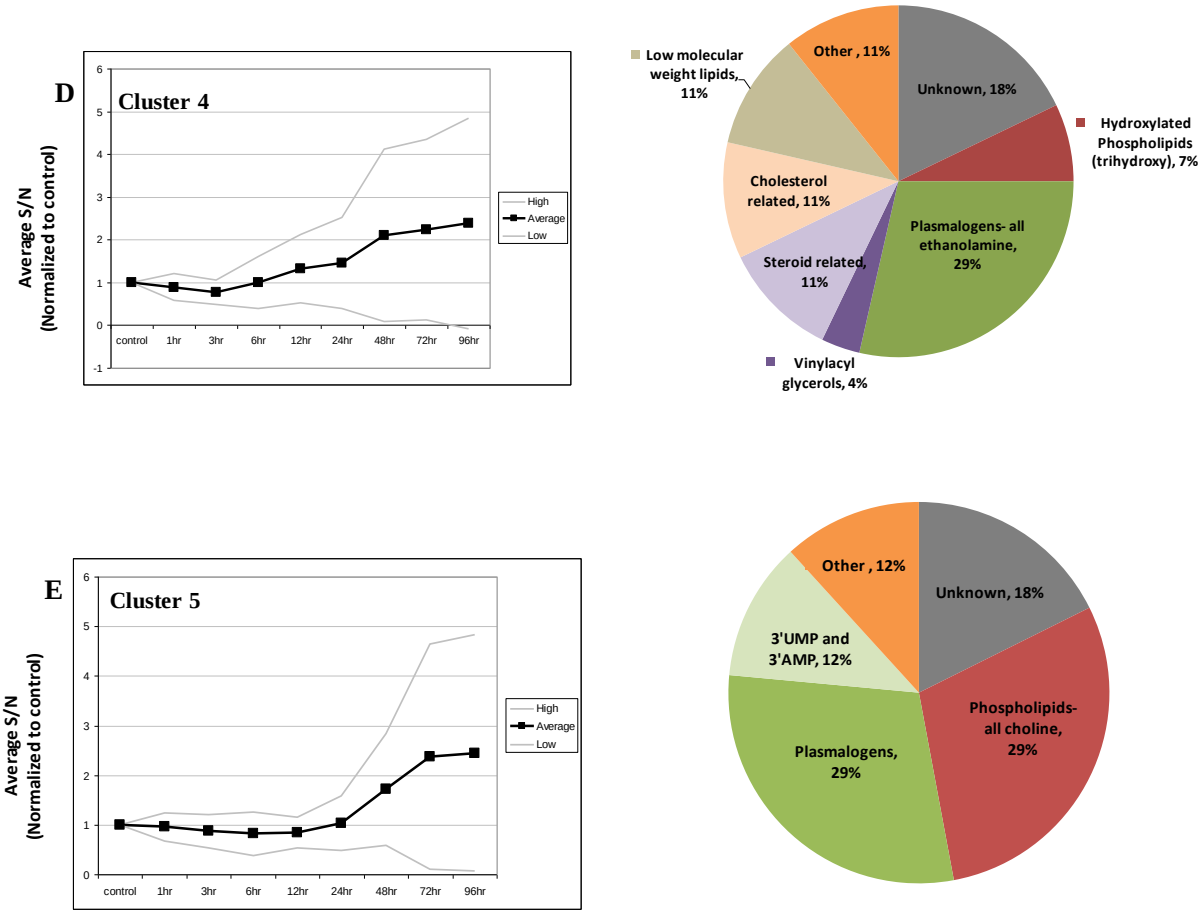

Figure 4-14 (d,e) A graphical representation of the pattern of expression and class of metabolites clustered together in a hierarchical clustering analysis (Pearson correlation with complete linkage) of the U937 differentiation data.
The average of the control normalized S/N of the masses in each of the clusters has been graphed in a line plot on the left hand side. The grey lines above and below the average S/N represent the standard deviations between the masses within each cluster. The column graphs on the right hand side of the figure show the putatively identified metabolite classes of each cluster, as well as the percentage that each class contributes to the cluster.

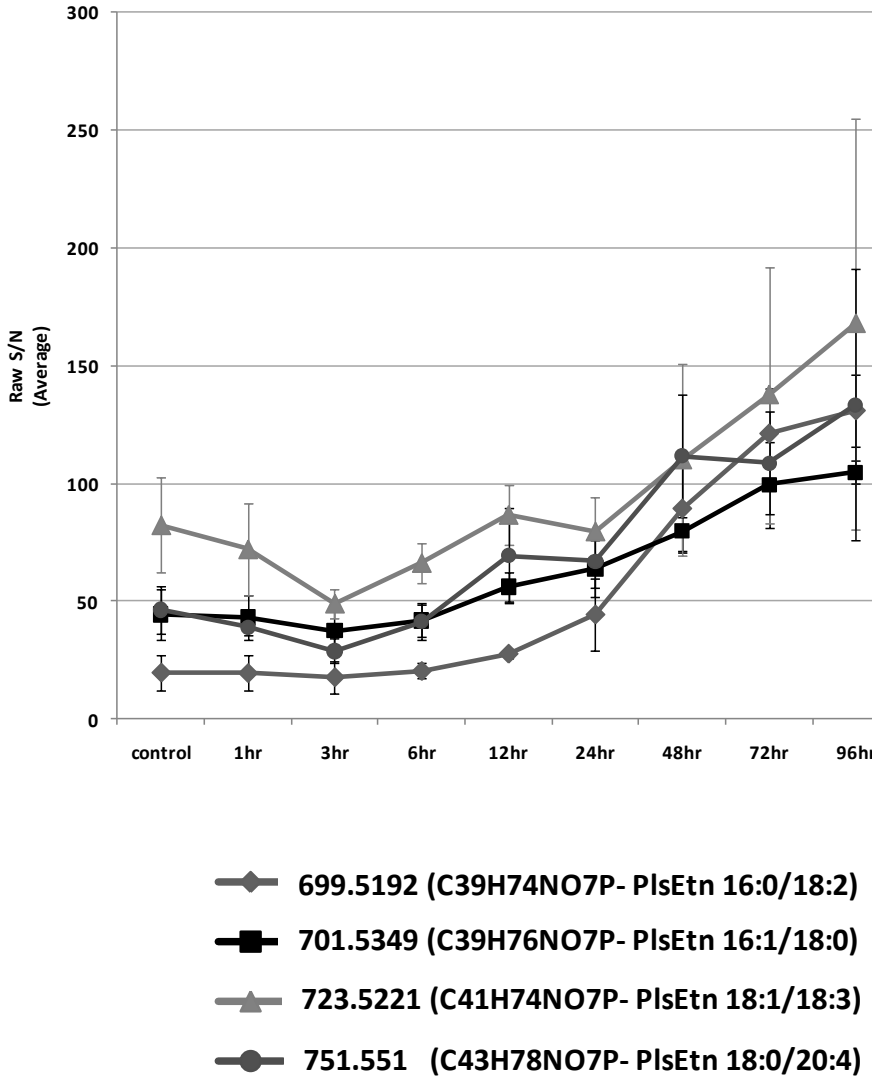

Figure 4.15 Ethanolamine plasmalogen (PlsEtn) profiles during the differentiation of U937 cells.

The average relative intensities (raw S/N) of select ethanolamine plasmalogens during the differentiation of U937 cells. The error bars represent the standard deviation between triplicate samples. The formula and the potential fatty acid side chains of each mass are listed in the legend of the figure. The error bars represent the standard deviation between replicate samples. (F-test's of these masses resulted in $p<0.001$)

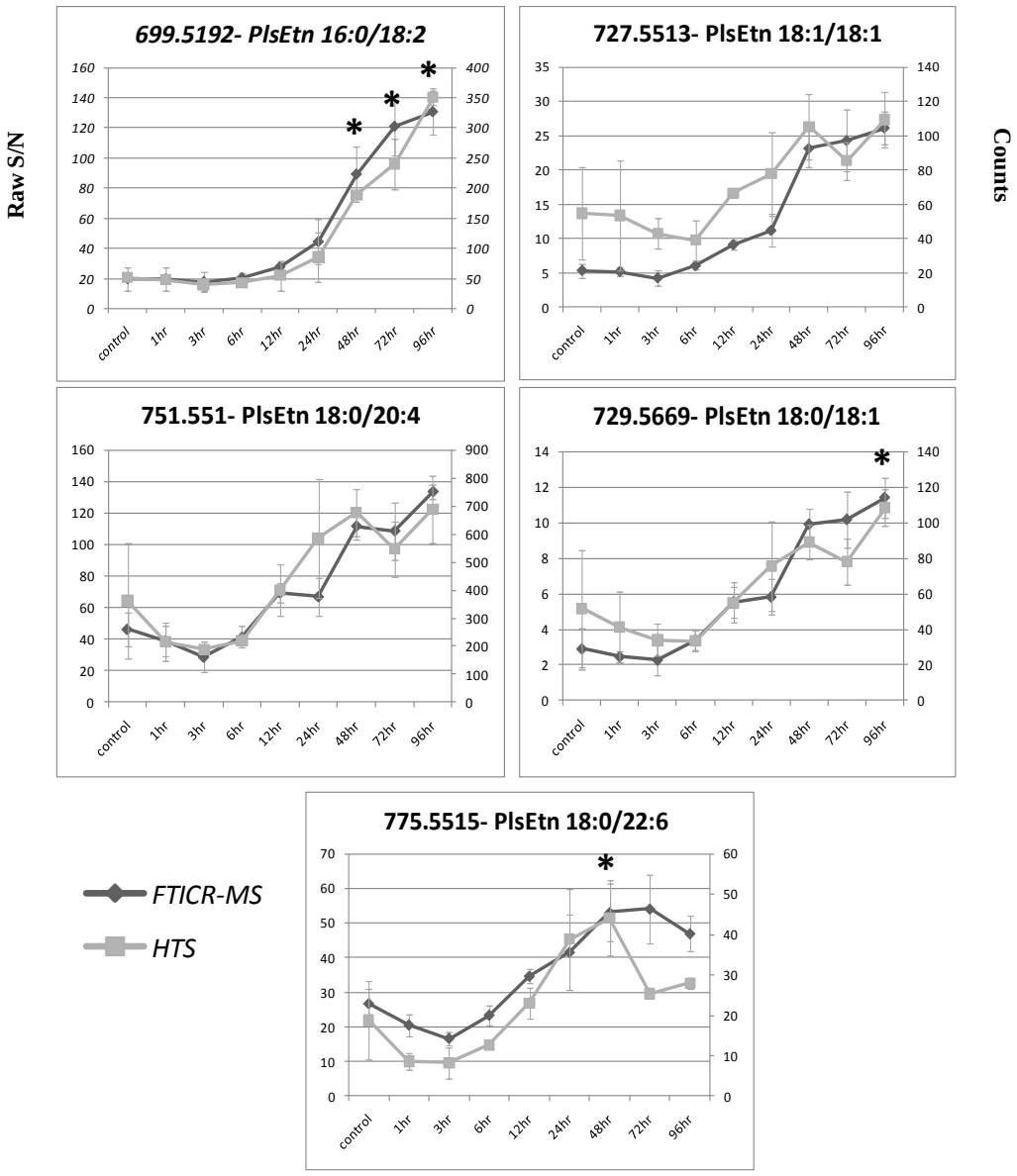

Figure 4.16 FTICR-MS and triple-quadrupole analyses of ethanolamine plasmalogens, in U937 cells as they differentiate.

Cell extracts were analyzed with multiple reaction monitoring- triple quadrupole method. The five graphs have the FTICR-MS data plotted on the primary y axis and the high throughput data is plotted on the secondary y axis. The error bars represent the standard deviation between replicate samples. FTICR-MS data (F-test, $p<0.001$), triple-quadrupole data * $p<0.05$ relative to the control time point.

the predicted matching plasmalogens from the FTICR-MS is shown in Figure 4.16. The increased levels of PlsEtn 16:0/18:2, PlsEtn 18:1/18:1, PlsEtn18:0/20:4, PlsEtn 18:0/18:1 and PlsEtn 18:0/22:6 closely resemble the increased levels of the corresponding masses detected in the FTICR-MS analysis. The increases of the PlsEtn in the U937 cells begin between 12 and 24 hours after the PMA treatment.

4.2.4 Real Time Polymerase Chain Reaction of Peroxisome Related Transcripts in Differentiating U937 cells

The increase in ether lipids during the differentiation suggested a possible role of enzymes involved in ether lipid synthesis or peroxisomal activity. The transcript levels of several key enzymes in the pathway were therefore assessed in the monocytes (controls) and macrophages (cells treated with PMA for 48 hours) using real-time polymerase chain reaction (RT-PCR) (Figure 4.17). Surprisingly, the transcript levels of dihydroxyacetone-phosphate acyltransferase (DHAPAT), a key enzyme in the synthesis of ether lipids, decreased following 48 hours of PMA treatment (Figure 4.17a). The experiments were repeated with consistent results, prompting an examination of some of the other genes involved in ether lipid synthesis and peroxisomal function. The transcript levels of fatty acid synthase (FASN), the key enzyme in fatty acid synthesis, also decreased slightly during differentiation (Figure 4.17a). 1-Acyl-Sn-Glycerol-3-.Phosphate Acyltransferase (AGPAT1 and 2), another key enzyme in the ether lipid synthesis pathway was also examined using RT-PCR, which also showed decreased levels as the U937 cells differentiated (AGPAT1 more significantly) (Figure 4.17a). Pex11a is typically used as a marker of peroxisome proliferation, and also decreases as the cells differentiate (Figure 4.17a). Glycerol-3-phosphate acyltransferase (GPAT) catalyzes the initial and rate limiting step in phospholipid synthesis, and was also detected at significantly lower levels in the differentiated U937 cells as compared to the levels detected in the monocytes (Figure 4.17a). Catalase activity, as another peroxisomal marker, was also measured in the cells and found to decreases during differentiation (data not shown). The results were intriguing, as it was expected that an increase in the transcription of genes encoding enzymes involved in ether lipid synthesis or peroxisome activity would have been detected. Two genes that are known to have increased expression in differentiating U937 cells, SRC and αV-integrin (ITGAV) (Kitamura *et al.*, 2004; Shrivastav *et al.*, 2008), were tested. Both SRC and ITGAV

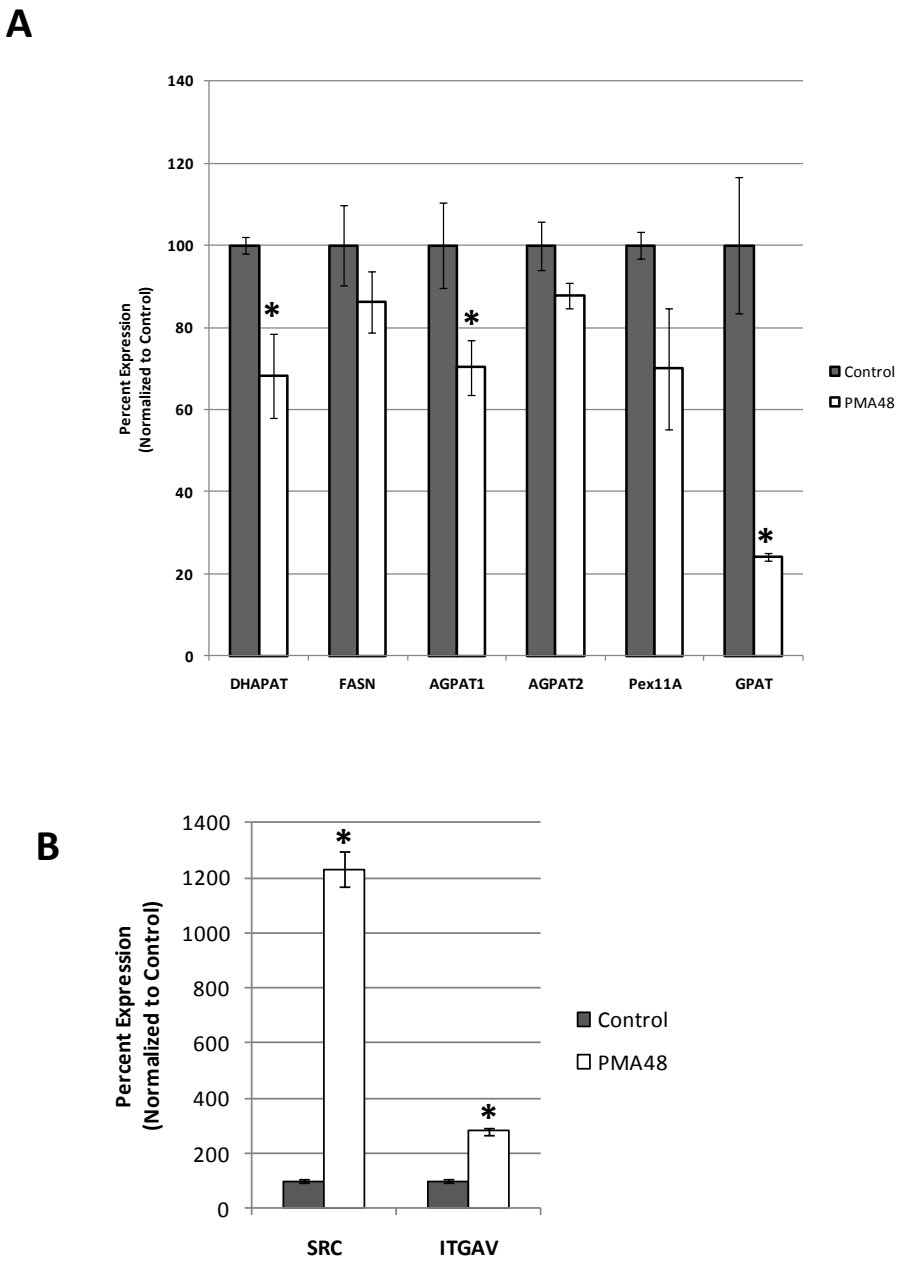

Figure 4.17 Percent expression of peroxisome related transcripts in differentiating U937 cells as detected with real time PCR (RT-PCR).
a. Peroxisome related transcript levels in monocytes (control) and macrophages (PMA 48 hr). Results have been normalized to the control. DHAPAT- dihydroxyacetone-phosphate acyltransferase, FASN- fatty acid synthase, AGPAT- 1-acyl-sn-glycerol-3-phosphate acyltransferase, Pex11A- peroxisomal membrane protein 11A, GPAT- glycerol-3-phosphate acyltransferase. **b**. Percent expression of gene transcripts known to increase during differentiation. SRC- Sarcoma gene, ITGAV- αV integrin. * $p<0.05$ relative to control. The error bars represent the standard deviation between replicate samples.

expression significantly increased during differentiation of the U937 cells (Figure 4.17b) as expected, further solidifying that the detected decrease in the transcription of the genes related to ether lipid synthesis and peroxisome proliferation during differentiation was real.

4.2.5 Citrate Export Inhibition in Differentiating U937 Cells

The question which emerged from these studies was whether the induction of the plasmalogens was a requirement for differentiation, or merely an association. I also questioned if there was a dependence on *de novo* synthesis of fatty acids during the induction of plasmalogen synthesis. 1,2,3-Benzenetricarboxylic acid (BTA) is a compound that prevents the export of citrate out of the mitochondria through the inhibition of the tricarboxylate carrier in the mitochondrial inner membrane (Kajimoto *et al.*, 2005). The inhibition of the tricarboxylate carrier subsequently reduces the amount of citrate available in the cytoplasm to be converted into acetyl CoA, which is required for *de novo* synthesis of fatty acids and cholesterol. Once exported out of the mitochondria, citrate has multiple fates. It is first broken down by ATP-citrate lyase which generates acetyl coenzyme A (AcCoA) and oxaloacetic acid (OAA) (Wellen *et al.*, 2009). The AcCoA is used for fatty acid synthesis, cholesterol synthesis and for the acetylation of histones (Costello and Franklin, 2005; Wellen *et al.*, 2009).

U937 cells were pre-treated with BTA for 3 hours prior to the PMA treatment to ensure that citrate export was inhibited prior to the induction of differentiation. After 24 hours of co-treatment with BTA and PMA, the U937 cells showed no morphological signs of differentiating, including lack of adherence (Figure 4.18). Cells still in suspension at 24 hours after treatment with both BTA and PMA were stained with Trypan blue and were found to be viable. The co-treated suspended cells were then rinsed with PBS, and then re-plated in fresh RPMI media lacking PMA and BTA. Within 6 hours of being plated in new media, the cells become adherent, and within 48 hours they showed a morphological differentiated phenotype (Figure 4.18). The results suggest that PMA does indeed initiate a terminal differentiation program, but one which can be reversibly blocked by preventing mitochondrial citrate export.

The levels of phospholipids during these treatments were subsequently measured. A comprehensive assessment of ethanolamine plasmalogen (PlsEtn) and Phosphatidylethanolamine (PtdEtn) levels using a triple-quadrupole tandem mass spectrometer was performed on the cell pellet extracts from the BTA experiment, including; control, BTA,

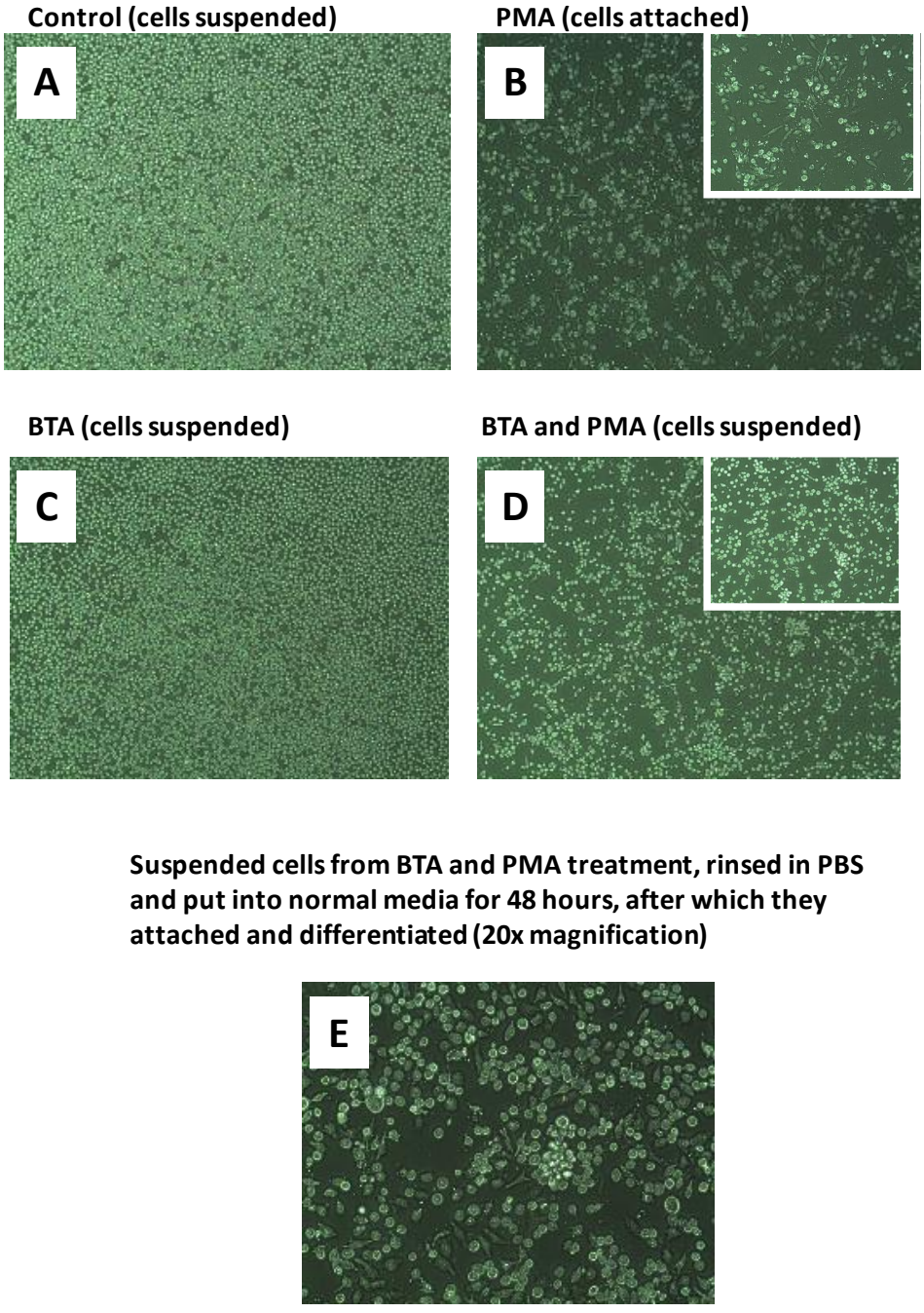

Figure 4.18 Photographs of U937 cells that have been treated with PMA and 1,2,3 benzene tricarboxylic acid (BTA).
Images from microscope at 10x and 20x magnification. **A**) Monocytic U937 cells (control). **B**) Differentiated U937 cells, PMA treated for 48 hours, cells adherent. **C**) U937 cells treated with BTA for 48 hours, cells in suspension. **D**) U937 cells treated with BTA and PMA for 24 hours, cells in suspension. **E**) Re-plated cells, BTA and PMA removed, cells are now adherent.

PMA, BTA and PMA, and re-plated samples (Figure 4.19). The relative levels of a PlsEtn and a PtdEtn, with the same specific fatty acid side chains, in all treatment combinations are shown.

The first four bars in each plot show the relative levels of the lipids in monocytes (undifferentiated) in the absence and presence of BTA (Figure 4.19). BTA treatment caused a significant decrease ($p<0.05$) in most of the PtdEtn analyzed in the monocytes (Table 4.4). The PtdEtn that did not appear to be affected by the BTA treatment were those with 18:0/18:3, 18:1/18:3, 18:1/20:4 and 18:1/22:6 fatty acid side chain combinations. Interestingly, the BTA treatment appeared to cause a decrease in the PlsEtn that contained either an 18:1 or 18:2 at the sn2 position, and either no change or slight increase in the PlsEtn that contained an 18:3, 20:4 or 22:6 at the sn2 position in the undifferentiated U937 cells.

The next four bars in each of the plots shows the relative levels of PlsEtn and PtdEtn in PMA treated U937's in the absence and presence of BTA (Figure 4.19). The first column in this group shows the relative levels of PlsEtn in differentiated (48 hour PMA treated) U937 cells, and all of the measured plasmalogens significantly increase as the cells differentiate ($p<0.05$) (consistent with the results of the FTICR-MS analysis). Interestingly, the PtdEtn do not increase during PMA-induced differentiation. In fact, the only significant changes detected were decreased levels of those containing arachidonic acid (16:0/22:6), or docosahexaenoic acid (16:/20:4) (Figure 4.19) (Table 4.4). When the cells were co-treated with BTA and PMA all of the PtdEtn in the panel decreased to similar, or lower, levels that were detected in the BTA treated monocytes (Figure 4.19). The PlsEtn containing 18:1, 18:2 or 18:3 in the sn2 position decrease in the cells co-treated with PMA and BTA, to the levels detected in the monocytes treated with BTA alone (Figure 4.19) (Table 4.4). The PlsEtn which contain either 20:4 or 22:6 in the sn2 position either remain at the same relative levels that were detected in the differentiated cells, or show a significant increase as in the case of the lipids that contain either 18:1 or 18:0 in the sn1 position (Figure 4.19) (Table 4.4).

Following 24 hours of BTA- PMA co-treatment, and no visual signs of differentiation, monocyte cells still in suspension were washed and re-plated in fresh media lacking BTA or PMA. The relative phospholipid levels 48 hours after re-plating are shown in the last two bars of the plots in Figure 4.19. As previously mentioned, when the cells were co-treated with both BTA and PMA they did not complete the differentiation process. However, once these cells were rinsed and plated in fresh media they attached to the plate surface within 6 hours. The

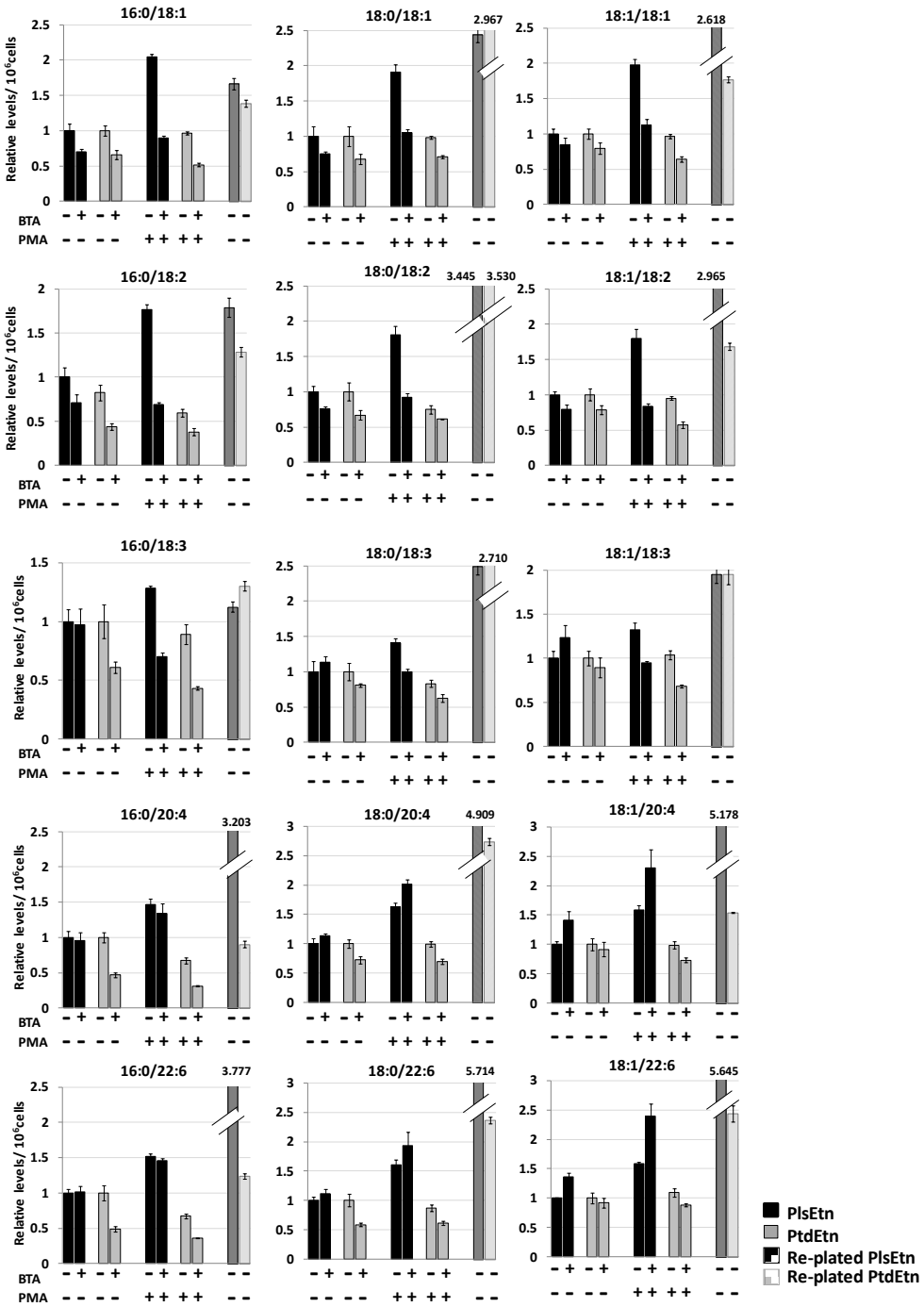

Figure 4.19 High throughput analysis of phosphatidylethanolamines (PtdEtn) and plasmenylethanolamines (PlsEtn) in U937 cells that have been treated with PMA and 1,2,3 benzene tricarboxylic acid (BTA).

Each graph shows the relative levels of PtdEtn and PlsEtn with the same fatty acid side chains per million cells. Data has been normalized to the control sample (no BTA or PMA). Statistics for these graphs is presented in Table 4.4. The error bars represent the standard deviation between replicate samples.

Table 4.4 The univariate *t*-test analyses for the results of the high throughput analysis of U937 cells treated with PMA and/or BTA (presented in Figure 4.19).

Each value in the table is the two-tailed *t*-test result for the comparison of different treatments (listed on the left hand side of each table) for each lipid analyzed (listed at the top of each table). If P-value<0.05, the cell has been grayed. (C-control, BTA- 1,2,3 Benzene Tricarboxylic Acid, PMA- Phorbol 12-myristate 13-acetate)

A

	16:0/18:1		16:0/18:2		16:0/18:3		16:0/20:4		16:0/22:6	
	PtdEtn 16:0/18:1	PlsEtn 16:0/18:1	PtdEtn 16:0/18:2	PlsEtn 16:0/18:2	PtdEtn 16:0/18:3	PlsEtn 16:0/18:3	PtdEtn 16:0/20:4	PlsEtn 16:0/20:4	PtdEtn 16:0/22:6	PlsEtn 16:0/22:6
C vs BTA	0.0032	0.0071	0.0018	0.0251	0.0110	0.8066	0.0003	0.6246	0.0014	0.7785
C vs PMA	0.4623	0.0001	0.0368	0.0004	0.3145	0.0089	0.0023	0.0023	0.0069	0.0002
C vs PMA & BTA	0.0004	0.1380	0.0006	0.0086	0.0024	0.0086	0.0001	0.0210	0.0005	0.0003
C vs Replated	0.0230	0.0165	0.0679	0.0233	0.0630	0.2964	0.3768	0.0003	0.0701	0.0003
PMA vs PMA & BTA	1.9672E-05	2.6543E-06	0.0004	8.4517E-06	0.0008	1.4686E-05	0.0001	0.2374	0.0001	0.0998
PMA vs Replated	0.0137	0.0754	0.0123	0.8980	0.0133	0.1364	0.0663	0.0008	0.0020	0.0006
BTA vs PMA & BTA	0.0194	0.0031	0.0081	0.6778	0.0041	0.0267	0.0015	0.0190	0.0041	0.0009
BTA vs Replated	0.0023	0.0038	0.0028	0.0079	0.0015	0.2636	0.0088	0.0003	0.0007	0.0003
PMA & BTA vs Replated	0.0010	0.0084	0.0013	0.0066	0.0005	0.0084	0.0026	0.0007	0.0003	0.0005

B

	18:0/18:1		18:0/18:2		18:0/18:3		18:0/20:4		18:0/22:6	
	PtdEtn 18:0/18:1	PlsEtn 18:0/18:1	PtdEtn 18:0/18:2	PlsEtn 18:0/18:2	PtdEtn 18:0/18:3	PlsEtn 18:0/18:3	PtdEtn 18:0/20:4	PlsEtn 18:0/20:4	PtdEtn 18:0/22:6	PlsEtn 18:0/22:6
C vs BTA	0.0231	0.0430	0.0165	0.0080	0.0596	0.2245	0.0068	0.0563	0.0030	0.0948
C vs PMA	0.8140	0.0009	0.0361	0.0007	0.0951	0.0107	0.9177	0.0005	0.1353	0.0007
C vs PMA & BTA	0.0242	0.5806	0.0063	0.2437	0.0088	0.9834	0.0029	0.0001	0.0039	0.0026
C vs Replated	0.0003	0.0031	0.0002	0.0007	0.0001	0.0044	0.0001	4.1625E-05	0.0004	0.0002
PMA vs PMA & BTA	0.0001	0.0002	0.0140	0.0003	0.0079	0.0006	0.0013	0.0026	0.0023	0.0859
PMA vs Replated	0.0002	0.0726	0.0001	0.0033	1.6543E-05	0.0117	0.0001	0.0001	0.0002	0.0004
BTA vs PMA & BTA	0.4489	0.0006	0.2243	0.0101	0.0064	0.0498	0.5414	0.0001	0.3979	0.0044
BTA vs Replated	0.0001	0.0013	0.0001	0.0004	1.2966E-05	0.0054	0.0001	4.3190E-05	0.0001	0.0002
PMA & BTA vs Replated	0.0001	0.0028	0.0001	0.0006	1.1892E-05	0.0036	0.0001	0.0001	0.0001	0.0006

C

	18:1/18:1		18:1/18:2		18:1/18:3		18:1/20:4		18:1/22:6	
	PtdEtn 18:1/18:1	PlsEtn 18:1/18:1	PtdEtn 18:1/18:2	PlsEtn 18:1/18:2	PtdEtn 18:1/18:3	PlsEtn 18:1/18:3	PtdEtn 18:1/20:4	PlsEtn 18:1/20:4	PtdEtn 18:1/22:6	PlsEtn 18:1/22:6
C vs BTA	0.0264	0.0954	0.0247	0.0112	0.2555	0.0608	0.4070	0.0107	0.3046	0.0008
C vs PMA	0.4530	0.0001	0.4008	0.0006	0.5242	0.0071	0.8412	0.0005	0.2363	7.7039E-06
C vs PMA & BTA	0.0015	0.1170	0.0016	0.0116	0.0025	0.3500	0.0130	0.0019	0.0906	0.0003
C vs Replated	0.0010	0.0006	0.0031	0.0006	0.0138	0.0096	0.0009	2.1574E-05	0.0066	0.0015
PMA vs PMA & BTA	0.0003	0.0002	0.0002	0.0003	0.0003	0.0011	0.0036	0.0167	0.0082	0.0026
PMA vs Replated	0.0006	0.0178	0.0016	0.0055	0.0151	0.0370	0.0001	4.2563E-05	0.0081	0.0024
BTA vs PMA & BTA	0.0370	0.0218	0.0090	0.4305	0.0335	0.0218	0.0624	0.0103	0.4974	0.0012
BTA vs Replated	0.0005	0.0005	0.0009	0.0004	0.0103	0.0286	0.0009	4.6309E-05	0.0053	0.0020
PMA & BTA vs Replated	0.0002	0.0008	0.0004	0.0004	0.0047	0.0073	8.2596E-06	0.0003	0.0047	0.0059

analysis of lipid levels in the re-plated cells revealed statistically significant increases in all of the phosphatidylethanolamines analyzed in comparison to the levels of these lipids in the cells treated with both PMA and BTA (Figure 4.19) (Table 4.4). The analysis of plasmalogens in the re-plated cells revealed that PlsEtn16:0/18:1, PlsEtn16:0/18:2 and PlsEtn16:0/18:3 increased to levels similar to those detected in the PMA treated cells (Figure 4.19). The remaining PlsEtn levels significantly increased in the re-plated cells, to levels more than two fold greater than in the PMA treated cells (Figure 4.19) (Table 4.4). Interestingly, the PtdEtn levels in the re-plated cells also varied depending on the fatty acid side chains at the sn1 and the sn2 position of the lipid. The ethanolamine plasmalogens containing either arachidonic acid (22:6) or docosahexaenoic acid (20:4) in the sn2 position showed the most significant increase (Figure 4.19) (Table 4.4).

Since citrate is required for cholesterol synthesis through the production of acetyl-CoA precursors through the activity of citrate lyase, I examined total cholesterol levels to determine if the inhibition of citrate from the mitochondria would impact cholesterol synthesis. An assessment of total cholesterol levels, using a triple-quadrupole tandem mass spectrometer, was performed on the cell pellet extracts from the BTA experiment, including; control, BTA, PMA, BTA and PMA combination treatment, and re-plated samples. Similar to the phospholipid results, increased cholesterol levels were detected in the 48 hour PMA treatment, which reflects the increase observed in the FTICR-MS data (Figure 4.20). The treatment of the U937 cells, undifferentiated, with BTA for 24 and 48 hours decreased total cholesterol levels in the cells. The U937 cells that were pre-treated with BTA prior to the PMA treatment show decreased levels of total cholesterol, in comparison to the levels detected in the PMA treated cells. When the cells that were originally treated with BTA and PMA were rinsed and re-plated in fresh media the total cholesterol levels increased to the levels detected in the cells treated with PMA for 48 hours. Since both plasmalogen and cholesterol levels were affected by BTA treatment during differentiation, I examined the third possible metabolic fate of acetyl-CoA, which is histone acetylation. A recent publication shows that histone acetylation in mammalian cells is dependent on the generation of cytosolic AcCoA by ATP-citrate lyase (Wellen *et al.*, 2009).

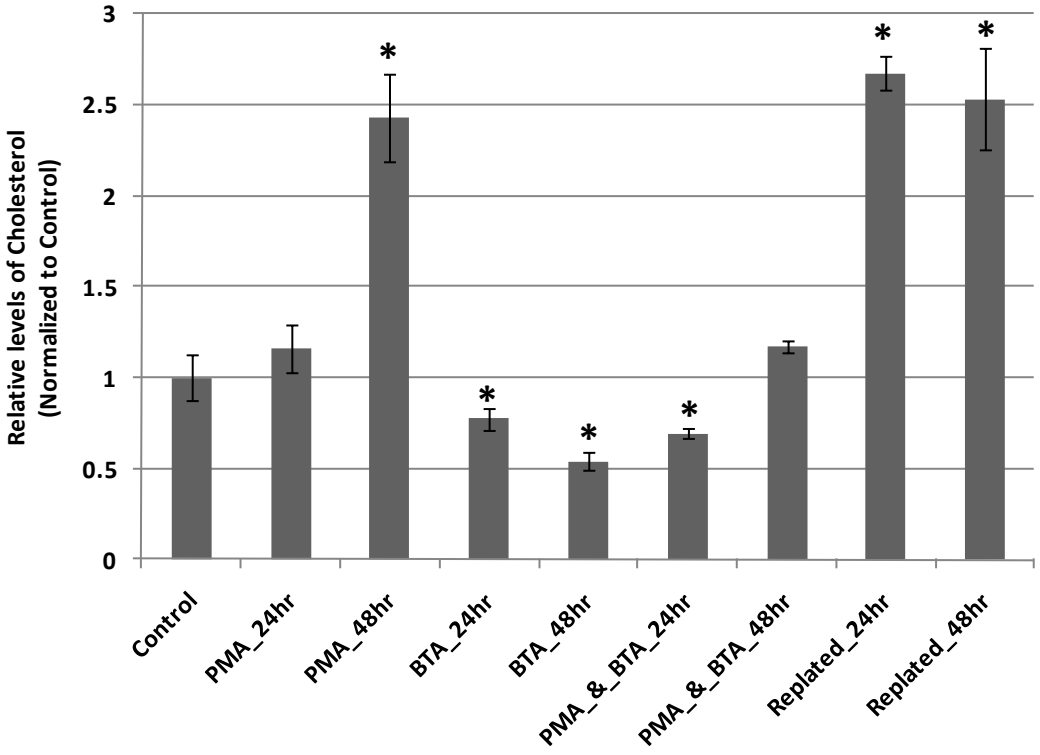

Figure 4.20 Analysis of cholesterol in U937 cells that have been treated with PMA and 1,2,3 benzene tricarboxylic acid (BTA).

The values have been normalized to the level of cholesterol in the control (un-differentiated) cells. *$p<0.05$ relative to the control time point. The error bars represent the standard deviation between replicate samples.

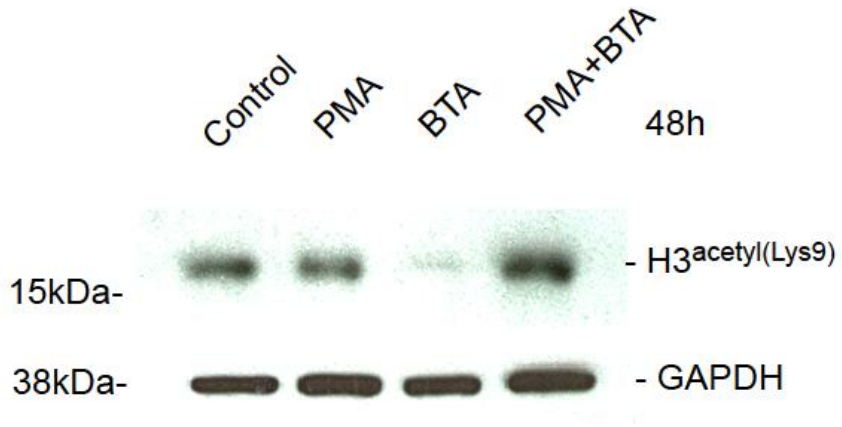

Figure 4.21 The effects of PMA and BTA treatment on histone 3 acetylation in U937 cells.
U937 cells were treated with the indicated compounds for 48 hours. Protein lysates were resolved by SDS-PAGE and probed for acetylated Histone3 ($H3^{acetyl(Lys9)}$) by Western blot analysis. GAPDH was used as loading control.

Western blot analysis of the BTA treated cells showed a remarkable reduction of acetylation of histone 3 ($H3^{acetyl}$) (Figure 4.21). Interestingly, when the cells were treated with both BTA and PMA the acetylation of H3 was not inhibited. Although the results show that the BTA alone can block H3 acetylation, this can be over-ridden by the activation of PKC. This result suggests that PMA may activate a different pathway that is capable of acetylating histones or generating cytosolic citrate or AcCoA.

4.2.6 Discussion

Comprehensive metabolomic analysis of differentiating human promyelomonocytic leukemic cell line U937 revealed dramatic alterations in multiple classes of glycerophospholipids. The most significant, and novel finding, is that preferential increase of plasmalogens, relative to diacyl phospholipids, occurring between 6 and 48 hours post PMA induced differentiation (Figure 4.22A-B). Multiple Reaction Monitoring (MRM) Triple Quadrupole mass spectrometry was used to confirm these results. The monocyte form of the cell is a small spherical cell which is free-floating in the media. Within 3 hours of the addition of PMA to the media, the cells became adherent and begin to differentiate. This dramatic physical change would likely require a major alteration in membrane composition, and consistent with our results, may be modulated by significant increases in phospholipids and plasmalogens. An increase in the percentage of plasmalogens in the cell membrane will result in a more fluid and flexible membrane. Plasmalogens also have a number of other functions in cells: they mediate membrane dynamics, they act as antioxidants in the presence of reactive species, they store polyunsaturated fatty acids (PUFAs), and have been found to be involved in intracellular signalling in cells (Nagan and Zoeller, 2001; Brites *et al.*, 2004). Interestingly, an elevation of the phosphatidylethanolamine pool, including plasmalogens, was also detected when P19 teratocarcinoma cells where induced to differentiate into cardiac myocytes (Fotheringham *et al.*, 2000). In another study researchers determined that the elevation of phosphatidylethanolamine levels in the differentiating P19 cells was not essential for differentiation to proceed (Xu *et al.*, 2000).

It is quite conceivable that the increased levels of ethanolamine plasmalogens during the differentiation of U937 cells may be due to the dramatic changes in the membrane structure

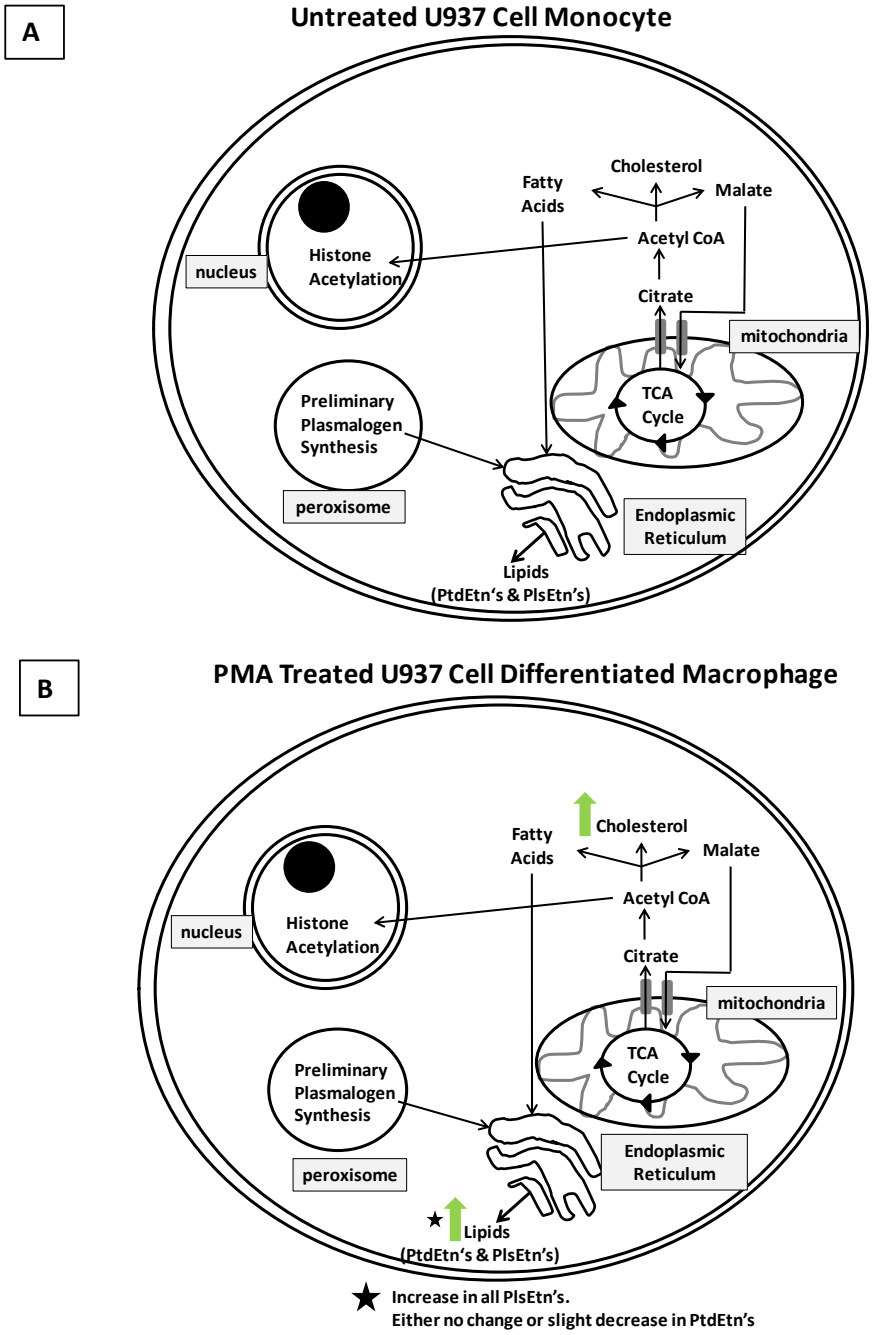

Figure 4.22(A-D) A summary of the results attained from the analyses of U937 cells during differentiation and BTA inhibition of differentiation.
Lipid synthesis and histone acetylation in U937 cells. **A)** The monocyte form of the cell, is considered to be the control of the experiment. Simplified pathways for lipid synthesis and histone acetylation are shown. The relative levels of lipids and histone acetylation detected in the monocyte cells is considered to be baseline for all other comparisons. **B)** U937 cell treated with phorbol 12-myristate 13-acetate (PMA). Increased levels of cholesterol and plasmalogens (PlsEtn) are observed, as illustrated with green arrows, as compared to the levels detected in the monocyte cells. Figure continued on next page.

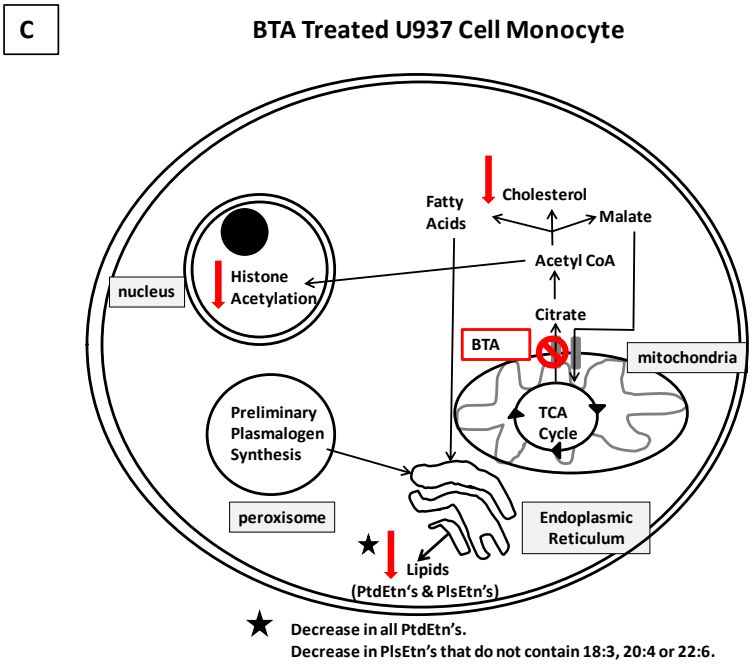

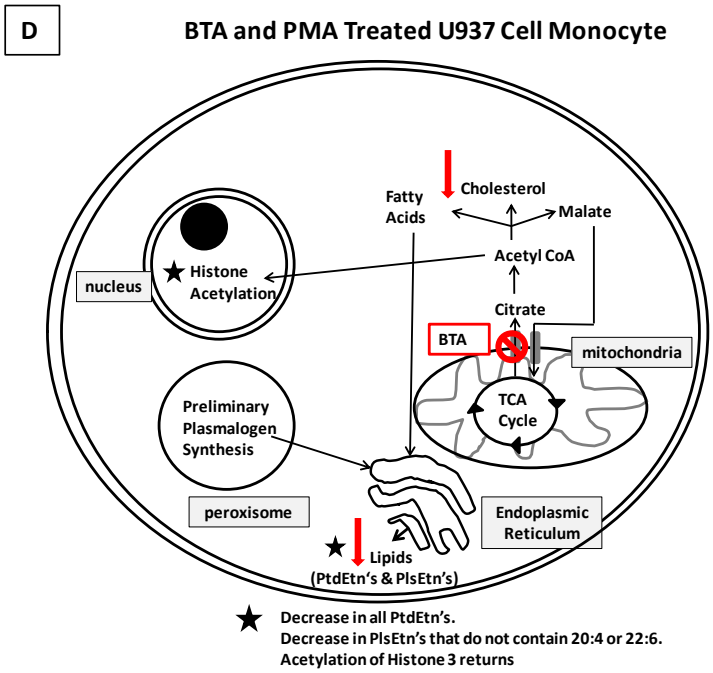

Figure 4.22C-D A summary of the results attained from the analyses of U937 cells during differentiation and BTA inhibition of differentiation (continued from previous page).
C) Inhibition of citrate export from mitochondria with 1,2,3-Benzenetricarboxylic acid (BTA) (red strikethrough). Decreased levels of phospholipids and cholesterol were detected (red arrows). Acetylation of histone 3 (H3) was also decreased (red arrow). **D)** Co-treatment with BTA and PMA. Decreased levels of phospholipids and cholesterol were detected (red arrows). Acetylation of Histone 3 similar to levels detected in PMA treated cells.

E

Re-plated cells (originally treated with BTA and PMA), grown in regular media without PMA

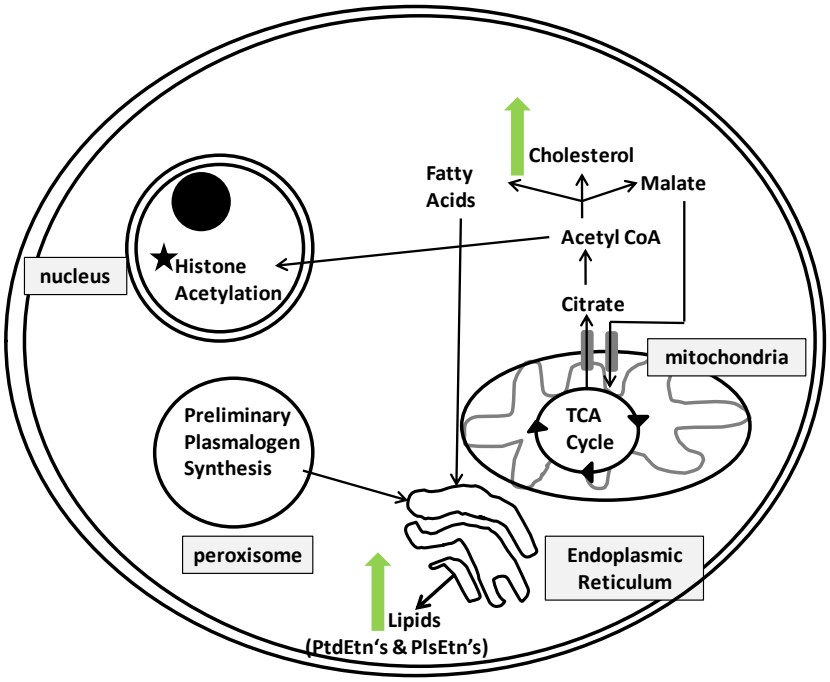

Figure 4.22E A summary of the results attained from the analyses of U937 cells during differentiation and BTA inhibition of differentiation (continued from previous page).
E) Cells that were treated with both BTA and PMA were removed from their media, rinsed and re-plated in fresh media without BTA or PMA. After a period of 48 hours in the fresh media increased levels of phospholipids and cholesterol were detected (green arrows). Due to a reduced number of cells collected it was not possible to analyze histone acetylation.

of the cells as they shift from monocytes to macrophages. Phospholipid mixtures containing diacylphospholipids generally form lamellar gel at low temperatures, and mixtures containing plasmalogens become liquid-crystalline at the same temperature (Brites *et al.*, 2004). An increase in the percentage of plasmalogens in the cell membrane will result in a more fluid and flexible membrane (Lohner, 1996). It is also possible that the increase of plasmalogens detected in the macrophage cells is due to a self-protection mechanism. Macrophages release reactive oxygen species (ROS), known as a respiratory burst, in response to phagocytosis (Forman and Torres, 2001). The increased production of ROS, such as H_2O_2 and superoxide, in U937 cells plays an important function and characteristic during differentiation (Harris and Ralph, 1985). These reactive oxygen species could be very damaging unless the cell can develop a method of protecting itself. One of the key roles of plasmalogens is to protect the cell from reactive oxygen species, which may explain why an increase of these particular phospholipids would be necessary in U937 cells as they differentiate. The vinyl-ether bond in plasmalogens increases the lipid susceptibility to oxidative attack in comparison to their diacyl counterparts (Brites *et al.*, 2004). Plasmalogens can protect cells from oxidative stress by scavenging radicals at the vinyl-ether linkage. Plasmalogens have also been shown to be capable of inhibiting iron-induced peroxidation of PUFAs and copper-induced oxidation of lipoproteins (Brites *et al.*, 2004).

Ethanolamine plasmalogens, especially those containing arachidonic acid, have also been recently identified as major components of lipid rafts in cellular membranes (Pike *et al.*, 2002). Lipid rafts are specialized cholesterol-enriched lipid domains that facilitate interactions between lipid and protein components of signalling pathways, regulate membrane trafficking, and cytoskeletal composition (Fan *et al.*; Pike *et al.*, 2002). Several signalling components are highly enriched in lipid rafts, such as: Heteromeric G proteins, growth factor receptors, SRC family kinases, MAP kinase and protein kinase C (Pike *et al.*, 2002). It is hypothesized that the enrichment of arachidonic acid containing plasmalogens in lipid rafts may be for the production of free arachidonic acid during cellular signalling (Pike *et al.*, 2002). In another study a relationship was identified between lipid rafts and pro-survival signalling pathways induced by reactive oxygen species (Yang *et al.*, 2006).

The question that these results raised was whether the induction of plasmalogens was required for differentiation, or merely an associated effect. One way to address this was to

block the *de novo* synthesis of fatty acids using citrate export inhibitor 1,2,3-Benzenetricarboxylic acid (BTA). The BTA treatment in the monocytic U937 cells caused a reduction in growth and in the synthesis of lipids, including: cholesterol, phosphatidylethanolamines and ethanolamine plasmalogens (with the exception of those that contain linolenic acid (18:3), arachidonic acid (20:4), or docosahexanoic acid (22:6)) (Figure 4.22C). Another interesting observation is that plasmalogens containing essential fatty acids, linoleic acid (18:2) and linolenic acid (18:3), are affected by both PMA and BTA treatments. As the cells are not capable of synthesizing these fatty acids it is somewhat perplexing as to how they are incorporated into the lipids detected. It is possible that they are in the foetal bovine serum that is added to the serum and then transported into the cell. The inhibition of citrate export from the mitochondria also affected the acetylation of histone 3.

Cells co-treated with BTA and PMA (BTA was added 3 hours prior to PMA) showed decreased levels of all phosphatidylethanolamines, as well as ethanolamine plasmalogens (with the exception of those containing arachidonic acid or docosahexanoic acid) (Figure 4.22D). It is interesting that histone-3 acetylation was not inhibited in the combination treatment, as seen in the BTA treated cells, suggesting that an alternative method of acetylation can be induced with PMA treatment. Numerous gene expression changes are likely initiated during differentiation, and therefore acetylation of histones would be required. Recently published work shows that PMA treatment of LNCaP cells, a prostate cancer cell line, resulted in overall acetylation of histones H3 and H4 (Rowe *et al.*, 2008). Rowe's group determined that PMA treatment lead to the induction of KAI1, a metastasis suppressor down-regulated in many human cancers (Rowe *et al.*, 2008). Another interesting finding was that when a PKC inhibitor, apigenin, was added to the cells the acetylation of H3 by PMA was blocked (Rowe *et al.*, 2008). Interestingly, acetylation of H4 was not blocked by the PKC inhibitor, suggesting the effect of PMA on H4 acetylation may not be specifically regulated by the PKC pathway (Rowe *et al.*, 2008).

When the media from the combination treatment is removed, and the cells are rinsed and re-fed with normal media, plasmalogens and cholesterol increase to the same levels detected in the PMA treated cells (Figure 4.22E). After re-plating the cells in fresh media the cells attached to the plate surface and appeared to differentiate without new addition of PMA. These findings suggest that PMA is able to initiate the differentiation process but the inhibition of

citrate export prevents the process from completing. U937 cells may require plasmalogens and cholesterol in order to differentiate; however, further experiments will be required in order to prove this hypothesis.

4.3 Phenotypic Transformations of Cancer Cells

4.3.1 Comprehensive Non-Targeted Metabolic Analysis of CNA14 Cells Grown at 34°C and 39°C

Transformation of a normal cell into a cancer cell is accomplished by a multitude of phenotypic changes including: self-sufficiency in growth signals, insensitivity to anti-growth signals, tissue invasion and metastasis, limitless replicative potential, sustained angiogenesis and evading apoptosis (Hanahan and Weinberg, 2000). To determine whether metabolic changes are associated with the transformation of normal cells into a cancer cell, a metabolomic analysis was completed on a cell line harbouring a temperature sensitive mutant of an oncogene. CNA14 cells were derived from a parental rat fibroblast cell line, Rat2, and contain a temperature sensitive mutation of the oncogene $p130^{gag\text{-}fps}$. CNA14 cells have a normal phenotype at 39ºC but are tumourigenic at 34ºC, due to the apparent incompatibility between a temperature-sensitive version of the oncogene $p130^{gag\text{-}fps}$ (functional at 34ºC, but not at 39ºC) and p53 (present at 39ºC, but absent at 34ºC). The CNA14 cells grown at 34ºC and 39ºC are phenotypically different (Figure 4.23). The cells grown at 39ºC are normal fibroblast cells, whereas the cells that are grown at 34ºC no longer have the morphology of fibroblasts. Western blot analyses, previously completed by Dr. R. Warrington, on the CNA14 cells grown at 34 ºC, 37 ºC and 39ºC showed that at 39ºC p53 is present and that $p130^{gag\text{-}fps}$ is absent, and the reverse is seen in the cells grown at 34ºC, where $p130^{gag\text{-}fps}$ is present and p53 is no longer detected (un-published data). Both p53 and $p130^{gag\text{-}fps}$ are detected in the cells grown at 37ºC, and therefore negate each other at this temperature. The objective therefore was to characterize differences between cells grown at the two temperatures. Since the metabolic and transcriptomic comparisons are being made with essentially ‘isogenic’ cells, the results obtained from this particular study should provide many new insights into the molecular differences between tumourigenic and normal cells.

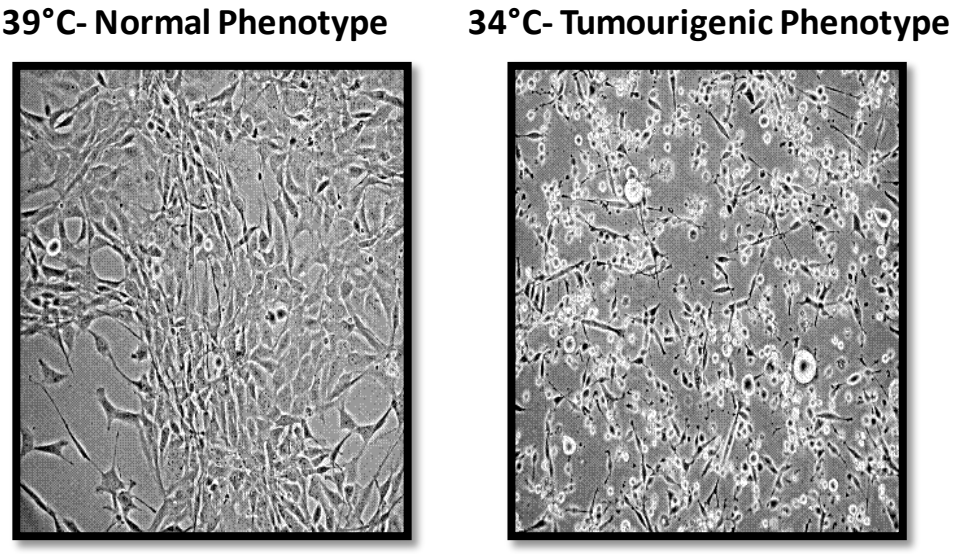

Figure 4.23 CNA14 cells, grown at 39˚C and 34˚C, show different phenotypes at each temperature.
CNA14 cells grown at 39˚C have a morphology consistent with fibroblast cells. When the cells are grown at 34˚C they become irregular in shape, with some cells appearing elongated and narrow, and others almost spherical.

Included in this experiment were three control cell lines (grown at 34 ºC, 37 ºC and 39ºC): the parental cell line (Rat2), a rat fibroblast cell line (NW16) expressing the wild type version of the $p130^{gag\text{-}fps}$ oncogene, and a mouse embryonic cell line ($10T_{1/2}$) to ensure that the metabolic changes that were observed were due to changes in growth phenotype and not the result of the temperature shift.

A principal component analysis (PCA) of the control cell lines, NW16, 10T1/2 and Rat2, showed that there were very little metabolic differences due to temperature change ($p<0.01$, $\log_2$ normalized) (Figure 4.24). The NW16 cells and Rat2 cells cluster tightly together, regardless of the temperature they were grown at. In comparison, the CNA14 cells grown at the three different temperatures clearly separate. This suggests that the metabolic differences seen in CNA14 cells at each temperature were a result of the alteration in growth phenotype rather than an effect of the temperature shift alone.

The data sets of two duplicate CNA14 experiments were combined (2011 metabolites), resulting in the comparison of four replicates. A hierarchical cluster (Pearson correlation, complete linkage, $p<0.01$, $\log_2$ normalized) was completed on the dataset, resulting in 2 distinct clusters of metabolites. The first cluster contains metabolites elevated in the cells grown at 39ºC (normal phenotype), and the second cluster contains the metabolites elevated in the cells grown at 34ºC (tumourigenic phenotype) (Figure 4.25). The masses elevated in the CNA14 cells grown at 39ºC were putatively identified as glycerophosphocholine (parental and adduct forms), phospholipids, triacylglycerols (TAGs) and vinyl acyl glycerols (VAGs) (Table 4.5). The masses in the second cluster, those elevated in the cells grown at 34ºC, have been putatively identified as ethanolamine and choline phospholipids and plasmalogens (Table 4.6). Glycerophosphocholine is a precursor for phospholipids and ether lipids, and was elevated in the CNA14 cells grown at 39°C (Figure 4.26). Some of the other putatively identified classes of metabolites elevated in the CNA14 cells grown at 39°C include TAGs, VAGs and phosphatidylethanolamines (Figure 4.26). The phospholipids, including plasmalogens, which are elevated in the tumour cells, are at very low levels or absent in the normal cells (Figure 4.26).

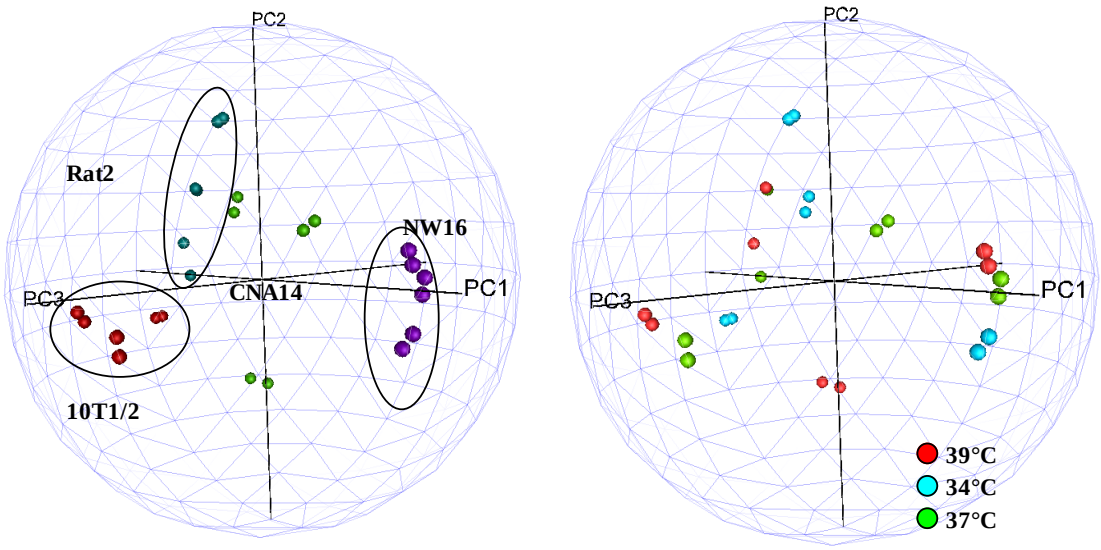

Figure 4.24 Principal component analysis (PCA) of CNA14, Rat2, 10T1/2 and NW16 cell lines grown at 34°C, 37°C and 39°C.
The closer the samples cluster together in a PCA plot the more metabolically similar they are. The further the samples separate from each other along PC1 the more metabolically different the samples are. The plot on the left hand side of the figure is coloured by cell line, and the plot on the right is coloured by temperature.

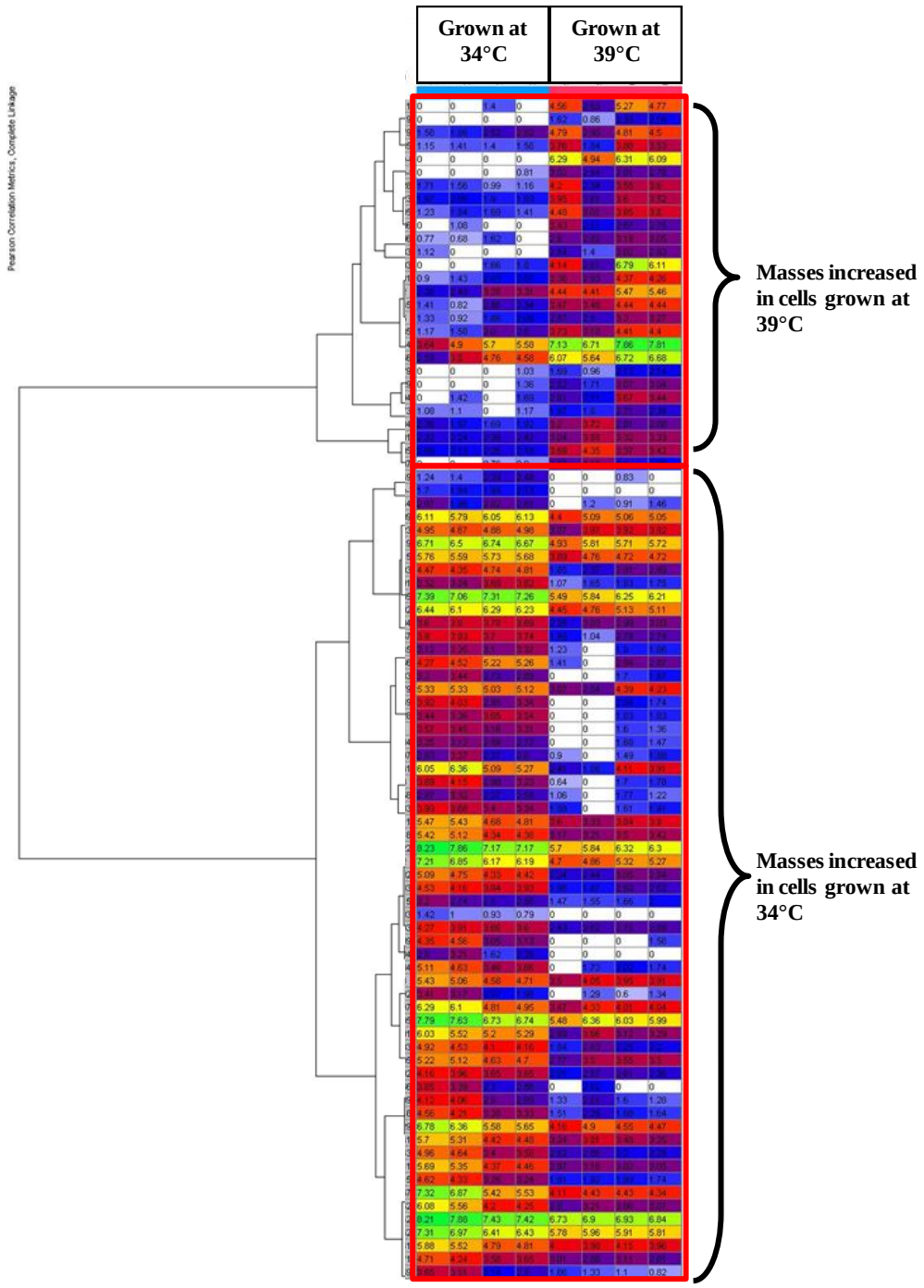

Figure 4.25 A hierarchical cluster, Pearson correlation with complete linkage, of CNA14 cells (grown at 34˚C and 39˚C).
The top one third of the array contains masses that are detected at elevated levels in the CNA14 cells grown at 39°C, and the masses in the bottom two thirds of the array are detected at elevated levels in the CNA14 cells grown at 39°C. (F-test- $p<0.01$, data is log2 normalized)

Table 4.5 Deduced metabolite identifications of the masses decreased in the CNA14 cells grown at 34°C (tumourigenic phenotype) as compared to the cells grown at 39°C (normal phenotype).

This table is an expansion of the first cluster in Figure 4.25. The first column contains the metabolite identification. Some masses are identified as the parent form of the molecule, where as others are adduct forms of the molecule (containing a sodium or potassium adduct for example), this information is listed in the second column. The theoretical mass of the assigned metabolite is listed in the third column and the corresponding formula in the fourth column. The PPM error calculated between the theoretical mass and detected mass (in the sixth column) is listed in the fifth column. The analytical mode that the mass was detected in is listed in the seventh column. The p-value calculated across the samples is listed in the eighth column. The 2-demensional array of the data is shown on the right hand side of the table. The colours in the array represent the relative intensity of the mass in each sample (the legend for colours is located at the bottom of the table).

								34°C				39°C			
							temperature								
dBase_Match	Adduct	T_Mass	Formula	Error	Detected Mass	Analysis Mode	P_Value	2	2	3	3	5	5	6	6
Glycerylphosphorylcholine	parent	257.1028	$C_8H_{20}NO_6P$	0.09	257.1028	1101	0.0011								
-	-	-	-	-	333.2761	1204	0.0019								
Phosphatidylethanolamine, arachidonic, arachidic	parent	795.5778	$C_{45}H_{82}NO_8P$	0.26	795.578	1203	0.0079								
C13					796.5809	1203	0.0085								
Glycerylphosphorylcholine	Na	257.1028	$C_8H_{20}NO_6P$	0.1	279.0848	1101	1.82E-06								
Phosphatidylethanolamine, linolenic, caprylic, hydroxy	parent	617.3693	$C_{31}H_{56}NO_9P$	0.76	617.3688	1202	2.58E-05								
15-Rosene-5,19-diol; 5?-form, 19-Tigloyl	parent	388.2977	$C_{25}H_{40}O_3$	0.91	388.2981	1203	0.0028								
Spirost-5-en-3-ol; (3?,25R)-form, Hexadecanoyl	parent	652.5431	$C_{43}H_{72}O_4$	0.21	652.5432	1203	0.0023								
Diacylglyceroplasmalogen, EPA, arachidic	parent	654.5587	$C_{43}H_{74}O_4$	0.43	654.5584	1203	0.0005								
C13	-	-	-	-	655.5618	1203	0.0006								
Phosphatidylethanolamine, lignoceric, arachidonic,	parent	883.6302	$C_{49}H_{90}NO_{10}P$	0.03	883.6302	1202	0.0006								
losarcol, INN	K-K	861.9069	$C_{21}H_{29}I_3N_4O_9$	0.77	937.8193	1203	0.0033								
Glycerylphosphorylcholine	K	257.1028	$C_8H_{20}NO_6P$	0.05	295.0587	1101	0.0093								
1,3,7-Cembratrien-11-ol; (1E,3E,7E,11?)-form, Ac	parent	332.2715	$C_{22}H_{36}O_2$	0.81	332.2718	1204	0.0031								
Phosphatidylethanolamine, arachidonic, arachidic	parent	795.5778	$C_{45}H_{82}NO_8P$	0.39	795.5781	1202	0.002								
C13	-	-	-	-	796.5825	1202	0.0045								
Phosphatidylethanolamine, lignoceric, EPA, dihydroxy	parent	881.6146	$C_{49}H_{88}NO_{10}P$	1.34	881.6134	1202	0.006								
-	-	-	-	-	529.3163	1202	0.0085								
Phosphatidylethanolamine, arachidonic, arachidic	parent	795.5778	$C_{45}H_{82}NO_8P$	3.15	795.5803	1204	0.0044								
C13	-	-	-	-	796.5834	1204	0.0056								
-	-	-	-	-	615.3539	1202	0.0079								
-	-	-	-	-	935.8019	1203	0.0029								
triacylglyceride, myristic, EPA, lignoceric	parent	936.8146	$C_{61}H_{108}O_6$	0.17	936.8144	1203	0.0094								
triacylglyceride, myristic, arachidonic, lignoceric	parent	938.8302	$C_{61}H_{110}O_6$	2.35	938.828	1203	0.0073								
C13					778.5727	1201	0.0034								
Phosphatidylethanolamine, EPA, arachidic	Na	793.5621	$C_{45}H_{80}NO_8P$	0.62	815.5436	1201	0.0001								
Phosphatidylethanolamine, arachidonic, arachidic	Na	795.5778	$C_{45}H_{82}NO_8P$	0.05	817.5597	1201	0.0005								
C13					818.5628	1201	0.0007								

Low Intensity — High Intensity

Table 4.6 Deduced metabolite identifications of the masses elevated in the CNA14 cells grown at 34°C as compared to the cells grown at 39°C.

This table is set up in the same manner as Table 4.5, for a complete description of the table please see previous figure. These are the masses in the second cluster of the HCA in Figure 4.25.

34°C 39°C

temperature							
dBase_Match	Adduct	T_Mass	Formula	Error	Detected Mass	Analysis Mode	P_Value
1-(2-Isopropyl-1-methylcyclobutyl)-4-methyl-4-nonene-1,8-	parent	278.2246	$C_{18}H_{30}O_2$	2.23	278.2252	1204	0.0049
-	-	-	-	-	573.485	1203	5.96E-07
Diacylglyceroplasmalogen, oleic, linolenic	parent	600.5117	$C_{39}H_{68}O_4$	1.07	600.5111	1201	0.0044
Phosphatidalethanolamine, arachidonic, oleic, hydroxy	parent	765.5309	$C_{43}H_{76}NO_8P$	0.87	765.5302	1201	0.0009
C13					766.5334	1201	0.0023
Phosphatidylcholine, arachidonic, linoleic	parent	805.5621	$C_{46}H_{81}NO_8P^+$	1.91	805.5606	1201	0.0019
C13	-	-	-	-	806.5636	1201	0.0015
Phosphatidalethanolamine, oleic, linoleic, hydroxy	Na	741.5309	$C_{41}H_{76}NO_8P$	0.11	763.5129	1201	0.0003
C13					764.5158	1201	0.0001
N-methylphosphatidylethanlamine, linolenic, arachidic	parent	783.5778	$C_{44}H_{82}NO_8P$	0.4	783.5781	1201	0.0005
C13	-	-	-	-	784.581	1201	0.0002
N-methylphosphatidylethanlamine, linolenic, arachidic	K	783.5778	$C_{44}H_{82}NO_8P$	0.92	821.5344	1201	0.0034
13-Hydroxy-3-cleroden-15-oic acid; (ent-13?)-form, Me ester	parent	336.2664	$C_{21}H_{36}O_3$	0.16	336.2665	1203	0.0067
Diacylglyceroplasmalogen, arachodonic, myristic	parent	572.4804	$C_{37}H_{64}O_4$	1.33	572.4812	1203	0.0045
Phosphatidylethanolamine,linolenic, palmitic	parent	713.4996	$C_{39}H_{72}NO_8P$	3.71	713.5022	1204	0.0066
C13	-	-	-	-	365.2989	1201	0.0083
Phosphatidylethanolamine, lauric, caprylic, hydroxy	parent	539.3223	$C_{25}H_{50}NO_9P$	2.08	539.3212	1202	0.0079
Phosphatidalethanolamine, linoleic, palmitic (plasmalogen)	parent	699.5203	$C_{39}H_{74}NO_7P$	0	699.5203	1202	0.0049
Phosphatidylethanolamine, palmitoleic, palmitoleic	parent	687.484	$C_{37}H_{70}NO_8P$	0.96	687.4833	1204	0.0028
Phosphatidylethanolamine, linoleic, linolenic	parent	737.4996	$C_{41}H_{72}NO_8P$	2.37	737.4978	1201	0.001
C13	NH_4	755.5911	$C_{43}H_{81}NO_9$	0.68	772.6183	1201	0.0034
Reticulatamol	parent	534.5012	$C_{35}H_{66}O_3$	1.32	534.5019	1203	0.0097
Phosphatidalethanolamine, linoleic, palmitic (plasmalogen)	parent	699.5203	$C_{39}H_{74}NO_7P$	0.57	699.5199	1204	0.0061
Phosphatidalethanolamine, linoleic, palmitic (plasmalogen)	parent	699.5203	$C_{39}H_{74}NO_7P$	0.29	699.5201	1203	0.003
1,9-Tridecanediol; 1-Docosanoyl	Na	538.5325	$C_{35}H_{70}O_3$	3.63	560.5164	1203	0.0058
C13					770.602	1201	0.0033
14-Hydroxyheneicosanoic acid, 9Cl	Na	342.3134	$C_{21}H_{42}O_3$	0.16	364.2954	1201	0.0011
-	-	-	-	-	757.4954	1201	0.0018
Phosphatidylcholine, linoleic, palmitic	parent	757.5621	$C_{42}H_{81}NO_8P^+$	1.14	757.563	1201	0.0022
C13					758.5661	1201	0.002
Phosphatidalcholine, linoleic, stearic (plasmalogen)	parent	769.5985	$C_{44}H_{85}NO_7P^+$	0.73	769.5991	1201	0.0002
Phosphatidalcholine, nervonic, lauric (plasmalogen)	parent	771.6142	$C_{44}H_{87}NO_7P^+$	1.06	771.615	1201	0.0003
C13	-	-	-	-	772.5825	1201	0.0015
Phosphatidalcholine, linoleic (plasmalogen)	parent	519.3316	$C_{26}H_{51}NO_7P^+$	0.24	519.3317	1201	0.0003
Phosphatidylethanolamine, linoleic, arachidic	parent	771.5778	$C_{43}H_{82}NO_8P$	1.18	771.5787	1201	0.0003
Phosphatidalethanolamine,linolenic, palmitic (plasmalogen)	parent	697.5046	$C_{39}H_{72}NO_7P$	0.07	697.5046	1204	0.0009
C13	-	-	-	-	700.5238	1203	0.0004
N,N-dimethylphosphatidylethanlamine, linoleic, myristic	parent	715.5152	$C_{39}H_{74}NO_8P$	0.7	715.5157	1201	0.0034
N,N-dimethylphosphatidylethanlamine, arachodonic, myristic	parent	739.5152	$C_{41}H_{74}NO_8P$	0.4	739.5149	1201	0.003
C13					742.571	1201	0.0092
Phosphatidylcholine, linoleic, myristic	Na	729.5308	$C_{40}H_{77}NO_8P^+$	0.26	751.5126	1201	0.0097
Phosphatidylcholine, linoleic, palmitic	Na	757.5621	$C_{42}H_{81}NO_8P^+$	0.94	779.5448	1201	0.0095
Phosphatidalethanolamine, oleic, linoleic, hydroxy	parent	741.5309	$C_{41}H_{76}NO_8P$	0.5	741.5305	1201	0.0001
C13	-	-	-	-	742.5332	1201	0.0003
Phosphatidylcholine,linolenic, palmitic	Na	755.5465	$C_{42}H_{79}NO_8P^+$	0.87	777.5291	1201	0.0005
C13					778.5322	1201	0.0002
Phosphatidylethanolamine,linolenic, palmitic	parent	713.4996	$C_{39}H_{72}NO_8P$	1.19	713.4987	1201	0.0066
Phosphatidalethanolamine, linolenic, linolenic (plasmalogen)	Na	719.489	$C_{41}H_{70}NO_7P$	1.32	741.47	1201	0.0099
Phosphatidalcholine, oleic, palmitoleic (plasmalogen)	parent	741.5673	$C_{42}H_{81}NO_7P^+$	0.58	741.5677	1201	0.0018
N,N-dimethylphosphatidylethanlamine, linoleic, palmitic	parent	743.5465	$C_{41}H_{78}NO_8P$	0.67	743.546	1201	0.0029
C13					744.5493	1201	0.0041
Phosphatidalcholine, logniceric, caprylic (plasmalogen)	parent	717.5672	$C_{40}H_{81}NO_7P^+$	1.21	717.5681	1201	0.0043
Phosphatidalcholine, nervonic, capric (plasmalogen)	parent	743.5829	$C_{42}H_{83}NO_7P^+$	0.16	743.583	1201	0.0011
C13					744.5863	1201	0.0015
Phosphatidylcholine, linoleic, myristic	parent	729.5308	$C_{40}H_{77}NO_8P^+$	0.6	729.5304	1201	0.0067
C13					730.5338	1201	0.0062
Phosphatidalcholine, linoleic, stearic, hydroxy (plasmalogen)	parent	785.5935	$C_{44}H_{85}NO_8P^+$	0.2	785.5933	1201	0.0042
C13					786.5964	1201	0.0062
Phosphatidalcholine, behinic, lauric (plasmalogen)	parent	745.5985	$C_{42}H_{85}NO_7P^+$	0.31	745.5983	1201	0.0041
C13	-	-	-	-	746.6017	1201	0.0071
C13	-	-	-	-	718.5712	1201	0.0059

Low Intensity | High Intensity

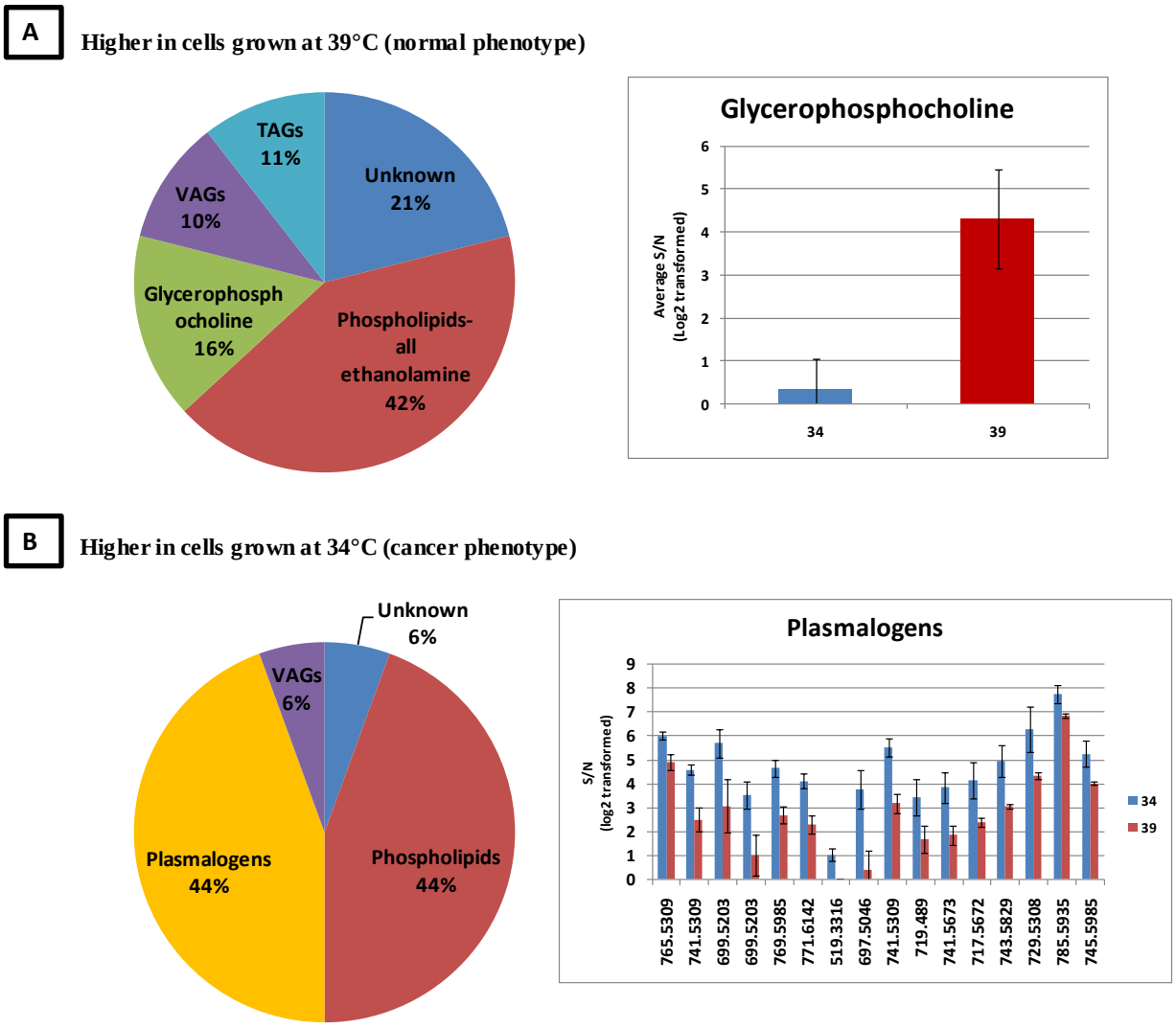

Figure 4.26(A,B) A graphical representation of the pattern of expression, and class, of metabolites that differ between CNA14 cells grown at 39°C and 34°C.

A) The classes of metabolites that were detected at higher levels in the CNA14 cells growing at 39°C (normal phenotype). The graph on right hand side shows levels of glycerophosphocholine in cells grown at 39°C. **B)** The classes of metabolites that were detected at higher levels in the CNA14 cells growing at 34°C (tumourigenic phenotype). Levels of plasmalogens in the cells grown at 34°C are shown in the graph on the right hand side. The error bars represent the standard deviation between replicate samples.

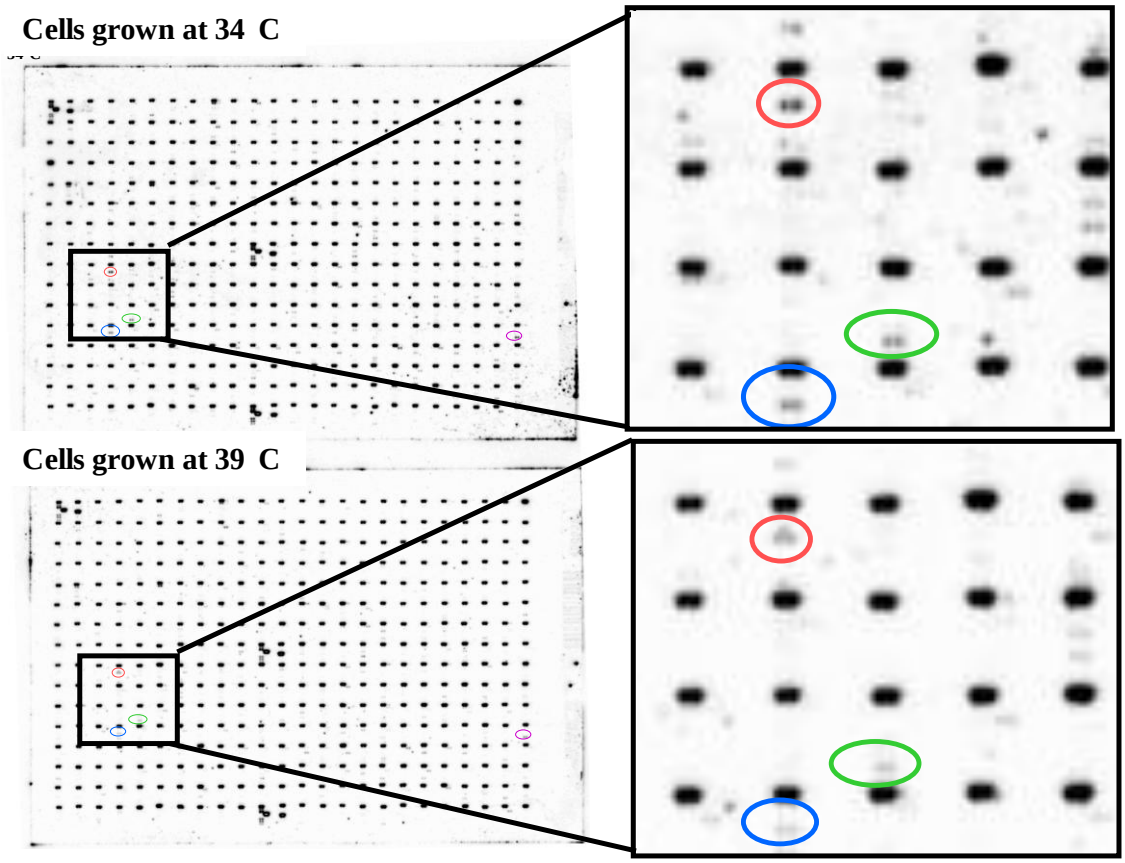

Figure 4.27 Scans of the phosphorimaging screens of two BD Atlas™ plastic rat 4K microarrays (BD Biosciences Clontech).
The microarray of the CNA14 cells grown at 34°C is on top and the microarray of the CNA14 cells grown at 39°C is on the bottom. An example of some of the differences between the arrays has been expanded on the right hand side. A complete list of the significant gene expression differences (minimum two-fold difference) between the cells grown at the two temperatures is located in Table 4.7.

4.3.2 Gene Expression of CNA14 Cells at 34ºC and 39ºC

Due to the apparent metabolic diversity between the CNA14 cells grown at 34ºC and 39ºC, it was decided to investigate whether any genes were responsible for the metabolic differences detected. A BD AtlasTM plastic rat 4K microarray (BD Biosciences Clontech) was used, as per manufacturer's directions, to analyze the gene expression differences between the CNA14 cells grown at 34°C and 39°C. The analysis revealed variability in gene expression between the CNA14 cells grown at 34ºC and those grown at 39ºC (Figure 4.27). The majority of differences between the two different temperatures appear to be higher expression in the tumourigenic phenotype (34ºC) as compared to the normal phenotype (39ºC). The significant gene expression differences (at least a twofold difference in expression) between the CNA14 cells grown at 34 and 39ºC are summarized in Table 4.7. The genes highlighted grey (under the name column in the table) are those that have higher expression levels in the cells grown at 34ºC, and those that are white have higher expression levels in the cells grown at 39ºC.

There was an increase in the expression of hypoxia inducible factor 1 (HIF-1α) which has not only been found to be important in the metabolic adaptation to hypoxia through its role in the conversion of glucose to lactate, but it also actively suppresses the TCA cycle by trans-activating the gene that encodes pyruvate dehydrogenase kinase 1 (PDK1) (Kim *et al.*, 2006) (Figure 4.28). HIF-1α is believed to be a metabolic switch that is responsible for shunting glucose metabolism from the mitochondria to glycolysis in order to continue production of ATP and to prevent the synthesis of reactive oxygen species (Kim *et al.*, 2006). Increased expression of two glycolytic enzymes, lactate dehydrogenase and enolase1α, were detected in the cells grown at 34°C. The increase in glycolytic enzymes in the 'tumourigenic' CNA14 cells suggests that the Warburg phenomenon may be occurring in the cells that are expressing the oncogene. Expression of the gene that encodes for zymogen granule membrane protein was also found to be greater in the cells grown at 34ºC. The zymogen granule membrane protein is a major glycosylphosphatidylinositol anchored membrane glycoprotein that is associated with cholesterol and lipid rafts (Kalus *et al.*, 2002). I also detected an increase in the expression of the gene that encodes the mitochondrial uncoupling protein which attenuates mitochondrial reactive oxygen species (ROS) production and protects the cell against cellular damage (Brand and Esteves, 2005). It was also interesting that ornithine carbamoyltransferase,

Table 4.7(A,B) Gene expression differences between CNA14 cells grown at 34°C and 39°C.
Genes were selected as significant if expression was at least twofold different between the cells grown at 34°C or 39°C. The first table contains the genes that are reduced in the cells grown at 34°C. The following two pages contain the genes that are elevated in the cells grown at 34°C.

A. Genes with reduced expression in the CNA14 cells grown at 34°C as compared to levels detected in the CNA14 cells grown at 39°C.

	avg 34	sd 34	%SD	avg 39	sd 39	%SD	ratio	log(ratio)	Name
1	33.491	0.882	2.634	128.810	27.471	21.327	0.260	**-1.943**	tubulin T beta15
2	53.825	6.028	11.199	189.129	7.960	4.209	0.285	**-1.813**	small proteoglycan I (biglycan), bone (BSPG1) (bone/cartilage proteclycan 1 precursor)
3	341.304	38.437	11.262	1144.216	132.588	11.588	0.298	**-1.745**	ornithine carbamoyltransferase
4	78.701	0.716	0.910	250.809	37.036	14.767	0.314	**-1.672**	collagen alpha2(I) (col1a2)
5	175.048	4.865	2.779	516.718	114.495	22.158	0.339	**-1.562**	src related tyrosine kinase
6	144.709	13.550	9.364	421.080	80.932	19.220	0.344	**-1.541**	early growth response 3
7	274.590	14.315	5.213	738.818	45.499	6.158	0.372	**-1.428**	growth response protein (CL-6)
8	298.339	2.919	0.978	802.544	39.278	4.894	0.372	**-1.428**	salivary proline-rich protein (RP15)
9	50.111	8.356	16.675	133.898	17.091	12.764	0.374	**-1.418**	secreted acidic cystein-rich glycoprotein (osteonectin)
10	162.388	16.624	10.237	409.534	60.010	14.653	0.397	**-1.335**	isoprenylated 67 kD protein
11	345.294	43.588	12.623	821.553	38.891	4.734	0.420	**-1.251**	hemopexin
12	192.006	9.003	4.689	449.169	7.048	1.569	0.427	**-1.226**	isovaleryl Coenzyme A dehydrogenase
13	33.791	0.345	1.020	72.858	13.304	18.261	0.464	**-1.108**	hereditary haemochromatosis-like protein
14	127.326	3.990	3.134	263.553	12.770	4.845	0.483	**-1.050**	farnesyl pyrophosphate synthetase, testis-specific
15	51.531	0.836	1.623	104.451	9.590	9.181	0.493	**-1.019**	defensin-2, beta

Table 4.7 continued.

B. Genes with increased expression in the CNA14 cells grown at 34°C as compared to levels detected in the CNA14 cells grown at 39°C (table continued on next page).

	avg 34	sd 34	%SD	avg 39	sd 39	%SD	ratio	log(ratio)	Name
1	174.376	25.560	14.658	33.596	5.747	17.106	5.190	**2.376**	lin-10 protein homolog (lin-10)
2	991.176	42.538	4.292	196.215	17.034	8.681	5.051	**2.337**	zymogen granule membrane protein GP-2
3	133.163	27.637	20.755	28.488	1.100	3.860	4.674	**2.225**	cytochrome P450, subfamily XIB, polypeptide 1 (steroid 11-beta-hydroxylase)
4	187.630	17.664	9.414	40.164	5.694	14.177	4.672	**2.224**	synaptonemal complex protein 3
5	141.068	5.972	4.233	33.508	1.849	5.518	4.210	**2.074**	coatomer protein beta'-COP
6	144.649	3.081	2.130	40.995	0.240	0.586	3.528	**1.819**	espin
7	328.336	13.981	4.258	105.161	8.978	8.538	3.122	**1.643**	macrophage migration inhibitory factor (MIF); glutathione-binding 13-kDa protein
8	1150.100	160.474	13.953	368.819	4.145	1.124	3.118	**1.641**	enolase 1, alpha
9	426.335	96.891	22.727	141.470	7.941	5.613	3.014	**1.591**	ribosomal protein S26
10	581.868	18.558	3.189	207.435	5.749	2.771	2.805	**1.488**	lactate dehydrogenase A
11	74.593	15.624	20.945	27.098	1.142	4.214	2.753	**1.461**	toll-like receptor 4
12	161.284	13.992	8.675	59.169	0.027	0.045	2.726	**1.447**	acidic ribosomal protein P0
13	259.504	7.306	2.815	95.401	1.299	1.362	2.720	**1.444**	ribosomal protein L14
14	665.599	100.093	15.038	253.136	29.760	11.757	2.629	**1.395**	phospholamban
15	424.368	28.182	6.641	162.144	8.385	5.171	2.617	**1.388**	crystallin B alpha
16	357.969	27.324	7.633	138.053	23.168	16.782	2.593	**1.375**	cytochrome P450, an olfactory-specific steroid hydroxylase
17	916.591	38.210	4.169	354.343	18.311	5.167	2.587	**1.371**	neuraminidase 2
18	480.415	27.821	5.791	186.416	21.091	11.314	2.577	**1.366**	ribosomal protein L6
19	68.166	19.242	28.228	26.609	1.193	4.484	2.562	**1.357**	Phosphocholine cytidylyltransferase
20	414.855	73.171	17.638	163.675	24.590	15.023	2.535	**1.342**	ubiquitin carboxy-terminal hydrolase L1
21	276.458	7.011	2.536	110.376	16.757	15.181	2.505	**1.325**	cyclic nucleotide phosphodiesterase (CaM-PDE)
22	66.999	2.611	3.897	27.205	2.835	10.423	2.463	**1.300**	toll-like receptor 4
23	427.553	61.974	14.495	178.321	7.250	4.065	2.398	**1.262**	diacylglycerol kinase 90kD
24	120.941	10.131	8.377	50.450	7.746	15.355	2.397	**1.261**	late gestation lung protein 2 (Lgl2)
25	96.703	20.870	21.582	40.738	6.986	17.149	2.374	**1.247**	protein tyrosine phosphatase and tensin homolog/mutated in multiple advanced cancers protein (PTEN/MMAC1)
26	460.348	58.686	12.748	196.535	2.691	1.369	2.342	**1.228**	phospholipase B
27	73.888	3.649	4.938	31.706	2.286	7.209	2.330	**1.221**	sec22 homolog (rsec22)
28	161.014	5.450	3.385	70.189	0.256	0.365	2.294	**1.198**	uncoupling protein 2, mitochondrial
29	382.298	32.817	8.584	167.595	0.223	0.133	2.281	**1.190**	medium-chain S-acyl fatty acid synthetase thio ester hydrolase (MCH)
30	65.763	4.642	7.059	28.961	3.555	12.275	2.271	**1.183**	integrin alpha 7A

Table 4.7 continued.

B. Continued (Genes with increased expression in the CNA14 cells grown at 34°C as compared to levels detected in the CNA14 cells grown at 39°C).

	avg 34	sd 34	%SD	avg 39	sd 39	%SD	ratio	log(ratio)	Name
31	60.420	9.652	15.975	26.976	0.546	2.025	2.240	**1.163**	thyroid hormone responsive protein
32	166.233	12.321	7.412	74.970	1.821	2.429	2.217	**1.149**	ribosomal protein L41
33	107.719	10.163	9.435	48.590	3.037	6.250	2.217	**1.149**	protein inhibitor of neuronal nitric oxide synthase (PIN)
34	288.423	5.109	1.771	130.870	16.631	12.708	2.204	**1.140**	ubiquitin and ribosomal protein S27a
35	152.605	25.474	16.692	69.423	6.817	9.819	2.198	**1.136**	heterogeneous nuclear ribonucleoprotein A/B
36	364.698	2.351	0.645	166.600	27.146	16.294	2.189	**1.130**	protein-glutamine gamma-glutamyltransferase
37	56.851	9.763	17.174	25.973	0.004	0.014	2.189	**1.130**	ninjurin 2
38	1060.816	67.361	6.350	484.883	11.282	2.327	2.188	**1.129**	ribosomal protein L29
39	775.376	33.978	4.382	357.403	44.855	12.550	2.169	**1.117**	hydroxyindole-O-methyltransferase
40	5771.263	302.398	5.240	2666.318	196.261	7.361	2.165	**1.114**	tubulin alpha 1 (TUBA1)
41	63.155	13.633	21.587	29.336	2.077	7.080	2.153	**1.106**	tropomyosin non-muscle isoform NM1 (TPM-gamma)
42	636.124	17.658	2.776	296.044	24.019	8.113	2.149	**1.103**	130 kD-Ins(1,4,5)P3 binding protein
43	125.803	2.450	1.948	58.999	1.925	3.263	2.132	**1.092**	guanine nucleotide binding protein beta 2 subunit
44	97.716	7.879	8.063	45.941	3.424	7.453	2.127	**1.089**	carboxypeptidase E (CPE); CPH
45	518.283	90.930	17.545	244.746	48.630	19.869	2.118	**1.082**	PHAS-I
46	247.280	21.132	8.546	117.259	2.028	1.729	2.109	**1.076**	D-beta-hydroxybutyrate dehydrogenase
47	153.445	3.942	2.569	72.866	0.320	0.439	2.106	**1.074**	cytochrome c oxidase polypeptide Vb (COX5B)
48	66.298	11.091	16.729	31.499	1.204	3.822	2.105	**1.074**	dishevelled-1 (dvl-1)
49	497.139	47.123	9.479	239.894	0.327	0.136	2.072	**1.051**	ATP synthase, subunit c, P2 gene
50	1054.455	134.856	12.789	511.901	17.991	3.514	2.060	**1.043**	acyl-CoA synthetase ll, brain
51	65.414	9.017	13.785	31.959	1.837	5.747	2.047	**1.033**	histone H1-0
52	71.465	6.230	8.717	35.028	6.608	18.865	2.040	**1.029**	mitogen-activated protein kinase kinase 1 (MAP kinase kinase 1; MAPKK1; MAP2K1; PRKMK1); MAPK/ERK
53	108.053	0.735	0.681	53.070	3.528	6.649	2.036	**1.026**	2,4-dienoyl-CoA reductase precursor
54	96.134	12.008	12.491	47.340	3.129	6.610	2.031	**1.022**	aldehyde oxidase (female form)
55	395.285	25.870	6.545	195.826	16.566	8.459	2.019	**1.013**	ribosomal protein S10
56	69.576	5.351	7.691	34.559	3.817	11.044	2.013	**1.010**	testis enhanced gene transcript
57	921.485	178.389	19.359	458.810	46.524	10.140	2.008	**1.006**	Ig germline gamma-1 H-chain C-region
58	69.410	12.120	17.461	34.606	5.857	16.924	2.006	**1.004**	histone H3.3
59	85.058	4.465	5.250	42.446	1.575	3.711	2.004	**1.003**	nuclear pore complex protein nup155
60	80.854	7.992	9.885	40.358	1.018	2.523	2.003	**1.002**	zinc finger protein (pMLZ-4)
61	2843.238	410.256	14.429	1419.364	139.744	9.846	2.003	**1.002**	peptidylprolyl isomerase A (cyclophilin A)
62	63.086	6.390	10.130	34.069	2.158	6.336	1.852	**0.889**	hypoxia-inducible factor-1 alpha (Hif1a) *

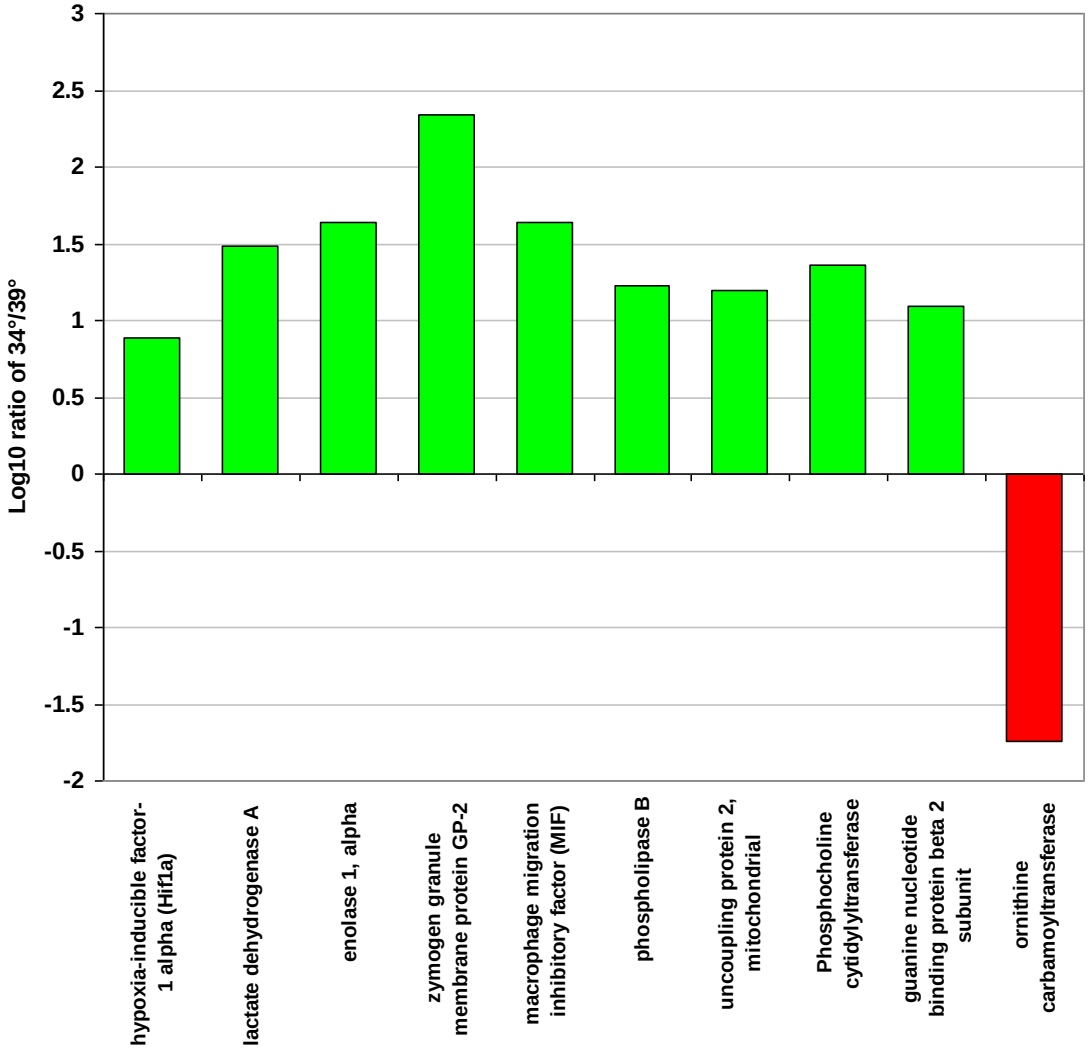

Figure 4.28 The $\log_{10}$ ratio of the expression of selected genes at 34°C as compared to those in the cells grown at 39°C.

These particular genes were selected due their particular relevance to glycolysis and lipid synthesis. The green depicts the genes which are expressed at higher levels in the tumourigenic phenotype and the red is for the gene expressed at a higher level in the normal phenotype.

the second enzyme in the urea cycle which converts ornithine to citrulline, was found to be reduced in the cells grown at 34ºC. The urea cycle produces fumarate, which feeds into the TCA cycle. Therefore, it is possible that the decrease in ornithine carbamoyltransferase is another mechanism that the cancer cell has developed to prevent the TCA cycle from functioning. These connections are hypotheses of the relationships that may exist between the results of the transcriptomics and the metabolomics data, and therefore further research will be required to either confirm or refute them.

There are many interesting expression differences in CNA14 cells grown at 34°C and 39ºC, including zymogen granule membrane protein GP-2. It encodes for a major glycosylphosphatidylinositol anchored membrane glycoprotein that is associated with cholesterol and lipid rafts (Kalus *et al.*, 2002). It is significantly higher (5 times) in the CNA14 cells that were grown at 34ºC. There are also a group of genes that encode for ribosomal proteins that are considerably higher in the tumourigenic cells, indicating increased cell growth. Elevated transcript levels of hydroxyindole-O-methyltransferase (HIOMT) were also detected in the cells grown at 34 ºC. HIOMT catalyzes the final reaction in the melatonin synthesis pathway, and has been detected at elevated levels in pineal parenchymal tumor (PPT) cells (Fukuda *et al.*, 2010). Mitochondrial uncoupling protein 2 (UCP2) transcript levels were also elevated in the cells grown at 34 ºC. UCP2 attenuates mitochondrial ROS production, therefore protection the cell against cellular damage, as well as catalyzing the export of fatty acids and anions out of the mitochondria (Baffy, 2010) . Elevated levels of dishevelled-1 (dvl-1) transcripts were found in the tumourigenic cells. The Dishevelled family of proteins play a regulatory role in the WNT signalling pathway and have been found to be elevated in numerous cancers (Zhao *et al.*, 2010). Phospholipase B converts phospholipids into fatty acids, by cleaving both fatty acid residues from the phospholipids (Morgan *et al.*, 2004), and is found to be expressed at a higher level in the 34ºC cells. Macrophage migration inhibitory factor (MIF) promotes malignant cell transformation (Mitchell, 2004) and the gene which encodes it is at a higher level of expression in the CNA14 cells grown at 34ºC. The gene for D-beta-hydroxybutarate dehydrogenase, was expressed twice as high in the tumourigenic form of CNA14. The gene product is a membrane enzyme that requires lecithin for activity and plays an essential role in energy metabolism (Grover *et al.*, 1975). The gene which encodes for lactate dehydrogenase A, which catalyzes the interconversion of pyruvate to lactate and the

oxidation of hydroxybutyrate (Koukourakis *et al.*, 2006), is also elevated in the CNA14 cells grown at 34ºC. Another important enzyme in the glycolytic pathway, enolase 1 alpha, is a cytoplasmic glycolytic enzyme that is responsible for the formation of phosphoenolpyruvate (Chang *et al.*, 2003) and was also found to be elevated in the cells grown at 34ºC.

There were only a few genes that showed higher expression in the CNA14 cells grown at 39ºC as compared to the cells grown at 34ºC. The gene encoding secreted acidic cysteine-rich glycoprotein (also known as osteonectin) is one of the genes with higher expression in the normal cells. The gene product regulates the activity of fibroblast growth factor 2 and has an antiproliferative effect (Yan and Sage, 1999). The gene which encodes for ornithine carbamoyltransferase, the second enzyme in the urea cycle which converts ornithine to citrulline, is also significantly higher in the cells grown at 39ºC.

4.3.3 Temperature Shift

I was interested to know if the oncogenic phenotype was reversible. The cells that had been originally grown at 34 ºC were shifted to 39 ºC, and the cells grown at 39 ºC were shifted to 34 ºC. The PCA of the CNA14 temperature shift experiment shows a clear separation of the cells originally grown at 34ºC and 39ºC along principal component 1 (PC1) (Figure 4.29). Interestingly, the temperature shift did not result in a conversion of metabolic profiles even after a shift of 96 hours. Although the cells appeared to phenotypically change when temperature shifted, metabolically there was very little change. Movement of the samples along principal components 2 and 3 was also examined and it became evident that the differences between the cells grown at 34ºC and shifted to 39ºC were found along PC2 and movement of the 39ºC cells, being shifted to 34ºC, was found along PC3 (Figure 4.29). These results may prove that it is not possible to metabolically shift CNA14 cells from a normal profile to a tumour profile (and tumour to normal) within 96 hours. Although phenotypically they may have appeared to take on characteristics of the other cell type, their metabolic pathways do not significantly change. This suggests that oncogenic transformation, metabolically, is irreversible.

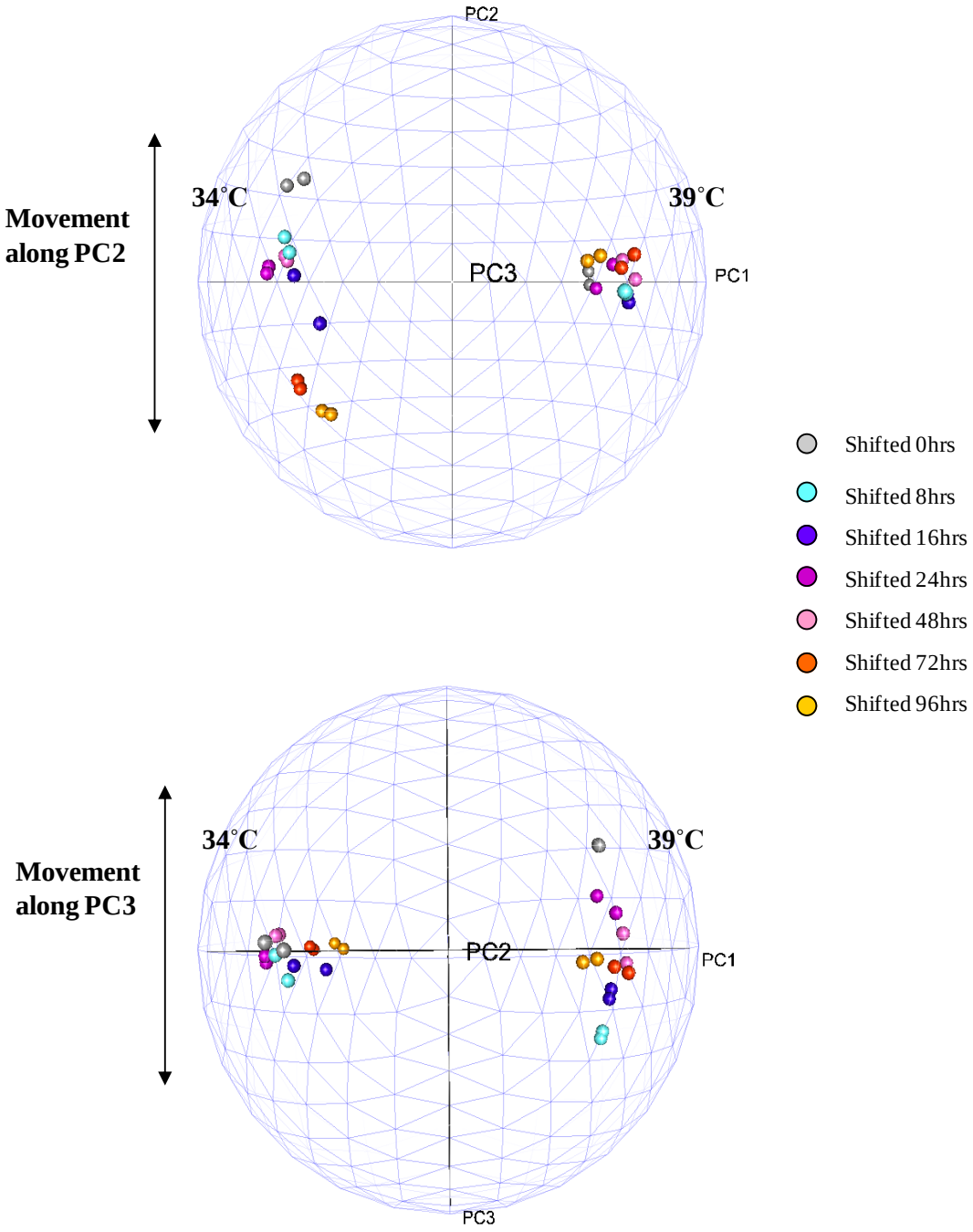

Figure 4.29 PCA of CNA14, cells grown at 34°C and shifted to 39°C, and cells grown at 39°C and shifted to 34°C.
The PCA of the temperature shift experiments, from the PC2 and PC3 views. The cells shifted from 34˚C to 39˚C show movement along PC2, whereas the cells shifted from 39˚C to 34˚C show movement along PC3.

4.3.4 Discussion

In the metabolomic analysis of CNA14 cells, a dramatic increase was observed in phospholipids (phosphatidylcholines, phosphatidylethanolamines, and plasmalogens) as well as triacylglycerols and diacylglycerols in the cells grown at 34°C (tumourigenic phenotype) compared to the cells grown at 39°C (showing a normal phenotype). There are a few phospholipids that are found to be moderately elevated in the normal cells; however, the majority of those detected were higher in the tumour phenotype. There is also a difference in the level of glycerophosphocholine in the cells grown at the two temperatures. Much higher levels were observed in the normal cells as compared to near absent levels in the transformed phenotype. This observation suggests that glycerophosphocholine may be a precursor molecule for the lipids that are elevated in the cells grown at 34°C.

In our attempt to explain these observations, I methodically searched the literature for any previous reports linking metabolic deregulation to known cellular changes that occur in cancer. In 1926, Warburg proposed a model of tumourigenesis involving altered energy production in tumours (Langbein *et al.*, 2006). This model, which is now known as the Warburg hypothesis, states that cancer cells shift to a high level of aerobic glycolysis, even in the presence of oxygen, and low respiration to metabolize glucose (Warburg, 1956). Under normal physiological conditions, cellular energy metabolism is preferentially based on oxidative phosphorylation, which is considerably more efficient than glycolysis. Warburg hypothesized an alternative state of energy metabolism in cancer systems, which included an impaired mitochondrial function and increased dependence on glycolysis as a source of energy, even under aerobic conditions (Warburg, 1956). According to this hypothesis, the ability of cancer cells to generate ATP via mitochondrial respiration is impaired, which likely triggers alternative metabolic pathways by the over-expression of glycolytic enzymes. This alternative method of energy production may be a response, or perhaps a requirement, due to the rapid growth of cancer cells and consequently the expansion of a tumour mass which may result in an insufficient supply of blood to the tissue. This would create a hypoxic environment with limited mitochondrial respiration, causing cancer cells to utilize the glycolytic pathway as its main source of energy (Xu *et al.*, 2005). If the cancer cells automatically switch to glycolysis,

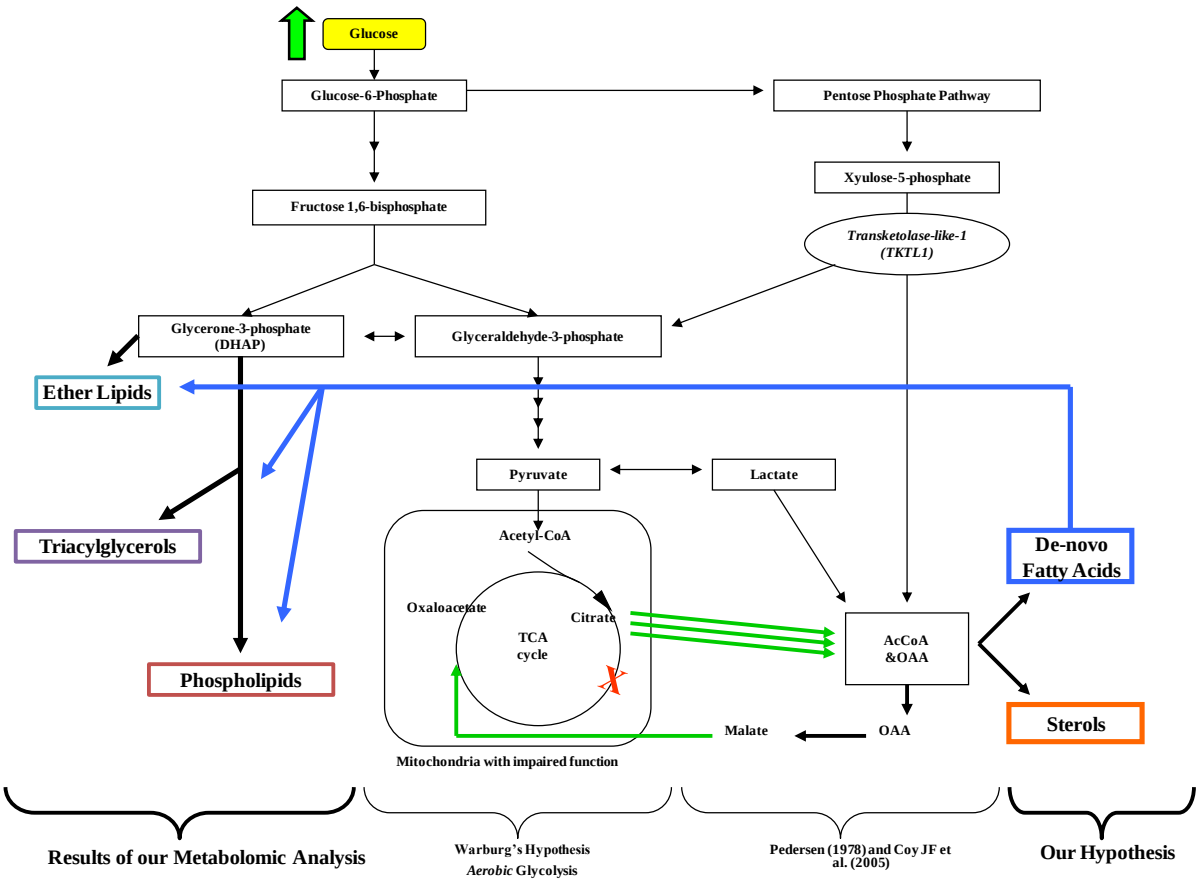

Figure 4.30 A model of glycolysis and lipid synthesis in cancer.
This model is a compilation of well known metabolic pathways, such as glycolysis and the pentose phosphate pathway, cancer induced alterations to metabolic pathways and the results of our analysis of CNA14 cells. Glucose uptake is increased in most cancer cells (green arrow). The increased glucose in the cell is metabolized by the glycolytic pathway or the pentose phosphate pathway. Citrate is exported out of the mitochondria in most cancer cells (three green arrows) and is used to synthesize cytosolic acetyl-CoA. The coloured boxes highlight the metabolites detected at increased levels in our analyses.

rather than respiration as a source of energy, then a lack of oxygen will not prevent the cells from growing.

The metabolic pathways are initially altered in cancer systems with the increased uptake of glucose in the cells (Figure 4.30). The result of the increased levels of glucose is an up-regulation of both glycolysis and the pentose phosphate pathway. As mentioned previously, cancer cells typically utilize *aerobic* glycolysis (even in the presence of oxygen) as a source of energy, which is known as the Warburg effect. This effect can be seen in the model with an increase in glycolysis and increased lactate production. Typically in normal cells citrate is converted into isocitrate, which then proceeds into the TCA cycle (Costello and Franklin, 2005). Tumour cells have also been found to exhibit both a truncated TCA cycle and an increase in the export of citrate out of the mitochondria into the cytoplasm (Parlo and Coleman, 1984).

The export of citrate depletes the availability of citrate for oxidation and therefore may likely be the cause of the limited respiration observed in the cancer cells. Reduced levels of mitochondrial aconitase, the enzyme responsible for the conversion of citrate into isocitrate, have also been reported in cancer systems and may also lead to the truncation of the TCA cycle (Ristow, 2006).

Another important observation regarding cancer metabolism, made over half a century ago, was that tumours have an increased rate of de-novo fatty acid synthesis (Medes *et al.*, 1953). Numerous researchers have exploited this finding and through the inhibition of fatty acid synthesis have arrested cell proliferation and induced the death of the diseased cells in various types of cancer (Pizer *et al.*, 1996; Brusselmans *et al.*, 2005). These observations clearly fit the model created (Figure 4.30) as de-novo fatty acid synthesis would be required in order for the cancer cells to increase the synthesis of the multiple classes of lipids found to be at elevated levels in the cells expressing the cancer phenotype.

There has been a recent discovery of a transketolase like gene (TKTL1) that is up-regulated in most cancers as well as numerous neurodegenerative diseases and diabetes (Coy *et al.*, 2005). It encodes a transketolase enzyme that enables the conversion of xylulose 5-phosphate into glyceraldehyde-3-phosphate and Acetyl-CoA (Langbein *et al.*, 2006). The conversion of xylulose 5-phosphate into glyceraldehyde-3-phosphate, which is unique to cancer systems, may signify the level of importance that the products of glycolysis have in

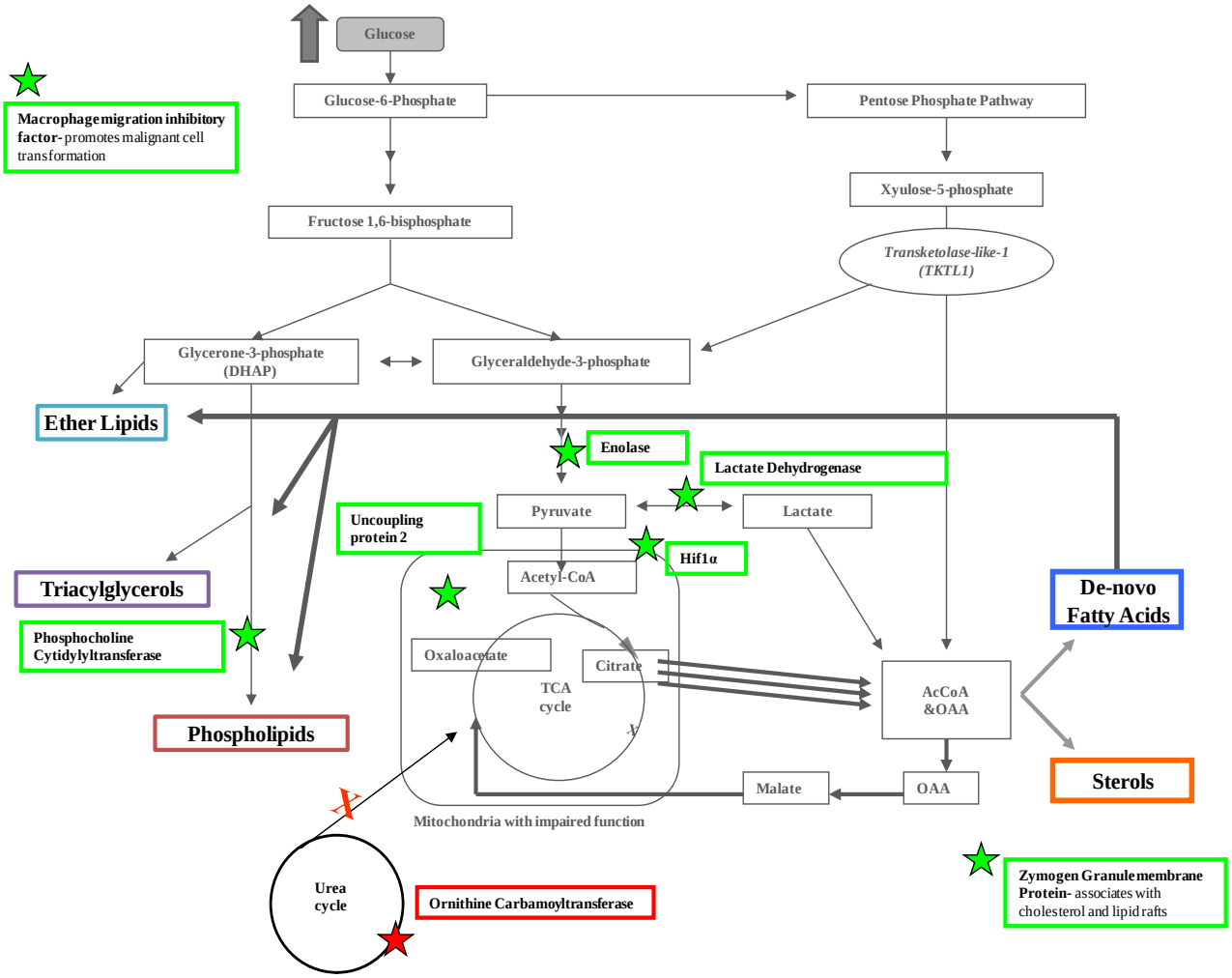

Figure 4.31 The model of glycolysis and lipid synthesis in cancer, in combination with the results of the gene expression analysis of the CNA14 cells.
Some of the key results of the gene expression analysis have been overlaid with the metabolic changes that have been associated with cancer development and progression. The green (increased in CNA14 cells grown at 34°C) and red (decreased in CNA14 cells grown at 34°C) boxes highlight the gene changes, and the other coloured boxes highlight the metabolites that were detected at elevated levels (in the CNA14 cells grown at 34°C) in our analyses.

cancer development. This discovery clearly fits into the presented model and further suggests that a cancer cells heavily relies on glycolysis and the related end-products for the development of the cancer phenotype.

Some of the gene expression differences that were detected in the CNA14 cells have been overlaid onto the glycolysis and lipid synthesis model that was discussed above (Figure 4.31). In the analysis of transcriptional changes occurring in the CNA14 system, increases of two glycolytic genes encoding lactate dehydrogenase and enolase 1 alpha were detected in the cells grown at 34ºC which show the transformed phenotype. It was also interesting that ornithine carbamoyltransferase, the second enzyme in the urea cycle which converts ornithine to citrulline, was found to be reduced in the cells grown at 34ºC. The urea cycle produces fumarate, which feeds into the TCA cycle. Therefore, it is possible that the decrease in ornithine carbamoyltransferase is another mechanism that the cancer cell has developed to prevent the TCA cycle from functioning. These connections are hypotheses of the relationships that may exist between the results of the transcriptomics and the metabolomics data, and therefore further research will be required to either confirm or refute them.

Recent findings in cancer research have rekindled interest in Warburg's theory, including an observation that, during tumourigenesis, an increase in glucose uptake and lactate production occurs and that the fully transformed state is most dependent on glycolysis and minimally dependent on the mitochondria for ATP synthesis (Ramanathan *et al.*, 2005). One major reason for the shift to glycolysis in cancer systems is likely to provide a source of acetyl CoA for the mitochondrial synthesis of citrate, which provides the source for cytosolic acetyl CoA (Costello and Franklin, 2005). Cytosolic acetyl CoA is the essential precursor molecule for the synthesis of fatty acids, which in turn are the major building blocks for lipid molecules. The strong correlation between the rate of aerobic glycolysis and the aggressiveness of the cancer likely indicates that the glycolytic phenotype offers a significant proliferative advantage and may be a crucial component of the malignant phenotype (Gatenby and Gillies, 2004).

There have also been many connections made between cancer causing genes and glucose metabolism, including AKT which has been found to stimulate glucose metabolism in cancer cells, as well as AMP-activated protein kinase which links glucose metabolism and cell cycle (Langbein *et al.*, 2006). Reports have also showed that mitochondria in rapidly growing tumour cells are generally smaller and show less cristae than mitochondria from normal tissues,

and also that the actual number of mitochondria in tumour cells is reduced (Ristow, 2006). The fact that the glycolytic rate in cancers is increased has been detected and reported by many researchers over the past 70 years. It is still unknown whether this is due to the reduced mitochondria activity, or rather that the mitochondria activity is reduced due to the increased glycolytic activity.

It is well known that the inactivation of the p53 tumour suppressor gene has been found to occur in almost half of all human tumours (Mori *et al.*, 2004), and recently it was found that p53 modulates the balance between the utilization of the glycolytic and respiratory pathways (Matoba *et al.*, 2006). A recently published review suggests that there are four main advantages for aerobic glycolysis in cancer: the cells will be able to survive fluctuating levels of oxygen, the lactic acid produced during glycolysis conditions their environment for tumour invasion and suppresses anticancer immune effectors, the cells can metabolize glucose through the pentose phosphate pathway which in turn generates NADPH, and lastly cancer cells can use the glycolytic intermediates for anabolic reactions (Kroemer and Pouyssegur, 2008).

Despite numerous reports by many different researchers whose research complements, or supports, Warburg's theory, the underlying cause of the effect is still not well understood. It is also unknown if the same causes always underlie this effect in cancers, or if genetic influences play any part (Unwin *et al.*, 2003). The glycolytic phenotype in cancer is believed to be present because it offers a growth advantage and not because it is the result of a secondary response from another pathway during carcinogenesis (Gatenby and Gillies, 2004). The glycolytic phenotype suppresses apoptosis and the by-products of glycolysis contribute to the degradation of the extracellular matrix, and increase cell mobility and metastatic potential (Bonnet *et al.*, 2007). Recently it was also discovered that activated T cells also have dramatically increased metabolic requirements, and in order to meet the energy and biosynthetic needs the T cells increase glucose uptake and employ aerobic glycolysis (Cham *et al.*, 2008; Maciver *et al.*, 2008).

All of these pieces of information add strength to the hypothesis of the pivotal role of glycolysis in cancer systems and the dependence that the cells have on the products of glucose metabolism for the development and progression of cancer. Our discovery of significant changes in lipid synthesis in cancer systems, as well as during the fundamental cellular

processes involved in cancer development, may provide the evidence required to understand the correlation between cancer and glycolysis.

5 Final Conclusions and Future Directions

The results presented in this thesis have demonstrated that non-targeted metabolomic profiling approaches can reveal non-intuitive insights into basic cellular processes. The biochemical composition of biological material associated with particular cellular or physiological responses can be characterized first, followed by the generation of hypotheses based on the data collected. This type of analysis represents a non-traditional scientific approach, in that specific hypotheses regarding the response of interest are generated subsequent to the analysis. The use of a FTICR-MS in non-targeted metabolomic analyses has allowed the detection of a broad range of metabolites, including both known and novel molecules, in three independent models. This would not have been possible if a targeted approach had been solely utilized. The results of the metabolomic analyses suggest that particular lipid alterations are associated with all of the cellular processes being investigated. During the cell cycle, TAGs and VAGs were detected at elevated levels at the key regulatory checkpoints in the cell cycle. Plasmalogens were detected at elevated levels during differentiation of monocytes into macrophages. Furthermore, elevated lipids, in particular plasmalogens, were detected in cells expressing a temperature sensitive oncogene.

These results suggest that alterations in the metabolism of specific classes of lipids may be not only essential in cell growth, proliferation, and differentiation, but also a requirement in cancer development. Cellular membranes are formed by amphipathic lipids, such as phospholipids and plasmalogens, which contain hydrophilic and hydrophobic regions. Cellular membranes not only segregate the external environment from the internal components of the cells, but they also enable the production of discrete organelles within the cell. Lipids are required not only as structural components of the cell, but also for basic cellular functions such as cell signalling and energy storage. It would therefore be logical that during fundamental cellular processes, such as cell cycle, differentiation and transformation, significant changes in lipid content would occur.

During the cell cycle elevated levels of triacylglycerols (TAGs) and vinyl acylglycerols (VAGs) were detected as the cells approached the mitotic phase of the cycle. An increase of phospholipase C (PLC) transcript levels was also detected in the cells prior to cell division. Phospholipase C is a class of enzymes that cleave phospholipids to release the phosphate head group of the molecule. One type of lipid that PLC cleaves is phosphatidylinositol 4,5-

bisphosphate (PIP_2), which results in the production of inositol 1,4,5-triphosphate (IP_3) and diacylglycerol (DAG). PLC can also cleave ethanolamine plasmalogens, resulting in the production of VAGs and ethanolamine phosphates. DAGs and VAGs are involved in the activation of protein kinase C, which in turn regulates many different cellular processes (Ford *et al.*, 1989; Griner and Kazanietz, 2007). It has also been hypothesized that VAGs may be competitive inhibitors of DAGs for PKC, and therefore may regulate PKC-mediated responses (Nagan and Zoeller, 2001). PKC signalling has been implicated in growth control, differentiation and tumourigenesis (Fima *et al.*, 2001). Activation of PKC has been shown to regulate cell cycle progression during G1 and G2/M phases, either in a stimulatory or inhibitory manner (Fima *et al.*, 2001). PKC is also a major cellular receptor for phorbol esters, such as phorbol 12-myristate 13-acetate (PMA), which was used to initiate differentiation in U937 cells. It is conceivable that PLC activity, signalling lipids (DAGs and VAGs) and PKC signalling are integral in all three of the fundamental cellular processes examined for this thesis. DAG's are also precursors for phospholipids (phosphatidylethanolamines and phosphatidylcholines) as well as triacylglycerols. It is therefore possible that after the DAG has activated PKC it will either be converted into a phospholipid for cellular membranes or into a TAG for the storage of fatty acids, depending on the requirements of the cells at that time.

Plasmalogens were detected at elevated levels during differentiation of U937 cells and in CNA14 cells expressing a temperature sensitive oncogene $p130^{gag\text{-}fps}$. In addition to serving as structural components of cellular membranes, plasmalogens also function as sinks for polyunsaturated fatty acids, intracellular signalling molecules, mediators of membrane dynamics and endogenous antioxidants (Zoeller *et al.*, 1999; Nagan and Zoeller, 2001; Brites *et al.*, 2004). The monocyte form of the U937 cell is a small spherical cell which is free floating in the media. After the addition of PMA to the media, the cells become adherent and begin to differentiate within 3 hours. This dramatic physical change would likely require a major, if not a complete, alteration in membrane composition, and consistent with our results, may be modulated by significant increases in plasmalogens.

The results of our investigations have implicated glycerolipids, in particular phospholipids, in the process of cell cycle progression, differentiation and oncogenic transformation. The majority of phospholipids are contained in the cellular membranes of

cells, and it is therefore logical to assume that the membrane structure is being affected during these processes. Nutrient and ion transport, inter- and intracellular signalling, fusion, and receptor localization and interaction are all influenced by membrane composition. It is likely that phospholipid alterations in the cell would affect the membrane structure and in turn alter these important cellular mechanisms. Model membranes that are composed entirely of ethanolamine plasmalogens transform from lamellar gel to non-lamellar or non-bilayer structures at lower temperatures than membranes composed of diacyl species (Lohner, 1996). The non-bilayer areas of the membrane are more susceptible to increased leakage of the membranes to ions and allow membrane-membrane fusions (Glaser and Gross, 1994; Nagan and Zoeller, 2001). Membrane fusion is very important in several cellular processes including endocytosis and secretion (Nagan and Zoeller, 2001), both of which are characteristic of macrophage cells. Ethanolamine plasmalogens, especially those containing arachidonic acid, have also been recently identified as major components of lipid rafts in cellular membranes (Pike *et al.*, 2002). Lipid rafts are specialized cholesterol-enriched lipid domains that facilitate interactions between lipid and protein components of signalling pathways, regulate membrane trafficking, and cytoskeletal composition (Fan *et al.*; Pike *et al.*, 2002). Lipid rafts also contain transforming growth factor (TGF)-β receptors, which regulate cell growth, apoptosis, differentiation and migration (Zuo and Chen, 2009).

When *de novo* synthesis of lipids was inhibited with BTA treatment, the U937 cells were not able to complete the differentiation process. Interestingly, when the inhibitor was removed, plasmalogen and cholesterol levels dramatically increased and the cells completed the differentiation process, suggesting that U937 cells require plasmalogens and cholesterol in order to differentiate. However, further experiments will be required in order to prove this hypothesis. A direct inhibition of plasmalogen synthesis, such as a knockdown of DHAPAT, in U937 cells may provide insight into the necessity of these lipids during the differentiation process. It may also be interesting to analyze the cellular membranes of the U937 cells for non-lamellar regions and lipid rafts during differentiation to determine if the increase in plasmalogen levels is linked to these membrane structures.

In order for cells to grow and replicate they must generate enough energy and synthesize, or acquire, all of the biomolecules to double their cellular content. For highly proliferative cells, such as cancer cells, increased glucose uptake, up-regulated glycolysis, and reduced

cellular respiration (aerobic glycolysis or the Warburg effect) provide the cell with both the energy and metabolic intermediates required for rapid cell growth. This reprogramming of the cell's core metabolic pathway confers a selective growth advantage ideal for cancer progression. Interestingly, our examination of metabolic and gene expression differences in the CNA14 cells revealed increased levels of lipids and up-regulation of genes encoding glycolytic enzymes in the cells expressing the oncogene $p130^{gag\text{-}fps}$. A comparison of normal and transformed human cells would have been preferred; however, it is very difficult to culture normal cells and therefore was not feasible.

There are many different types of analytical approaches currently being used to further our understanding of human health and disease states. The question really becomes what actually defines a disease state? Some researchers may believe that the answer can be discovered at the gene or protein level. However, in order to measure the true health state of an individual one must not only consider the blueprint molecules, genes and proteins, but must also consider the phenotype. The phenotype of a cell or organism is the complement of its physical characteristics, comprised primarily of proteins and small molecules. Changes in phenotype result from genetic alterations, changes in environment (such as diet and lifestyle) and aging. Therefore, a metabolomics analysis in the study of human health, aging and disease can provide a wealth of knowledge unattainable with any other type of approach.

The major and still yet unanswered question to the observations reported in this thesis is whether the observed changes are the cause of specific processes, or whether they are merely side effects? It is possible that cancer cells require the *de novo* synthesis of lipids, and shifting the cell's core metabolic system to aerobic glycolysis provides the necessary metabolic intermediates and energy requirements. On the other hand, the synthesis of the lipids may just be a result of the cancer cell's requirement for aerobic glycolysis. Although the results presented in this thesis suggest that the lipid changes were a result of the three basic cellular processes being studied, it is possible that under real physiological conditions associated with human disease lipid changes may be the cause of the disease state. Mutations to certain enzymes, changes in diet and environment, or even decreases in thermodynamic stability due to aging could alter the composition of the cellular membranes (de Grey, 2002; Dennis *et al.*, 2009). Changes to the membrane structure could alter membrane lipid rafts and microdomain architecture, which may lead to de-regulation of the cell cycle or an inability to differentiate.

Future investigations should be focused on understanding why the increase of lipids occurs during these cellular processes and whether or not their *de novo* synthesis is a necessity or a side effect of upstream changes. As previously mentioned, directly inhibiting the synthesis of specific classes of lipids in each of the cell lines studied could provide insight into the importance of the lipids during the cellular processes of interest. It may also be interesting to create a knock-down animal model in which DHAPAT has been inhibited in the animal to determine if the animal's susceptibility to tumour development is altered with reduced plasmalogen levels. It would also be very interesting to characterize the membrane and phospholipid composition of biospecimens collected from subjects affected with various diseases. Better understanding how metabolic pathways work and how membrane composition can affect cellular mechanisms may one day lead to new approaches for their modulation, and potentially to new therapies.

6 BIBLIOGRAPHY

Aharoni, A., Ric de Vos, C.H., Verhoeven, H.A., Maliepaard, C.A., Kruppa, G., Bino, R., and Goodenowe, D.B. (2002). Nontargeted metabolome analysis by use of Fourier Transform Ion Cyclotron Mass Spectrometry. Omics *6*, 217-234.

Albi, E., Cataldi, S., Magni, M.V., and Sartori, C. (2004). Plasmalogens in rat liver chromatin: new molecules involved in cell proliferation. Journal of cellular physiology *201*, 439-446.

Albi, E., and Viola Magni, M.P. (2004). The role of intranuclear lipids. Biol Cell *96*, 657-667.

Alwine, J.C., Kemp, D.J., and Stark, G.R. (1977). Method for detection of specific RNAs in agarose gels by transfer to diazobenzyloxymethyl-paper and hybridization with DNA probes. Proceedings of the National Academy of Sciences of the United States of America *74*, 5350-5354.

Baffy, G. (2010). Uncoupling protein-2 and cancer. Mitochondrion *10*, 243-252.

Bajad, S.U., Lu, W., Kimball, E.H., Yuan, J., Peterson, C., and Rabinowitz, J.D. (2006). Separation and quantitation of water soluble cellular metabolites by hydrophilic interaction chromatography-tandem mass spectrometry. J Chromatogr A *1125*, 76-88.

Barrow, M.P., Burkitt, W.I., and Derrick, P.J. (2005). Principles of Fourier transform ion cyclotron resonance mass spectrometry and its application in structural biology. Analyst *130*, 18-28.

Bell, R.M., and Coleman, R.A. (1980). Enzymes of glycerolipid synthesis in eukaryotes. Annual review of biochemistry *49*, 459-487.

Bhalla, R., Narasimhan, K., and Swarup, S. (2005). Metabolomics and its role in understanding cellular responses in plants. Plant Cell Rep, 1-10.

Bino, R.J., Hall, R.D., Fiehn, O., Kopka, J., Saito, K., Draper, J., Nikolau, B.J., Mendes, P., Roessner-Tunali, U., Beale, M.H., *et al.* (2004). Potential of metabolomics as a functional genomics tool. Trends Plant Sci *9*, 418-425.

Bonnet, S., Archer, S.L., Allalunis-Turner, J., Haromy, A., Beaulieu, C., Thompson, R., Lee, C.T., Lopaschuk, G.D., Puttagunta, L., Bonnet, S., *et al.* (2007). A mitochondria-k(+) channel axis is suppressed in cancer and its normalization promotes apoptosis and inhibits cancer growth. Cancer cell *11*, 37-51.

Bradford, M.M. (1976). A rapid and sensitive method for the quantitation of microgram quantities of protein using the principle of protein-dye binding. Analyt. Biochem. *72*, 248-254.

Brand, M.D., and Esteves, T.C. (2005). Physiological functions of the mitochondrial uncoupling proteins UCP2 and UCP3. Cell metabolism *2*, 85-93.

Brites, P., Waterham, H.R., and Wanders, R.J. (2004). Functions and biosynthesis of plasmalogens in health and disease. Biochimica et biophysica acta *1636*, 219-231.

Browaeys-Poly, E., Perdereau, D., Lescuyer, A., Burnol, A.F., and Cailliau, K. (2009). Akt interaction with PLC(gamma) regulates the G(2)/M transition triggered by FGF receptors from MDA-MB-231 breast cancer cells. Anticancer research *29*, 4965-4969.

Brusselmans, K., De Schrijver, E., Verhoeven, G., and Swinnen, J.V. (2005). RNA interference-mediated silencing of the acetyl-CoA-carboxylase-alpha gene induces growth inhibition and apoptosis of prostate cancer cells. Cancer research *65*, 6719-6725.

Buchholz, A., Hurlebaus, J., Wandrey, C., and Takors, R. (2002). Metabolomics: quantification of intracellular metabolite dynamics. Biomol Eng *19*, 5-15.

Butcher, E.C., Berg, E.L., and Kunkel, E.J. (2004). Systems biology in drug discovery. Nature biotechnology *22*, 1253-1259.

Butte, A. (2002). The use and analysis of microarray data. Nat Rev Drug Discov *1*, 951-960.

Cham, C.M., Driessens, G., O'Keefe, J.P., and Gajewski, T.F. (2008). Glucose deprivation inhibits multiple key gene expression events and effector functions in CD8+ T cells. Eur J Immunol *38*, 2438-2450.

Chang, Y.S., Wu, W., Walsh, G., Hong, W.K., and Mao, L. (2003). Enolase-alpha is frequently down-regulated in non-small cell lung cancer and predicts aggressive biological behavior. Clin Cancer Res *9*, 3641-3644.

Cheong, H.T., Park, T.M., Ikeda, K., and Takahashi, Y. (2003). Cell cycle analysis of bovine cultured somatic cells by flow cytometry. Jpn J Vet Res *51*, 95-103.

Costello, L.C., and Franklin, R.B. (2005). 'Why do tumour cells glycolyse?': From glycolysis through citrate to lipogenesis. Mol Cell Biochem *280*, 1-8.

Coy, J.F., Dressler, D., Wilde, J., and Schubert, P. (2005). Mutations in the transketolase-like gene TKTL1: clinical implications for neurodegenerative diseases, diabetes and cancer. Clin Lab *51*, 257-273.

Danna, K., and Nathans, D. (1971). Specific cleavage of simian virus 40 DNA by restriction endonuclease of Hemophilus influenzae. Proceedings of the National Academy of Sciences of the United States of America *68*, 2913-2917.

Davies, G.F., Roesler, W.J., Juurlink, B.H., and Harkness, T.A. (2005). Troglitazone overcomes doxorubicin-resistance in resistant K562 leukemia cells. Leuk Lymphoma *46*, 1199-1206.

de Grey, A.D. (2002). The reductive hotspot hypothesis of mammalian aging: membrane metabolism magnifies mutant mitochondrial mischief. European journal of biochemistry / FEBS *269*, 2003-2009.

Deane, N.G., Parker, M.A., and Beauchamp, R.D. (2005). Cell proliferation: a matter of time and place. Surgery *138*, 1-7.

Dennis, J.W., Nabi, I.R., and Demetriou, M. (2009). Metabolism, cell surface organization, and disease. Cell *139*, 1229-1241.

Dunn, W.B., Bailey, N.J., and Johnson, H.E. (2005). Measuring the metabolome: current analytical technologies. Analyst *130*, 606-625.

Edwards, D., and Batley, J. (2004). Plant bioinformatics: from genome to phenome. Trends Biotechnol *22*, 232-237.

Erson, A.E., and Petty, E.M. (2004). CHFR-associated early G2/M checkpoint defects in breast cancer cells. Mol Carcinog *39*, 26-33.

Fagone, P., and Jackowski, S. (2009). Membrane phospholipid synthesis and endoplasmic reticulum function. Journal of lipid research *50 Suppl*, S311-316.

Fahy, E., Subramaniam, S., Brown, H.A., Glass, C.K., Merrill, A.H., Jr., Murphy, R.C., Raetz, C.R., Russell, D.W., Seyama, Y., Shaw, W., *et al.* (2005). A comprehensive classification system for lipids. Journal of lipid research *46*, 839-862.

Fan, J., Sammalkorpi, M., and Haataja, M. Lipid microdomains: structural correlations, fluctuations, and formation mechanisms. Phys Rev Lett *104*, 118101.

Fan, T.W., Lane, A.N., and Higashi, R.M. (2004). The promise of metabolomics in cancer molecular therapeutics. Curr Opin Mol Ther *6*, 584-592.

Farooqui, A.A., and Horrocks, L.A. (2001). Plasmalogens: workhorse lipids of membranes in normal and injured neurons and glia. Neuroscientist *7*, 232-245.

Fiehn, O. (2002). Metabolomics--the link between genotypes and phenotypes. Plant Mol Biol *48*, 155-171.

Fima, E., Shtutman, M., Libros, P., Missel, A., Shahaf, G., Kahana, G., and Livneh, E. (2001). PKCeta enhances cell cycle progression, the expression of G1 cyclins and p21 in MCF-7 cells. Oncogene *20*, 6794-6804.

Ford, D.A., Miyake, R., Glaser, P.E., and Gross, R.W. (1989). Activation of protein kinase C by naturally occurring ether-linked diglycerides. The Journal of biological chemistry *264*, 13818-13824.

Forman, H.J., and Torres, M. (2001). Redox signaling in macrophages. Mol Aspects Med *22*, 189-216.

Fotheringham, J., Xu, F.Y., Nemer, M., Kardami, E., Choy, P.C., and Hatch, G.M. (2000). Lysophosphatidylethanolamine acyltransferase activity is elevated during cardiac cell differentiation. Biochimica et biophysica acta *1485*, 1-10.

Fridman, E., and Pichersky, E. (2005). Metabolomics, genomics, proteomics, and the identification of enzymes and their substrates and products. Curr Opin Plant Biol *8*, 242-248.

Fukuda, T., Akiyama, N., Ikegami, M., Takahashi, H., Sasaki, A., Oka, H., Komori, T., Tanaka, Y., Nakazato, Y., Akimoto, J., *et al.* (2010). Expression of hydroxyindole-O-methyltransferase enzyme in the human central nervous system and in pineal parenchymal cell tumors. J Neuropathol Exp Neurol *69*, 498-510.

Futreal, P.A., Coin, L., Marshall, M., Down, T., Hubbard, T., Wooster, R., Rahman, N., and Stratton, M.R. (2004). A census of human cancer genes. Nature reviews *4*, 177-183.

Gatenby, R.A., and Gillies, R.J. (2004). Why do cancers have high aerobic glycolysis? Nature reviews *4*, 891-899.

Glaser, P.E., and Gross, R.W. (1994). Plasmenylethanolamine facilitates rapid membrane fusion: a stopped-flow kinetic investigation correlating the propensity of a major plasma membrane constituent to adopt an HII phase with its ability to promote membrane fusion. Biochemistry *33*, 5805-5812.

Gonzalez-Mejia, M.E., and Doseff, A.I. (2009). Regulation of monocytes and macrophages cell fate. Front Biosci *14*, 2413-2431.

Goodenowe, D.B., Cook, L.L., Liu, J., Lu, Y., Jayasinghe, D.A., Ahiahonu, P.W., Heath, D., Yamazaki, Y., Flax, J., Krenitsky, K.F., *et al.* (2007). Peripheral ethanolamine plasmalogen deficiency: a logical causative factor in Alzheimer's disease and dementia. Journal of lipid research *48*, 2485-2498.

Gray, G.R. (2005). A global reorganization of the metabolome in Arabidopsis during cold acclimation is revealed by metabolic fingerprinting. Physiologia Plantarum *124*, 236-248.

Griner, E.M., and Kazanietz, M.G. (2007). Protein kinase C and other diacylglycerol effectors in cancer. Nature reviews *7*, 281-294.

Grover, A.K., Slotboom, A.J., de Haas, G.H., and Hammes, G.G. (1975). Lipid specificity of beta-hydroxybutyrate dehydrogenase activation. The Journal of biological chemistry *250*, 31-38.

Hahn, W.C., and Weinberg, R.A. (2002). Rules for making human tumor cells. N Engl J Med *347*, 1593-1603.

Hanahan, D., and Weinberg, R.A. (2000). The hallmarks of cancer. Cell *100*, 57-70.

Harris, P., and Ralph, P. (1985). Human leukemic models of myelomonocytic development: a review of the HL-60 and U937 cell lines. J Leukoc Biol *37*, 407-422.

Heeren, R.M., Kleinnijenhuis, A.J., McDonnell, L.A., and Mize, T.H. (2004). A mini-review of mass spectrometry using high-performance FTICR-MS methods. Anal Bioanal Chem *378*, 1048-1058.

Heijne, W.H., Kienhuis, A.S., van Ommen, B., Stierum, R.H., and Groten, J.P. (2005). Systems toxicology: applications of toxicogenomics, transcriptomics, proteomics and metabolomics in toxicology. Expert Rev Proteomics *2*, 767-780.

Higuchi, R., Fockler, C., Dollinger, G., and Watson, R. (1993). Kinetic PCR analysis: real-time monitoring of DNA amplification reactions. Biotechnology (N Y) *11*, 1026-1030.

Hood, L. (2003). Systems biology: integrating technology, biology, and computation. Mechanisms of ageing and development *124*, 9-16.

Hornberg, J.J., Bruggeman, F.J., Westerhoff, H.V., and Lankelma, J. (2006). Cancer: A Systems Biology disease. Biosystems.

Hsu, P.P., and Sabatini, D.M. (2008). Cancer cell metabolism: Warburg and beyond. Cell *134*, 703-707.

Igal, R.A., Caviglia, J.M., de Gomez Dumm, I.N., and Coleman, R.A. (2001). Diacylglycerol generated in CHO cell plasma membrane by phospholipase C is used for triacylglycerol synthesis. Journal of lipid research *42*, 88-95.

Iyer, V.R., Eisen, M.B., Ross, D.T., Schuler, G., Moore, T., Lee, J.C., Trent, J.M., Staudt, L.M., Hudson, J., Jr., Boguski, M.S., *et al.* (1999). The transcriptional program in the response of human fibroblasts to serum. Science (New York, N.Y *283*, 83-87.

Jacobs, J.P., Jones, C.M., and Baille, J.P. (1970). Characteristics of a human diploid cell designated MRC-5. Nature *227*, 168-170.

Kajimoto, K., Terada, H., Baba, Y., and Shinohara, Y. (2005). Essential role of citrate export from mitochondria at early differentiation stage of 3T3-L1 cells for their effective differentiation into fat cells, as revealed by studies using specific inhibitors of mitochondrial di- and tricarboxylate carriers. Molecular genetics and metabolism *85*, 46-53.

Kalus, I., Hodel, A., Koch, A., Kleene, R., Edwardson, J.M., and Schrader, M. (2002). Interaction of syncollin with GP-2, the major membrane protein of pancreatic zymogen granules, and association with lipid microdomains. The Biochemical journal *362*, 433-442.

Katan, M. (2005). New insights into the families of PLC enzymes: looking back and going forward. The Biochemical journal *391*, e7-9.

Kawamura, T., Kusakabe, T., Sugino, T., Watanabe, K., Fukuda, T., Nashimoto, A., Honma, K., and Suzuki, T. (2001). Expression of glucose transporter-1 in human gastric carcinoma: association with tumor aggressiveness, metastasis, and patient survival. Cancer *92*, 634-641.

Kell, D.B. (2004). Metabolomics and systems biology: making sense of the soup. Curr Opin Microbiol *7*, 296-307.

Kell, D.B. (2005). Metabolomics, machine learning and modelling: towards an understanding of the language of cells. Biochemical Society transactions *33*, 520-524.

Khalil, I.G., and Hill, C. (2005). Systems biology for cancer. Curr Opin Oncol *17*, 44-48.

Kim, J.W., Tchernyshyov, I., Semenza, G.L., and Dang, C.V. (2006). HIF-1-mediated expression of pyruvate dehydrogenase kinase: a metabolic switch required for cellular adaptation to hypoxia. Cell metabolism *3*, 177-185.

Kitamura, H., Nakagawa, T., Takayama, M., Kimura, Y., Hijika, A., and Ohara, O. (2004). Post-transcriptional effects of phorbol 12-myristate 13-acetate on transcriptome of U937 cells. FEBS letters *578*, 180-184.

Koukourakis, M.I., Giatromanolaki, A., Harris, A.L., and Sivridis, E. (2006). Comparison of metabolic pathways between cancer cells and stromal cells in colorectal carcinomas: a metabolic survival role for tumor-associated stroma. Cancer research *66*, 632-637.

Kristal, B.S. (2002). Practical Considerations and Approaches for Entry-Level Megavarite Analysis.

Kroemer, G., and Pouyssegur, J. (2008). Tumor cell metabolism: cancer's Achilles' heel. Cancer cell *13*, 472-482.

Kuhajda, F.P. (2000). Fatty-acid synthase and human cancer: new perspectives on its role in tumor biology. Nutrition *16*, 202-208.

Kuhajda, F.P. (2006). Fatty acid synthase and cancer: new application of an old pathway. Cancer research *66*, 5977-5980.

Kwon, H.J., and Kim, D.S. (2003). Production of nuclease activity in U937 cells by phorbol 12-myristate 13-acetate and lipopolysaccharide. Journal of biochemistry and molecular biology *36*, 520-523.

Lander, E.S., Linton, L.M., Birren, B., Nusbaum, C., Zody, M.C., Baldwin, J., Devon, K., Dewar, K., Doyle, M., FitzHugh, W., *et al.* (2001). Initial sequencing and analysis of the human genome. Nature *409*, 860-921.

Langbein, S., Zerilli, M., Zur Hausen, A., Staiger, W., Rensch-Boschert, K., Lukan, N., Popa, J., Ternullo, M.P., Steidler, A., Weiss, C., *et al.* (2006). Expression of transketolase TKTL1 predicts colon and urothelial cancer patient survival: Warburg effect reinterpreted. Br J Cancer *94*, 578-585.

Lewandrowski, U., Resemann, A., and Sickmann, A. (2005). Laser-induced dissociation/high-energy collision-induced dissociation fragmentation using MALDI-TOF/TOF-MS instrumentation for the analysis of neutral and acidic oligosaccharides. Analytical chemistry *77*, 3274-3283.

Lindqvist, A., Rodriguez-Bravo, V., and Medema, R.H. (2009). The decision to enter mitosis: feedback and redundancy in the mitotic entry network. The Journal of cell biology *185*, 193-202.

Little, J.L., and Kridel, S.J. (2008). Fatty acid synthase activity in tumor cells. Subcell Biochem *49*, 169-194.

Liu, B., Itoh, H., Louie, O., Kubota, K., and Kent, K.C. (2004a). The role of phospholipase C and phosphatidylinositol 3-kinase in vascular smooth muscle cell migration and proliferation. The Journal of surgical research *120*, 256-265.

Liu, C.T., Yu, K.C., and Ju, J.C. (2004b). Cell cycle stage analysis of rabbit foetal fibroblasts and cumulus cells. Reprod Domest Anim *39*, 385-390.

Lohner, K. (1996). Is the high propensity of ethanolamine plasmalogens to form non-lamellar lipid structures manifested in the properties of biomembranes? Chem Phys Lipids *81*, 167-184.

Macheda, M.L., Rogers, S., and Best, J.D. (2005). Molecular and cellular regulation of glucose transporter (GLUT) proteins in cancer. Journal of cellular physiology *202*, 654-662.

Maciver, N.J., Jacobs, S.R., Wieman, H.L., Wofford, J.A., Coloff, J.L., and Rathmell, J.C. (2008). Glucose metabolism in lymphocytes is a regulated process with significant effects on immune cell function and survival. J Leukoc Biol *84*, 949-957.

Malumbres, M., and Barbacid, M. (2001). To cycle or not to cycle: a critical decision in cancer. Nature reviews *1*, 222-231.

Marshall, A.G. (2002). Fourier transform ion cyclotron resonance detection: principles and experimental configurations. International Journal of Mass Spectrometry *215*, 59- 75.

Matoba, S., Kang, J.G., Patino, W.D., Wragg, A., Boehm, M., Gavrilova, O., Hurley, P.J., Bunz, F., and Hwang, P.M. (2006). p53 regulates mitochondrial respiration. Science (New York, N.Y *312*, 1650-1653.

Medes, G., Thomas, A., and Weinhouse, S. (1953). Metabolism of neoplastic tissue. IV. A study of lipid synthesis in neoplastic tissue slices in vitro. Cancer research *13*, 27-29.

Memili, E., Behboodi, E., Overton, S.A., Kenney, A.M., O'Coin, M., Zahedi, A., Rowitch, D.H., and Echelard, Y. (2004). Synchronization of goat fibroblast cells at quiescent stage and determination of their transition from G0 to G1 by detection of cyclin D1 mRNA. Cloning Stem Cells *6*, 58-66.

Menendez, J.A., Colomer, R., and Lupu, R. (2005). Why does tumor-associated fatty acid synthase (oncogenic antigen-519) ignore dietary fatty acids? Med Hypotheses *64*, 342-349.

Menendez, J.A., and Lupu, R. (2007). Fatty acid synthase and the lipogenic phenotype in cancer pathogenesis. Nature reviews *7*, 763-777.

Mills, G.B., and Moolenaar, W.H. (2003). The emerging role of lysophosphatidic acid in cancer. Nature reviews *3*, 582-591.

Mitchell, R.A. (2004). Mechanisms and effectors of MIF-dependent promotion of tumourigenesis. Cell Signal *16*, 13-19.

Morgan, C.P., Insall, R., Haynes, L., and Cockcroft, S. (2004). Identification of phospholipase B from Dictyostelium discoideum reveals a new lipase family present in mammals, flies and nematodes, but not yeast. The Biochemical journal *382*, 441-449.

Mori, N., Delsite, R., Natarajan, K., Kulawiec, M., Bhujwalla, Z.M., and Singh, K.K. (2004). Loss of p53 function in colon cancer cells results in increased phosphocholine and total choline. Mol Imaging *3*, 319-323.

Mullis, K.B. (1990). Target amplification for DNA analysis by the polymerase chain reaction. Ann Biol Clin (Paris) *48*, 579-582.

Nagan, N., and Zoeller, R.A. (2001). Plasmalogens: biosynthesis and functions. Progress in lipid research *40*, 199-229.

Naito, Y., Okada, M., and Yagisawa, H. (2006). Phospholipase C isoforms are localized at the cleavage furrow during cytokinesis. J Biochem *140*, 785-791.

Oliver, S.G., Winson, M.K., Kell, D.B., and Baganz, F. (1998). Systematic functional analysis of the yeast genome. Trends Biotechnol *16*, 373-378.

Park, W.Y., and Seo, J.S. (1995). Leucine zipper-like domain regulates the autophosphorylation and the transforming activity of P130gag-fps. Biochemical and biophysical research communications *211*, 447-453.

Parlo, R.A., and Coleman, P.S. (1984). Enhanced rate of citrate export from cholesterol-rich hepatoma mitochondria. The truncated Krebs cycle and other metabolic ramifications of mitochondrial membrane cholesterol. The Journal of biological chemistry *259*, 9997-10003.

Pastural, E., Ritchie, S., Lu, Y., Jin, W., Kavianpour, A., Khine Su-Myat, K., Heath, D., Wood, P.L., Fisk, M., and Goodenowe, D.B. (2009). Novel plasma phospholipid biomarkers of autism: mitochondrial dysfunction as a putative causative mechanism. Prostaglandins Leukot Essent Fatty Acids *81*, 253-264.

Pike, L.J., Han, X., Chung, K.N., and Gross, R.W. (2002). Lipid rafts are enriched in arachidonic acid and plasmenylethanolamine and their composition is independent of caveolin-1 expression: a quantitative electrospray ionization/mass spectrometric analysis. Biochemistry *41*, 2075-2088.

Piquemal, D., Commes, T., Manchon, L., Lejeune, M., Ferraz, C., Pugnere, D., Demaille, J., Elalouf, J.M., and Marti, J. (2002). Transcriptome analysis of monocytic leukemia cell differentiation. Genomics *80*, 361-371.

Pizer, E.S., Wood, F.D., Heine, H.S., Romantsev, F.E., Pasternack, G.R., and Kuhajda, F.P. (1996). Inhibition of fatty acid synthesis delays disease progression in a xenograft model of ovarian cancer. Cancer research *56*, 1189-1193.

Ramanathan, A., Wang, C., and Schreiber, S.L. (2005). Perturbational profiling of a cell-line model of tumorigenesis by using metabolic measurements. Proc Natl Acad Sci U S A *102*, 5992-5997.

Reemtsma, T. (2009). Determination of molecular formulas of natural organic matter molecules by (ultra-) high-resolution mass spectrometry: status and needs. J Chromatogr A *1216*, 3687-3701.

Ristow, M. (2006). Oxidative metabolism in cancer growth. Current opinion in clinical nutrition and metabolic care *9*, 339-345.

Rowe, A., Weiske, J., Kramer, T.S., Huber, O., and Jackson, P. (2008). Phorbol ester enhances KAI1 transcription by recruiting Tip60/Pontin complexes. Neoplasia (New York, N.Y *10*, 1421-1432, following 1432.

Sadowski, I., Stone, J.C., and Pawson, T. (1986). A noncatalytic domain conserved among cytoplasmic protein-tyrosine kinases modifies the kinase function and transforming activity of Fujinami sarcoma virus P130gag-fps. Mol Cell Biol *6*, 4396-4408.

Sanger, F., Nicklen, S., and Coulson, A.R. (1977). DNA sequencing with chain-terminating inhibitors. Proceedings of the National Academy of Sciences of the United States of America *74*, 5463-5467.

Schena, M., Shalon, D., Davis, R.W., and Brown, P.O. (1995). Quantitative monitoring of gene expression patterns with a complementary DNA microarray. Science (New York, N.Y *270*, 467-470.

Schorl, C., and Sedivy, J.M. (2007). Analysis of cell cycle phases and progression in cultured mammalian cells. Methods *41*, 143-150.

Schutgens, R.B., Schrakamp, G., Wanders, R.J., Heymans, H.S., Moser, H.W., Moser, A.E., Tager, J.M., Bosch, H.V., and Aubourg, P. (1985). The cerebro-hepato-renal (Zellweger) syndrome: prenatal detection based on impaired biosynthesis of plasmalogens. Prenat Diagn *5*, 337-344.

Seville, L.L., Shah, N., Westwell, A.D., and Chan, W.C. (2005). Modulation of pRB/E2F functions in the regulation of cell cycle and in cancer. Curr Cancer Drug Targets *5*, 159-170.

Sherr, C.J. (2000). The Pezcoller lecture: cancer cell cycles revisited. Cancer research *60*, 3689-3695.

Shrivastav, A., Varma, S., Lawman, Z., Yang, S.H., Ritchie, S.A., Bonham, K., Singh, S.M., Saxena, A., and Sharma, R.K. (2008). Requirement of N-myristoyltransferase 1 in the development of monocytic lineage. J Immunol *180*, 1019-1028.

Smith, H.O., and Wilcox, K.W. (1970). A restriction enzyme from Hemophilus influenzae. I. Purification and general properties. J Mol Biol *51*, 379-391.

Stallings, J.D., Tall, E.G., Pentyala, S., and Rebecchi, M.J. (2005). Nuclear translocation of phospholipase C-delta1 is linked to the cell cycle and nuclear phosphatidylinositol 4,5-bisphosphate. The Journal of biological chemistry *280*, 22060-22069.

Stallings, J.D., Zeng, Y.X., Narvaez, F., and Rebecchi, M.J. (2008). Phospholipase C-delta1 expression is linked to proliferation, DNA synthesis, and cyclin E levels. The Journal of biological chemistry *283*, 13992-14001.

Stenson, A.C., Marshall, A.G., and Cooper, W.T. (2003). Exact masses and chemical formulas of individual Suwannee River fulvic acids from ultrahigh resolution electrospray ionization Fourier transform ion cyclotron resonance mass spectra. Analytical chemistry *75*, 1275-1284.

Sulic, S., Panic, L., Dikic, I., and Volarevic, S. (2005). Deregulation of cell growth and malignant transformation. Croat Med J *46*, 622-638.

Sun, B., Murray, N.R., and Fields, A.P. (1997). A role for nuclear phosphatidylinositol-specific phospholipase C in the G2/M phase transition. The Journal of biological chemistry *272*, 26313-26317.

Tamayo, P., Slonim, D., Mesirov, J., Zhu, Q., Kitareewan, S., Dmitrovsky, E., Lander, E.S., and Golub, T.R. (1999). Interpreting patterns of gene expression with self-organizing maps:

methods and application to hematopoietic differentiation. Proceedings of the National Academy of Sciences of the United States of America *96*, 2907-2912.

Tenen, D.G. (2003). Disruption of differentiation in human cancer: AML shows the way. Nature reviews *3*, 89-101.

Tessema, M., Lehmann, U., and Kreipe, H. (2004). Cell cycle and no end. Virchows Arch *444*, 313-323.

Turkish, A., and Sturley, S.L. (2007). Regulation of triglyceride metabolism. I. Eukaryotic neutral lipid synthesis: "Many ways to skin ACAT or a DGAT". Am J Physiol Gastrointest Liver Physiol *292*, G953-957.

Unwin, R.D., Craven, R.A., Harnden, P., Hanrahan, S., Totty, N., Knowles, M., Eardley, I., Selby, P.J., and Banks, R.E. (2003). Proteomic changes in renal cancer and co-ordinate demonstration of both the glycolytic and mitochondrial aspects of the Warburg effect. Proteomics *3*, 1620-1632.

van Meer, G. (2005). Cellular lipidomics. Embo J *24*, 3159-3165.

van Meer, G., Voelker, D.R., and Feigenson, G.W. (2008). Membrane lipids: where they are and how they behave. Nat Rev Mol Cell Biol *9*, 112-124.

Velculescu, V.E., Zhang, L., Vogelstein, B., and Kinzler, K.W. (1995). Serial analysis of gene expression. Science (New York, N.Y *270*, 484-487.

Verhoeckx, K.C., Bijlsma, S., de Groene, E.M., Witkamp, R.F., van der Greef, J., and Rodenburg, R.J. (2004). A combination of proteomics, principal component analysis and transcriptomics is a powerful tool for the identification of biomarkers for macrophage maturation in the U937 cell line. Proteomics *4*, 1014-1028.

Villas-Boas, S.G., Mas, S., Akesson, M., Smedsgaard, J., and Nielsen, J. (2005a). Mass spectrometry in metabolome analysis. Mass Spectrom Rev *24*, 613-646.

Villas-Boas, S.G., Rasmussen, S., and Lane, G.A. (2005b). Metabolomics or metabolite profiles? Trends Biotechnol *23*, 385-386.

Warburg, O. (1956). On the origin of cancer cells. Science (New York, N.Y *123*, 309-314.

Warburg, O., Wind, F., and Negelein, E. (1927). The Metabolism of Tumors in the Body. J Gen Physiol *8*, 519-530.

Watson, A.D. (2006). Thematic review series: systems biology approaches to metabolic and cardiovascular disorders. Lipidomics: a global approach to lipid analysis in biological systems. Journal of lipid research *47*, 2101-2111.

Watson, J.D., and Crick, F.H. (1953). The structure of DNA. Cold Spring Harb Symp Quant Biol *18*, 123-131.

Wellen, K.E., Hatzivassiliou, G., Sachdeva, U.M., Bui, T.V., Cross, J.R., and Thompson, C.B. (2009). ATP-citrate lyase links cellular metabolism to histone acetylation. Science (New York, N.Y *324*, 1076-1080.

Werner, E., Heilier, J.F., Ducruix, C., Ezan, E., Junot, C., and Tabet, J.C. (2008). Mass spectrometry for the identification of the discriminating signals from metabolomics: current status and future trends. J Chromatogr B Analyt Technol Biomed Life Sci *871*, 143-163.

Winkles, J.A. (1998). Serum- and polypeptide growth factor-inducible gene expression in mouse fibroblasts. Prog Nucleic Acid Res Mol Biol *58*, 41-78.

www.cancer.ca (2010).

Xu, F.Y., Kardami, E., Nemer, M., Choy, P.C., and Hatch, G.M. (2000). Elevation in phosphatidylethanolamine is an early but not essential event for cardiac cell differentiation. Experimental cell research *256*, 358-364.

Xu, R.H., Pelicano, H., Zhou, Y., Carew, J.S., Feng, L., Bhalla, K.N., Keating, M.J., and Huang, P. (2005). Inhibition of glycolysis in cancer cells: a novel strategy to overcome drug resistance associated with mitochondrial respiratory defect and hypoxia. Cancer research *65*, 613-621.

Yan, Q., and Sage, E.H. (1999). SPARC, a matricellular glycoprotein with important biological functions. J Histochem Cytochem *47*, 1495-1506.

Yang, B., Oo, T.N., and Rizzo, V. (2006). Lipid rafts mediate H2O2 prosurvival effects in cultured endothelial cells. Faseb J *20*, 1501-1503.

Yeung, S.J., Pan, J., and Lee, M.H. (2008). Roles of p53, MYC and HIF-1 in regulating glycolysis - the seventh hallmark of cancer. Cell Mol Life Sci *65*, 3981-3999.

Zhao, Y., Yang, Z.Q., Wang, Y., Miao, Y., Liu, Y., Dai, S.D., Han, Y., and Wang, E.H. (2010). Dishevelled-1 and dishevelled-3 affect cell invasion mainly through canonical and noncanonical Wnt pathway, respectively, and associate with poor prognosis in nonsmall cell lung cancer. Mol Carcinog *49*, 760-770.

Zoeller, R.A., Lake, A.C., Nagan, N., Gaposchkin, D.P., Legner, M.A., and Lieberthal, W. (1999). Plasmalogens as endogenous antioxidants: somatic cell mutants reveal the importance of the vinyl ether. The Biochemical journal *338 (Pt 3)*, 769-776.

Zuo, W., and Chen, Y.G. (2009). Specific activation of mitogen-activated protein kinase by transforming growth factor-beta receptors in lipid rafts is required for epithelial cell plasticity. Mol Biol Cell *20*, 1020-1029.